NASA CR 73308
DAC-59819

Final Report

INCIPIENT SEPARATION OF A TURBULENT BOUNDARY LAYER AT HIGH REYNOLDS NUMBER IN TWO-DIMENSIONAL SUPERSONIC FLOW OVER A COMPRESSION CORNER

JANUARY 31, 1969

Prepared under Contract No. NAS7-589 by
McDonnell Douglas Astronautics Company – Western Division
Santa Monica, Calif.

for

AMES RESEARCH CENTER
NATIONAL AERONAUTICS AND SPACE ADMINISTRATION

DAC-59819

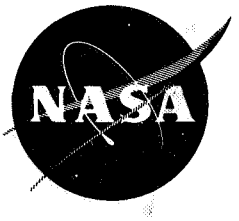

Final Report

INCIPIENT SEPARATION OF A TURBULENT BOUNDARY LAYER AT HIGH REYNOLDS NUMBER IN TWO-DIMENSIONAL SUPERSONIC FLOW OVER A COMPRESSION CORNER

By
G. J. THOMKE AND A. ROSHKO

Issued by Originator as Report DAC-59819
January 31, 1969

Prepared under Contract No. NAS7-589 by
McDonnell Douglas Astronautics Company – Western Division
Santa Monica, Calif.

for

AMES RESEARCH CENTER
NATIONAL AERONAUTICS AND SPACE ADMINISTRATION

ABSTRACT

An experimental study was made of the conditions necessary to promote incipient separation of a turbulent boundary layer in two-dimensional supersonic flow over a compression corner. The aim was to extend Kuehn's earlier results to higher Reynolds numbers. Measurements were obtained for Mach numbers in the range 2 to 5 and at Reynolds numbers, based on the boundary-layer thickness, in the range 10^6 to 10^7, nearly two orders of magnitude greater than those reported earlier. The main result was that the trend with Reynolds number established by Kuehn for the pressure rise for incipient separation does not continue to the high Reynolds number values of the present experiments; in fact, it is reversed. Pressure distributions were also obtained for conditions with and without separation. For the latter case, the upstream influence was considerably less than one boundary-layer thickness and the initial part of the pressure rise was practically a jump, suggesting that the oblique shock has its origin deep in the boundary layer.

FOREWORD

The research described herein was performed by the McDonnell Douglas Astronautics Company - Western Division under NASA Contract NAS7-589. The work was accomplished under the technical management of Mr. Donald M. Kuehn, NASA-Ames Research Center.

The authors are indebted to many staff members of the Douglas Aerophysics Laboratory, El Segundo, California, who contributed to the experimental program. Particular acknowledgement is made of the extensive help provided by Mr. W. E. Smith in preparing the experiment and report. Acknowledgement is also made of the support provided by Dr. J. Xerikos and Mr. R. A. Batchelder, MDAC-WD Advanced Aero/Thermodynamics Department, who carried out the numerical computations presented in the report.

CONTENTS

INCIPIENT SEPARATION OF A TURBULENT BOUNDARY LAYER AT HIGH REYNOLDS NUMBER IN TWO-DIMENSIONAL SUPERSONIC FLOW OVER A COMPRESSION CORNER

By G. J. Thomke and A. Roshko*

McDonnell Douglas Astronautics Company - Western Division
Santa Monica, Calif.

SUMMARY

An experimental study was made of the conditions necessary to promote incipient separation of a turbulent boundary layer in two-dimensional supersonic flow over a compression corner. The aim was to extend Kuehn's earlier results (ref. 1) for incipient separation to higher Reynolds numbers. This was accomplished by utilizing the thick (3- to 6-in.) boundary layer on the wall of a large supersonic wind tunnel, in conjunction with a ramp whose inclination was variable and controllable. Measurements were made at nominal Mach numbers of 2, 3, 4, and 5 for Reynolds numbers in the range 10^8 to 10^9 (equivalent flat plate values), approximately two orders of magnitude greater than those reported earlier. It was found that the trend with Reynolds number established by Kuehn for the pressure rise for incipient separation does not continue to the high Reynolds number values of the present experiments: in fact, it is reversed.

Pressure distributions were obtained for conditions with and without separation. For the latter case, the upstream influence was considerably less than one boundary-layer thickness and the initial part of the pressure rise was practically a jump, suggesting that the oblique shock has its origin deep in the boundary layer.

* Consultant; also Professor of Aeronautics, Graduate Aeronautical Laboratories, California Institute of Technology.

INTRODUCTION

A supersonic turbulent boundary layer can withstand without separation a certain amount of sudden pressure rise, such as that imposed by an impinging shock wave (ref. 2) or by a compression corner (ref. 3). It is not clear a priori how this maximum pressure rise will depend on Mach number and Reynolds number. In his experiments (ref. 1), Kuehn found that it increased with increasing Mach number, decreased with increasing Reynolds number (at M_o = 3 to 4), and seemed practically insensitive to Reynolds number at M_o = 2. The tendency, at least at the higher Mach numbers, of decreasing resistance to separation with decreasing skin friction coefficient seems intuitively correct, and is similar to the trend described by Chapman, Kuehn and Larson (ref. 4) for the separation pressure in the free-interaction region ahead of a fully separated flow. On the other hand, Zukoski (ref. 5) concludes from his correlation of data over a wide range of Reynolds number that the free-interaction separation pressure is independent of Reynolds number. Of course, the trends for plateau pressure or for separation pressure in the free-interaction region of a fully separated flow need not be similar to the trends for incipient separation conditions. But the plateau pressure must be lower than the pressure rise for incipient separation, and thus the latter could not continue to decrease indefinitely with increasing Reynolds number.

This question of the dependence of separation parameters on Reynolds number is of considerable practical importance; in addition, its accurate determination should be helpful in affording some understanding of the basic fluid mechanics.

The present experiments were motivated, to some extent, by the authors' earlier attempts (ref. 6) to find a simple correlation of Kuehn's data for the pressure rise for incipient separation. Assuming that the gross boundary-layer parameters, δ_o and C_{f_o}, determine the interaction with the free stream during the onset of separation, one is led to an analysis

like that used by Chapman, Kuehn and Larson for the free interaction problem, except that now one takes the pressure rise, Δp, to be given (applied) rather than free. This results in the rule $(\Delta p)_i \propto C_{f_o}$ (i.e., a linear dependence on C_{f_o} instead of the square root dependence found for a free interaction). A linear dependence of $(\Delta p)_i$ on C_{f_o} correlates Kuehn's data fairly well, as shown in figure 1, which implies

$$(\Delta p/p_o)_i/C_{f_o} = f(M_o)$$

Some results for incipient separation due to shock-wave boundary-layer interactions (ref. 1, 2, and 7) and the oft-quoted conditions for incipient separation on transonic airfoils (ref. 8) are also correlated on this figure. The correlation, however, is far from perfect, particularly at $M_o = 2$.

With increasing Reynolds number, C_{f_o} decreases. If one accepts the correlation given by figure 1, p_i/p_o should decrease as shown in figure 2, which is derived from figure 1 (cf. ref. 6). Shown for comparison in figure 2 are curves which Kuehn obtained by crossplotting his data.

The experiments reported here were therefore designed for as high a Reynolds number as possible in order to establish a trend with respect to Kuehn's results and to determine the merit of the correlation. In addition, the Reynolds number was varied over the widest range allowed by the wind tunnel operating parameters, in order to establish independently the Reynolds number trends over the range of these experiments.

SYMBOLS

C_f	local skin friction coefficient
M	Mach number
n	velocity profile parameter, e.g., $u/u_e = (y/\delta)^{1/n}$
p	pressure

Δp	pressure differential
Δp_d	orifice-dam pressure differential
r	reattachment point; also, recovery factor, r = 0.89
R	unit Reynolds number
R_δ	Reynolds number based on boundary-layer thickness
$R_{\bar{x}}$	equivalent flat-plate Reynolds number based on the distance from the virtual origin of the boundary layer
R_θ	Reynolds number based on boundary-layer momentum thickness
s	separation point
T	temperature
T_r	recovery temperature, $T_r = T_e [1 + r(\gamma - 1)M_o^2/2]$
u	velocity
$\bar{x}$	streamwise distance from virtual origin of the boundary layer
x	distance in the streamwise direction along the model surface (x = 0 at the hinge centerline)
y	distance along a normal to the model surface (y = 0 at the model surface)
z	distance in a spanwise direction (z = 0 at mid-span and is positive to the right looking upstream)
α	wedge angle for ramp
γ	ratio of specific heats, $\gamma = 1.4$ for air
Δ	dummy variable referring to δ, δ^* or θ
δ	boundary-layer thickness
δ^*	boundary-layer displacement thickness
θ	boundary-layer momentum thickness
ρ	density

Subscripts

c	condition at the corner (x = 0+)
e	condition at the outer edge of the boundary layer
i	condition for incipient separation
o	condition at the hinge centerline for $\alpha = 0$
R	condition at test section station 84.0 for a tunnel unit Reynolds number of 10^6/in.
t	tunnel total conditions

w	condition at the wall
1	condition downstream of the interaction calculated assuming the flow approaching the corner is turned inviscidly by an oblique shock for given values of M_o and α

APPARATUS AND TEST METHODS

Test Facility

The experiment was conducted in the McDonnell Douglas Astronautics Co. - Western Division (MDAC-WD) 4- by 4-foot Trisonic Wind Tunnel located at the Douglas Aerophysics Laboratory, El Segundo, California. The tunnel is an intermittent blowdown-to-atmosphere type facility. It is operative in the Mach number range 0.2 to 5.0 over a nominal unit Reynolds number range of 0.3×10^6 per in. to 3.6×10^6 per in. at stagnation temperatures from 60°F to 225°F. During a run, stagnation temperature decreases monotonically 10 to 15°F. The top and bottom walls of the nozzle are flexible plates which are automatically positioned for desired contours by means of electrically-driven screw jacks. The tunnel is equipped with a 12-ft long, porous-walled, transonic cart for testing in the Mach number range 0.7 to 1.2, and has an air-driven ejector system to facilitate low Reynolds number testing at supersonic Mach numbers.

The supersonic test section is normally 5 feet long, but for the present study the length was increased to 17 feet by placing the transonic cart in the tunnel circuit and replacing the porous walls with solid plates. In this configuration, the cart is essentially composed of a 48-in. square duct which passes through an 8-ft internal diameter by 12-ft long cylindrical outer shell. All parting lines, plate junctions, and screw-head recesses in the test section were sealed and faired in with tank sealer (MIL-S-75020) so as to provide a surface as aerodynamically smooth as possible, and to prevent high-pressure air from leaking into the test section from the chamber which existed between the duct and the outer shell.

The longitudinal Mach number gradient of the freestream is approximately -0.004/ft and -0.002/ft at M = 2 and 5, respectively. Flow uniformity is within $\pm$ 0.5-percent in Mach number. A more complete description of the tunnel is given in reference 9.

Model

The compression corner is formed by attaching a ramp to the floor of the tunnel test section (figs. 3 and 4). Because the floor (like the ceiling) is an extension of the nozzle, the boundary layer is free of distortions from flows such as those that are induced in the side wall boundary layers by the non-uniform pressure field in the nozzle. The ramp consists of a 36-in. square steel plate in two sections: the leading-edge section is 26-in. in length and hinged to the test section floor; the trailing-edge section is 10-in. long and is detachable. The hinge is mounted flush with respect to the ramp and floor surfaces. In order to minimize flow interaction problems associated with the test section sidewall boundary layers and bleed flow from or into the region where measurements are made, side-plates are fitted to the model (fig. 3). Each side-plate is 24-in. high, 72-in. long, and has a sharpened leading edge that is swept in the aft direction at an angle of 24 degrees with respect to the test section floor. An installation photograph of the model is shown in figure 4. The centerline of the hinge is located 148-in. downstream from the beginning of the supersonic test section, i.e., the end of the nozzle, which is at a fixed position. Sideplates are supported with brackets attached to the floor and sidewalls of the test section, and the 72-in. edges are centered about the hinge centerline. The hinge surface is sealed with a single layer of baggage tape (0.01-in. thick by 2-in. wide). The side edges of the ramp are fitted with O-ring seals which wipe against the side-plates, and the floor edge of each side plate is sealed with a gasket.

The ramp is hydraulically actuated, and its inclination (compression-corner angle, α) is continuously variable through the range 0 to 45

degrees. Movement of the ramp is accomplished with one 4-in. bore plus two 2.5-in. bore hydraulic cylinders. Provisions are made so that during a run the ramp can be deflected in a pitch-and-pause mode to a maximum of six preset values of α and hydraulically locked at each pause position.

Instrumentation

The ramp and test section are instrumented with 0.05-in. diameter pressure orifices and one copper-constantan thermocouple arranged as follows:

a) Sixty-five orifices are located on the centerline ($z = 0$) of the ramp and the tunnel floor. The orifices are spaced at 1-in. intervals near the hinge and 2-in. or 4-in. intervals at distances greater than 18 in. from the hinge.

b) A longitudinal row of 33 orifices are located at $z = 9.0$ in. These orifices are generally spaced at 2-in. intervals.

c) Spanwise rows of orifices are located at $x = -24.0$ in. (14 orifices), $x = -6.0$ in. (13 orifices), and $x = +2.0$ in. (15 orifices). The orifices are generally spaced at 2-in. intervals.

d) Twenty-four sets of orifices are placed in a staggered array in a region bounded by $-18 \leq z \leq 0$ in. and $-24 \leq x \leq 26$ in. Each set contains two orifices which are at the same x location but are generally separated a spanwise distance of one inch. A small wedge-shaped obstruction (0.05-in. high, 0.15-in. wide, 0.45-in. long), termed an orifice dam, is cemented to the model surface just upstream or downstream of each orifice. In each set, the orifice nearest the model centerline has a dam just upstream of it with the slanted surface facing the -x direction; the other has a dam just downstream of it with the slanted surface facing the +x direction. These orifice-dam sets are part of a technique, to be described later, for determining the flow reversal points in regions of separated flow.

e) One of the side plates is instrumented with 7 orifices. The orifices are on 2-in. centers along a normal to the floor at x = 0. The orifice nearest the floor is at a height y = 1.0 in.

f) Nineteen orifices are distributed on 6-in. centers along the centerline of the test section roof.

g) A copper-constantan thermocouple is imbedded 0.06 in. below the surface of the floor of the test section at x = -6.0 in.

Model pressures are sensed with 5-psia, 10-psia, and 15-psid transducers referenced to a near vacuum (approximately 15μ Hg). Most transducers were installed in pressure-switching devices. A known monitor pressure was applied to each transducer twice during each scanning cycle of the pressure switch (in effect, an in situ calibration of the transducer at each α). The accuracy of the system is estimated to be 0.25-percent of the full-scale range of the end instrument.

The ramp position indicator assembly consists of a ratchet, anti-backlash gear train, and potentiometer. The device is calibrated with an inclinometer. It is estimated that an accuracy of better than ± 0.05 degree was obtained in the measurement of α.

Procedure

The experiments were conducted at nominal Mach numbers 2, 3, 4, and 5, at two to four values of Reynolds number for each Mach number. During a run, data were obtained at constant Mach number and Reynolds number conditions by pitching the ramp in a pitch-and-pause mode to preset values of α, the number (from 1 to 5) depending upon available run time. Data were recorded at each α setting, and then tabulated and plotted on an "as-run" basis. The availability of as-run data was extremely helpful for the purpose of selecting values of α during the search for α_i.

A summary of test conditions is given in table 1. Reynolds number changes were accomplished primarily by changing tunnel total pressure. From 2 to 5 runs were required to obtain data reported for each R_o value shown in table 1. Reynolds number repeatability was within 2-percent of the average value obtained for a previous run. No valid data were obtained at $M = 2$ for $\alpha > 13$ degrees because the model blockage was too great to avoid shock-reflection interference from the upper wall.

The experimental method used to detect points of flow reversal is called the orifice-dam technique. A description of the dams and their arrangement was given in a previous section. Each orifice and dam combination is a rough approximation of a surface-pitot (Preston) tube. In "forward" flow, i.e., flow approaching the slanted surface, the orifice should show a decrease of pressure, compared to the clear surface pressure, since the orifice is on the "base" slide of the dam; whereas in "reverse flow", i.e., flow approaching from the base side of the dam, it should show an increase. As used in this study, the pressure differential between the orifices in a given orifice dam pair was positive if the flow at the surface were in a streamwise direction, it was negative if the flow were in a upstream direction, and it was zero at the reversal (stagnation) point.

RESULTS AND DISCUSSION

Boundary-Layer and Skin-Friction Data

The boundary-layer and skin-friction data presented in table 1 were derived from experimental results reported in reference 10. A brief description of that investigation will be given here for the sake of completeness in this report.

For the study (ref. 10), the tunnel configuration was almost identical to that used in the present experiment, the difference being that, except for required instrumentation, the test section was clear. Surface pressure, surface temperature, and pitot-pressure profile measurements were obtained for the boundary layer on the test section floor at stations

84.0 and 172.2 in. In addition, several surface pitot tubes, commonly referred to as Preston tubes, of 0.063-in. O.D. and 0.010-in. wall were distributed spanwise at both test stations. The surface pitots were mounted in a manner which duplicated, as nearly as possible, that reported by Hopkins and Keener (ref. 11) for their measurements. Measurements were obtained at nominal Mach numbers 2 to 5 in half Mach number increments for 1 to 5 values of tunnel unit Reynolds number for each Mach number.

Mach number profiles were computed in the usual way: the wall pressure was assumed constant through the boundary layer, and Rayleigh's pitot-static pressure formula was used to calculate M. Velocity and density profiles were calculated assuming that the temperature through the boundary layer was given by the following modified version of the expression obtained by Crocco for laminar flow:

$$T/T_e = T_w/T_e + (T_r/T_e - T_w/T_e)(u/u_e) - (T_r/T_e - 1)(u/u_e)^2 \quad (1)$$

By replacing u/u_e, T_w/T_e, and T_r/T_e in equation 1 with

$$u/u_e = (M/M_e)(T/T_e)^{1/2} \quad (2)$$

$$T_w/T_e = (T_w/T_t)\,[1 + (\gamma-1)M_e^2/2] \quad (3)$$

$$T_r/T_e = 1 + r\,(\gamma-1)M_e^2/2 \quad (4)$$

one arrives at a quadratic equation that is solvable for $(T/T_e)^{1/2}$ in terms of γ, r, T_w, T_t, M_e and M.

The boundary-layer thicknesses δ^* and θ were determined by integrating graphically the following expressions:

$$\delta^* = \int_0^\infty (1 - \rho u/\rho_e u_e)\, dy \quad (5)$$

$$\theta = \int_0^\infty (\rho u/\rho_e u_e)(1 - u/u_e)\, dy \quad (6)$$

The Mach number and velocity profiles were typical of those found for a turbulent boundary layer at high Reynolds number, i.e. the profiles were quite full, as shown in figure 5. Assuming that the outer portion of the velocity profile could be represented by a 1/n-type power law, n was determined to be the slope of the best straight-line fit to logarithmic values of y and u. The value for n ranged between 9 and 11 (cf. table 1). Because of the asymptotic behavior of the velocity at large y values, δ was arbitrarily selected to be the value of y at the point where the δ^* integrand was equal to 0.01 (fig. 5). This procedure yielded a consistent set of δ values amenable to analysis. Using the Preston-tube calibration equation developed by Hopkins and Keener (see fig. 8a of ref. 11) and the measured surface pitot pressure, etc., local skin-friction coefficients were calculated.

The relationship which gave the best fit to the boundary-layer thickness parameters was

$$\Delta/\bar{x} = f(M)/R_{\bar{x}}^{1/8} \tag{7}$$

where Δ is a dummy variable representing δ, δ^*, or θ, and f(M) is some function of Mach number. Furthermore, the skin-friction data correlated according to the rule

$$C_f = g(M)/R_\theta^{1/7} \tag{8}$$

One can arrive analytically at the foregoing expression for C_f by using equation 7 and the expression

$$d\theta/d\bar{x} = C_f/2 \tag{9}$$

which holds for two-dimensional compressible flow over a flat plate in zero pressure gradient. The form of equation (7) is identical to that given by Tucker (ref. 12) except that here the experimental data are proportional to $R^{-1/8}$, whereas Tucker proposed a $R^{-1/7}$ dependency. The

values of C_f calculated using the Preston-tube arrangement were found to be in agreement with those calculated using the measured R_θ values and the equations of reference 13. The effective origin of the boundary layer was determined for each M using equation (7) and the δ^* values measured at the two tunnel stations.

The values of M_o, δ_o, δ_o^*, θ_o, $\bar{x}_o$, and C_{f_o} given in table 1 were determined as follows:

a) Using the data of reference 10, the values of δ, δ^*, etc., existing at test section station 84.0 were determined for $R = 10^6/\text{in.}$

b) $\bar{x}_o$ was calculated using the equation

$$\bar{x}_o = \bar{x}_R + (148.0 - 84.0)/12 \tag{10}$$

c) δ_o, δ_o^*, and θ_o were then calculated from the following relationship obtained from equation (7),

$$\Delta_o/\Delta_R = (\bar{x}_o/\bar{x}_R)^{7/8}(10^6/R_o)^{1/8} \tag{11}$$

d) Similarly, using equation 8,

$$C_{f_o}/C_{f_R} = (R_{\theta_R}/R_{\theta_o})^{1/7} \tag{12}$$

e) M_o values were taken to be the values of M_e reported in reference 10 for tunnel station 172.2 in.

It is estimated that errors introduced through measurement and calculation procedures resulted in the following maximum uncertainties:

Quantity	Accuracy
δ	10%
δ^*	3%
θ	3%
C_f	10%
$\bar{x}$	10%
M	0.5%

Pressure Distributions

The pressure distributions measured on the model centerline are presented in figures 6 through 16 for the conditions given in table 1. The broken lines appearing in each figure represent the pressure rise corresponding to an ideal, oblique-shock compression of the flow for specific values of M_o and α. Positions of separation and reattachment are indicated by s and r, respectively. The flow-reversal points were determined from measurements made with the orifice dams. In each figure, the filled symbol located at x = 0 designates the pressure sensed on the instrumented side plate at a point 1 in. above the floor. It is shown for reference purposes only, and cannot be taken to represent the surface pressure because $dp/dy \neq 0$ in that region.

The two-dimensionality of the flow approaching the ramp, ramp length effects, hysteresis effects, and data repeatability are illustrated in figures 9(i), 13(a), 13(c), and 13(g), respectively. The slight difference between the two sets of measurements in figure 13(a) can be attributed to the 0.16-degree difference in α.

Flow Not Separated

The character of the pressure distributions at values of α below those for incipient separation was rather unexpected. For example, the data for $M_o = 2.95$ (figures 8, 9, and 10) show that there is little upstream influence ahead of the hinge for low values of α. The pressure rises abruptly, over a distance much less than one boundary-layer thickness. This feature is in sharp contrast with the data presented in reference 1,

where, at much lower Reynolds numbers, there was a much greater upstream "smoothening", extending over several boundary-layer thicknesses. For each Reynolds number condition, the surface pressure at x = 0 (not actually measured there, but determined by extrapolating through the values obtained for +x) increases with increasing α up to a limiting value. Only after this value is reached does the pressure distribution begin to develop upstream of the corner. The pressures at the downstream end of the ramp tend to rise above the ideal, oblique-shock values indicated in the figures; this tendency is pronounced for the larger α values. It is also noticed that points near the downstream end of each pressure distribution do not define a curve as smoothly as do all the others. This is almost certainly not due to errors in the instrumentation, but is probably a true indication of pressure variation in that region.

The features which characterize the $M_o = 2.95$ data appear also in figures 11 through 14 for $M_o = 3.93$, and in figures 15 and 16 for $M_o = 4.92$.

The small upstream influence and the rapid rise of pressure near the corner suggests that a pressure distribution may be idealized by a jump at x = 0, to some value p_c, followed by a gradual rise, over several boundary-layer thicknesses, toward the final value. The value of p_c is defined by extrapolating the measured pressure distribution back to x = 0. Such an idealized pressure distribution is sketched in figure 17(a) together with a model of the flow field that can account for it (the significance of M_m is discussed later). In this model, a small, inner portion of the boundary-layer profile is ignored and the outer portion is considered simply as a supersonic, rotational stream that interacts inviscidly with the ramp. The lower edge of this layer is defined by a Mach number M_w and is taken to be at the wall itself.

This idealized flow field model is nearly the same as that proposed by Rose et al (ref. 14) for the case of oblique-shock impingement on a turbulent boundary layer. In reference 14, the lower edge of the outer portion of the layer was defined by a characteristic break in the measured Mach number profile, which occurred at about 10 percent of the boundary-layer thickness, but here it is defined by the value of M_w which will give

the observed jump in pressure to p_c, due to the oblique shock wave initiated by the interaction of the $M = M_w$ steamline with the corner (fig. 17). As the oblique shock propagates into the regions of higher Mach number, it interacts with the vorticity or entropy layers, and produces compression waves which propagate downward onto the surface, resulting in the rising pressure sketched below it. To investigate the applicability of such a model, the case of figure 18 was computed by a method of characteristics program described in reference 15. The measured pressure distribution is extrapolated to a value at $x = 0$ chosen as p_c; this then determines the value of M_w, and the measured M profile (figure 5) is faired into this value at $y = 0$. The resulting, computed pressure distribution agrees very well with the measured one (figure 18). Variations of the initial choice of p_c and M_w indicate that the sensitivity is such that a reasonable choice can easily be made. Near the end of the pressure rise, at the last computed point shown, the flow next to the wall becomes subsonic and the characteristics computation cannot be continued. It is interesting that the measured pressure distribution follows the computed values smoothly up to the point but then begins to show some variation. Hence the earlier comment that those variations are real; it is believed that they are connected with the development of a sonic or subsonic region near the surface.

For the case calculated in figure 18 ($M_o = 3.93$, $\delta_o = 4.78$ in.), it was necessary to choose $M_w = 2.04$ to match the initial pressure jump. This value in the Mach number profile actually occurs at a distance of about 0.2 inch. from the wall. By contrast, the thickness of the viscous sublayer defined in the conventional way ($y^+ \doteq 10$) is about 0.004 in. (ref. 16). Thus, the thickness of the matching sublayer which determines M_w is considerably larger than that of the viscous sublayer, but still small compared to the boundary-layer thickness ($0.04\ \delta_o$ in the present case). How to determine it theoretically is the interesting question.

The Case at Mach Number 2

Figures 6 and 7, for $M_o = 1.95$ data, present quite a different picture from that obtained at higher Mach number. The slight pressure bump

upstream of the main interaction is probably extraneous; it may be due to weak waves originating at the vertex of each side plate. The pressure rise, then, again occurs abruptly, but now at about a half boundary-layer thickness upstream of the corner. More remarkable is the overshoot to values of pressure above those corresponding to the jump through a simple oblique shock wave. The overshoot is largest (about 50 percent) for the smallest ramp angle and becomes relatively smaller with increasing angle. After overshoot, the pressure dips down to the oblique shock value, in every case, and then increases again slightly.

An overshoot could occur for the following reason. Referring to figure 19, if M_w happens to be less than M_m, then in the interaction between an oblique shock originating from the corner with the layers at higher Mach number the family of waves directed downward toward the ramp surface (figure 17) initially are expansion waves and later become compression waves (once M_m is passed); the resulting surface distribution should resemble that sketched in part (b) of figure 17.

However, the observed overshoot in figure 6a for $\alpha = 5.16$ degrees, for example, is considerably higher than could be accounted for by an attached wave, and one has to conclude that the value of M_w is so low that the shock wave is detached from the corner. This idea is lent support by the fact that the initial pressure jump occurs not at the corner but upstream of it. To make calculations based on this model is obviously much more problematic than for the case with an attached wave and a fully supersonic field downstream of it.

Incipient Separation

The main objective of this investigation was to determine the conditions for incipient separation, i.e., the first appearance of flow reversal near the corner. The experimental method used to detect points of flow reversal is called the orifice-dam technique and is essentially an extension of that used previously (refs. 17 and 18) in base flow studies to detect the reattachment point.

An illustration of the results typically obtained and the method used to determine the incipient separation conditions is given in figure 20 for $M_o = 3.93$, $R_o = 0.443 \times 10^6$/in. In figure 20(a), the pressure differential, Δp_d, for each orifice-dam pair is normalized with respect to the freestream pressure, p_o, and plotted versus the x-location of the set. For $\alpha = 26.82$ degrees, the boundary layer separated near $x = -8$ in. and reattached near $x = 2$ in. (cf. fig. 11(h)). The data indicate that the boundary layer is not separated for $\alpha = 21.98$ degrees (cf. fig. 11(e)), and α_i is between 21.98 and 22.47 degrees. The method typically used to determine the incipient separation angle, α_i, is shown in figure 20(b), where the $\Delta p_d/p_o$ values obtained for the orifice-dam pair located one inch upstream of the corner are plotted versus α. The value for α at which the curve drawn through the experimental data intersects the $\Delta p_d/p_o = 0$ ordinate is taken to be α_i (for this case $\alpha_i = 22.4$ degrees). Also plotted on figure 20(b), for purpose of comparison, are data obtained for the orifice-dam pair located one inch downstream of the corner.

Kuehn (ref. 1) associated incipient separation with the first appearance of a kink in the pressure distribution near the corner. The development of such kinks is evident in figures 6 through 16. To define α_i accurately from the first appearance of a kink requires pressure distributions for a series of closely spaced values of α. Another possibility is to plot the variation of pressure near the corner against α and observe its behavior as it approaches the limiting value of p_c, described earlier. Such a plot is shown in figure 21 for the surface pressure orifice located one inch downstream of the corner. The break corresponds to $\alpha_i = 22.2$ degrees. (The kink pressure level at this point ($x = +1$) is $p/p_o = 3$ and is considerably higher than the kink pressure $p_c/p_o = 2.5$ at $x = 0$).

Still another way of plotting the data is illustrated in figure 22, where the trajectories of the points of flow reversal, that is, separation (s) and reattachment (r), are plotted against α. The values of s and r are determined from zero crossings in plots like that in figure 20b. The intersection of the s and r trajectories determines α_i, in this case

about 22.5 degrees, which compares well with the values 22.2 degrees and 22.4 degrees by the methods already described. A curious result is that, in all cases, this intersection apparently occurs at about one inch upstream of the corner, not at the corner itself. The apparent shift may be due to the finite height (0.05 in.) of the orifice dams which, near flow reversal, will project out of the separated region into the main flow and thus introduce error. However, because of the good agreement between values of α_i determined in this way with those found by the independent pressure kink method, corrections have not been attempted.

By these methods, values of α_i believed to be accurate to about 0.5 degree have been determined. A summary of the incipient separation conditions measured in this experiment is presented in table 2. The values tabulated for the ratio $(p_1/p_o)_i$ were obtained from reference 19. The conditions tabulated in table 2 are plotted in figures 23 and 24. Kuehn's interpolation (ref. 1) of his experimental results are presented in both figures, and in figure 24 the values predicted by the correlation given in reference 6 are also shown.

Figures 23 and 24 show that the trend with Reynolds number, established experimentally by Kuehn at values of R_{δ_o} nearly two order of magnitude lower than those of the present experiments, does not continue to the high values of the present study; in fact, it is reversed. The exception to the foregoing statement occurs at $M_o = 1.95$ where no measurable change in the incipient separation conditions was detected. The reason for the reversal in trend is not immediately apparent from the experimental data available in the literature, but it appears likely that the sublayer structure of the boundary layer approaching the corner plays a key role in the separation process.

Collectively, the results shown in figure 23 indicate that a minimum value for α_i exists as Reynolds number is varied at constant Mach number. Furthermore, the data suggest that, for constant Reynolds number, α_i may be approaching a limiting value with increasing Mach number.

Figure 24 shows that the correlation given in reference 6 does not hold at high R_{δ_o} values -- a result not entirely unanticipated. This is because the linear dependence of C_{f_o} established by the correlation leads to the result that the pressure rise for incipient separation continues to decrease indefinitely with increasing Reynolds number; and since the plateau pressure in the free-interaction region of a fully separated flow becomes independent of C_{f_o} (ref. 5), an impossible situation would occur at sufficiently high values of Reynolds number, viz., the plateau pressure would be higher than the pressure required for incipient separation.

Separated Regions

Though the present study was directed primarily toward determining the condition for incipient separation, a few measurements were obtained at conditions where the boundary layer was well-separated (cf. figs. 9i, 10e, 11h, 12g, 13g, 14d, 16e). In each case, the kink pressure at $x = 0$ is close to the value given by Zukoski (ref. 5) for the plateau pressure upstream of a forward-facing step at the same Mach numbers. However, a well-defined, constant-pressure, plateau region was never observed. As we might expect for $\alpha > \alpha_i$, the length of the separated region increased with α. The slope of the pressure rise near the beginning of the interaction is about twice Zukoski's value for the maximum slope near the beginning of a free interaction ahead of an upstream-facing step. It is not clear whether the difference is due to the difference in geometries, or that the flow is not sufficiently well separated in our examples. On the other hand, one should possibly ask why the pressure rise is not even steeper, since it is practically a jump for $\alpha < \alpha_i$. The explanation may be that, after separation, the turbulent or even more-organized fluctuations are greater than in the attached case, causing the foot of the shock to oscillate and give an apparent spread of the pressure rise, as suggested by Zukoski (ref. 5). The differences noted above, may possibly be traceable to different fluctuation amplitudes in the two geometries.

Reynolds number effects on the extent of the separation region are shown in figures 25 and 26, where the measured pressures are plotted versus

x and x/δ_o, respectively. The results show that an increase in Reynolds number produces a decrease in the separation length, in accordance with the trend for incipient separation.

CONCLUDING REMARKS

The finding that resistance to separation increases with increasing Reynolds number was unexpected, but it is very clearly shown by the results for incipient separation and the few data on separation length. Another important result was the clear demonstration of a boundary-layer flow in which the region of influence of some thin sublayer is very small so that most of the boundary layer may be treated simply as an inviscid, rotational flow. Such a model has been proposed, in various contexts, by a number of authors. Another aspect concerns the subcritical/supercritical nature of a supersonic boundary layer first described by Crocco and Lees (see, for example, ref. 20); clearly the boundary layer was supercritical in the present experiments.

The phenomena are perhaps less surprising when it is remembered that the viscous sublayer thickness, relative to the overall thickness δ, is (nearly) inversely proportional to the Reynolds number and, at the Reynolds numbers of these experiments, is very thin indeed. Still, the relation of the viscous sublayer to the sublayer that seems to be significant here is not evident and, indeed, presents an intriguing problem. Some understanding of this relation should throw light on the Reynolds number dependence and lead toward a more complete method of calculation. Unfortunately, profiles of the boundary layers in the interaction region were not obtained. These would be a useful aid for both the development and trial of theories. It is supposed that, for flow without separation, a calculation scheme similar to that used in the present study will also provide the correct velocity profiles downstream of the shock; a verification of this would be useful.

The results from the present experiment also prompt one to speculate about the course that the incipient separation angle would take with

still further increase of Reynolds number. Possibly it would level off when the angle became large enough to cause the foot of the shock to detach from the corner, as seems to be the case at M = 2.

REFERENCES

1. Kuehn, Donald M: Experimental Investigation of the Pressure Rise Required for the Incipient Separation of Turbulent Boundary Layers in Two-Dimensional Supersonic Flow. NASA Memo 1-21-59A, 1959.

2. Bogdonoff, S. M; Kepler, E. C.; and Sanlorenzo, E.: A Study of Shock Wave Turbulent Boundary Layer Interaction at M = 3. Rep. No. 222, Princeton Univ., Dept. of Aero. Eng., 1953.

3. Drougge, Georg: An Experimental Investigation of the Influence of Strong Adverse Pressure Gradients on Turbulent Boundary Layers at Supersonic Speeds. Presented at VIIIth International Congress on Theoretical and Applied Mechanics; Istanbul, Turkey, 1952. Also Rep. No. 46, Aero. Res. Inst. of Sweden, 1953.

4. Chapman, D. R.; Kuehn, D. M.; and Larson, H. K.: Investigation of Separated Flows in Supersonic Streams with Emphasis on the Effect of Transition. NACA Rep. 1356, 1958. (Supersedes NACA TN 3869)

5. Zukoski, E.E.: Turbulent Boundary Layer Separation in Front of a Forward-Facing Step. AIAA J., Vol. 3, No. 10, 1967, pp. 1746-1753.

6. Roshko, A.; and Thomke, G. J.: Correlations for Incipient Separation Pressure. Rep. No. DAC-59800, Douglas Aircraft Co., Inc., 1966.

7. Vas, I. E.; and Bogdonoff, S, M.: Interaction of a Shock Wave with a Turbulent Boundary Layer at M = 3.85. Rep. No. 294, Princeton Univ., Dept. of Aero. Eng., 1955.

8. Pearcey, H. H.: Shock-Induced Separation and its Prevention by Design and Boundary Layer Control. Boundary Layer and Flow Control, Pergamon Press, London, 1961, pp, 1166-1344.

9. Radattz, L.A.: The Douglas Aerophysics Laboratory Four-Foot Trisonic Wind Tunnel. Rep. No. DAC-59809, Douglas Aircraft Co., Inc., 1967.

10. Thomke, G. J.: Boundary-Layer and Skin-Friction Characteristics in the Supersonic Test Section of the Douglas Aerophysics Laboratory Four-Foot Trisonic Wind Tunnel. Unpublished report of the McDonnell Douglas Astronautics Co., Western Division.

11. Hopkins, Edward J.; and Keener, Earl R.: Study of Surface Pitots for Measuring Turbulent Skin Friction at Supersonic Mach Numbers - Adiabatic Wall. NASA TN D-3478, 1966.

12. Tucker, Maurice: Approximate Calculation of Turbulent Boundary-Layer Development in Compressible Flow. NACA TN 2337, 1951.

13. Komar, J. J.: Improved Turbulent Skin-Friction Coefficient Predictions Utilizing the Spalding-Chi Method. Rep. No. DAC-59801, Douglas Aircraft Co., Inc., 1966.

14. Rose, W. C; Murphy, J. D; and Watson, E. C.: Interaction of an Oblique Shock Wave with a Turbulent Boundary Layer. AIAA J., Vol. 6, No. 9, 1968, pp. 1792-1793.

15. Inouye, M.; Rakich, J. V.; and Lomax, H.: A Description of Numerical Methods and Computer Programs for Two-Dimensional and Axisymmetric Supersonic Flow Over Blunt-Nosed and Flared Bodies. NASA TN D-2970, August 1965.

16. Czarnecki, K. R.; and Monta, W. J.: Effects of Compressibility and Heat Transfer on the Laminar Sublayer of the Turbulent Boundary Layer. NASA TN D-1998, October 1964.

17. Roshko, A.; and Thomke, G. J.: Flow Separation and Reattachment Behind a Downstream-Facing Step. Rep. No. SM-43056-1, Douglas Aircraft Co., Inc., 1964.

18. Kuehn, D. M; and Monson, D. J.: Attached and Separated Boundary Layers on Highly Cooled Ablating and Non-Ablating Models at M = 13.8. NASA TN D-4041, 1967.

19. Dennard, J. S.; and Spencer, P. B.: Ideal-Gas Tables for Oblique-Shock Flow Parameters in Air at Mach Numbers from 1.05 to 12.0. NASA TN D-2221, 1964.

20. Klineberg, J. M.; and Lees, L.: Theory of Laminar Viscous-Inviscid Interactions in Supersonic Flow. AIAA Paper No. 69-7, Presented at AIAA 7th Aerospace Sciences Meeting, New York, January 1969.

TABLE 1. SUMMARY OF TEST CONDITIONS

M	M_0	T_{t_0} ($^\circ R$)	T_{w_0} ($^\circ R$)	$R_0 \times 10^{-6}$ (1/IN.)	$\bar{x}_0$ (FT)	δ_0 (IN.)	δ_0^* (IN.)	θ_0 (IN.)	n	$C_{f_0} \times 10^3$	α (DEG)
2	1.95	587	545	0.580	25.03	3.26	0.725	0.246	8.9	1.28	5.16, 9.03, 9.99, 11.08, 12.09, 12.60, 12.94
		608	555	1.022		3 08	0.684	0.237		1.18	8.96, 10.03, 10.97, 12.08, 13.00
3	2.95	585	536	0.411	31.83	4.56	1.210	0.250	10.5	1.05	18.95, 19.92, 21.03, 21.88
		592	536	0.752		4.21	1.118	0.231		0.94	10.00, 14.88, 16.84, 19.92, 20.46, 21.09, 21.52, 23.04, 25.00
		593	541	1.509		3.87	1.026	0.212		0.86	20.02, 21.45, 21.92, 21.96, 24.00
4	3.93	569	526	0.443	39.33	5.36	1.808	0.25	10.7	0.78	17.87, 18.85, 19.88, 21.98, 22.47, 23.44, 23.97, 26.82,
		566	524	0.734		5.04	1.701	0.242		0.72	14.99, 20.03, 21.05, 21.51, 22. 5, 23.04, 25.01
		549	529	1.140 ①		4.78	1.611	0.230		0.68	10.10, 14.66, 15.06, 16.88, 17.00, 19.04, 20.79, 22.65
		538	517	1.200		4.75	1.603	0.228		0.68	14.90, 18.55, 22.90, 24.86, 26.94
		538	517	1.200 ②		4.75	1.603	0.228		0.68	26.83, 24.92, 24.42, 23.42, 22.94
		591	535	1.743		4.52	1.525	0.217		0.64	23.00, 23.94, 25.05, 26.91
5	4.92	593	533	0.560	46.03	5.81	2.313	0.224	10.0	0.60	19.97, 21.09, 21.45, 22.98, 24.93
		633	537	0.959		5.49	2.183	0.211		0.55	14.86, 24.02, 24.93, 25.88, 26.96

① RAMP LENGTH REDUCED TO 26.0 INCHES FOR THIS SET OF CONDITIONS.

② FOR THIS SET OF α, THE RAMP WAS STEPPED FROM $\alpha = 0$ TO $\alpha = 26.83$ ON THE FIRST STEP; SUCCEEDING STEPS WERE FROM HIGH TO LOW α. OTHERWISE, RAMP MOVEMENT WAS ALWAYS FROM LOW TO HIGH α.

Table 2.

Summary of Measured Incipient Separation Conditions

M_0	$R_{\delta_0} \times 10^{-6}$	α_i (DEG)	$(P_1/P_0)_i$
1.95	1.891 3.148	12.8 12.8	1.95 1.95
2.95	1.874 3.166 5.840	19.5 19.7 20.3	3.61 3.65 3.77
3.93	2.374 3.699 5.700 7.878	22.4 22.5 22.7 23.0	5.92 5.92 6.02 6.13
4.92	3.254 5.265	23.4 23.7	8.65 8.82

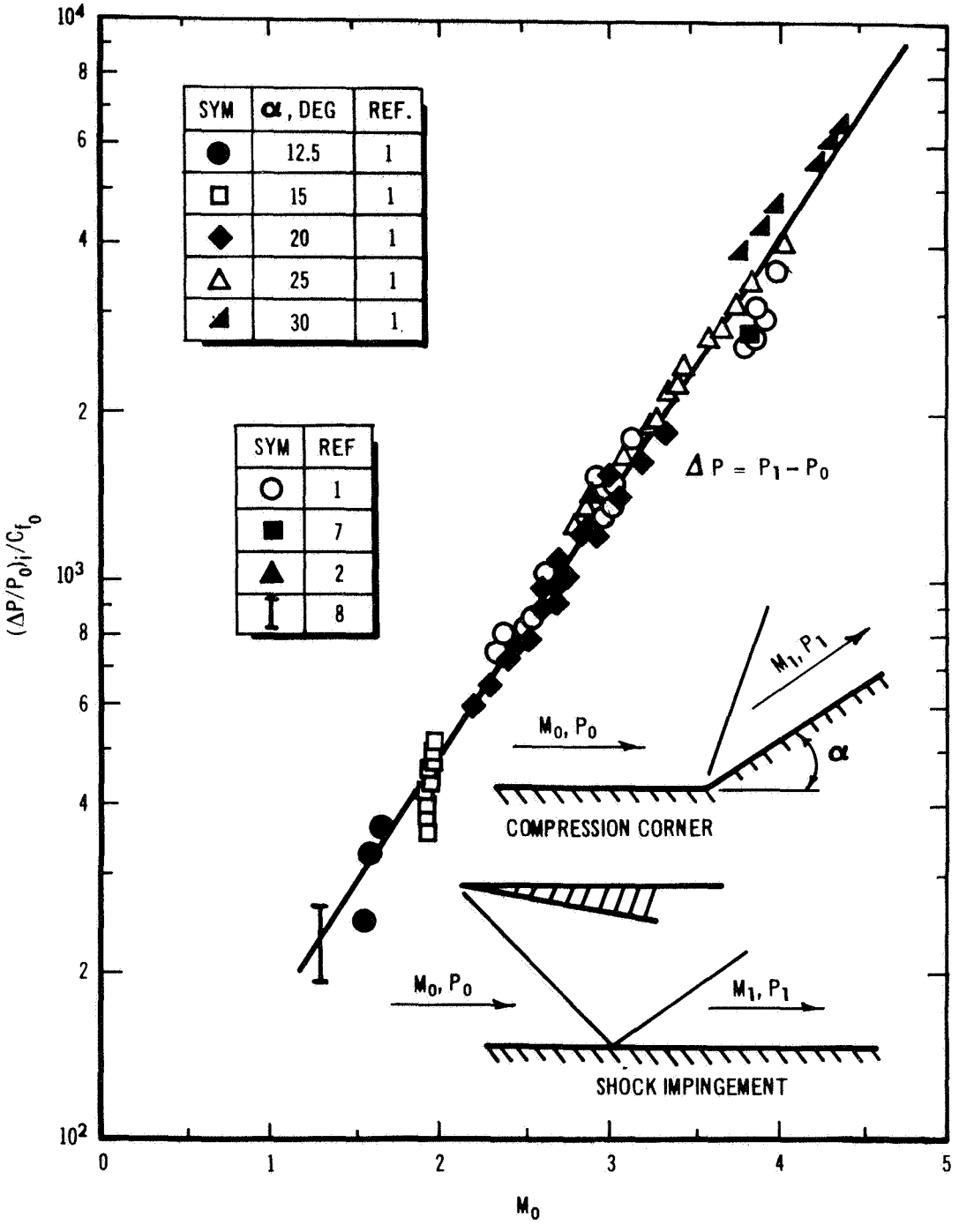

Figure 1. Similarity Correlation According To A Linear Skin-Friction Law

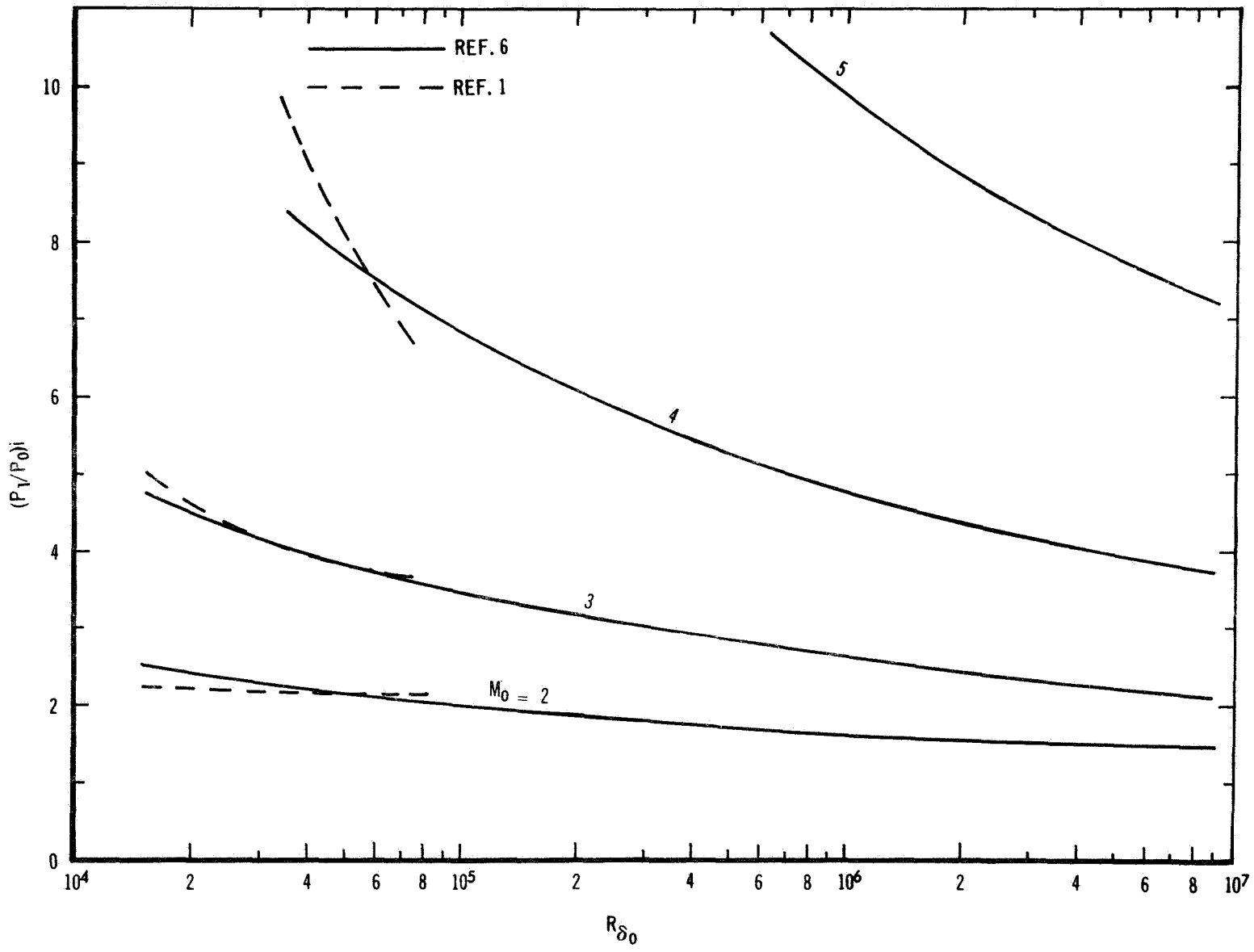

Figure 2. Pressure Rise for Incipient Separation of a Turbulent Boundary Layer According to the Similarity Correlation

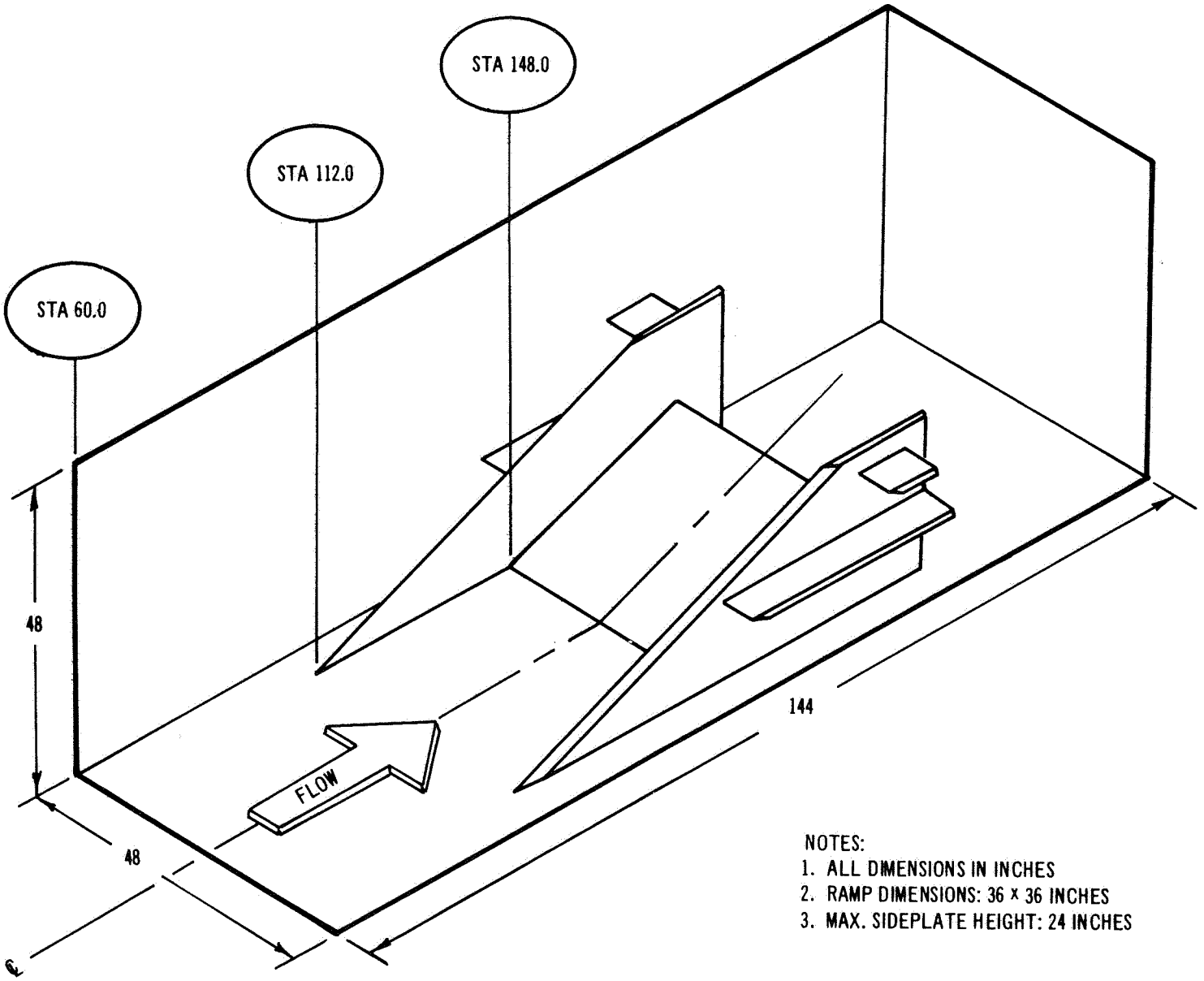

Figure 3. Installation Sketch

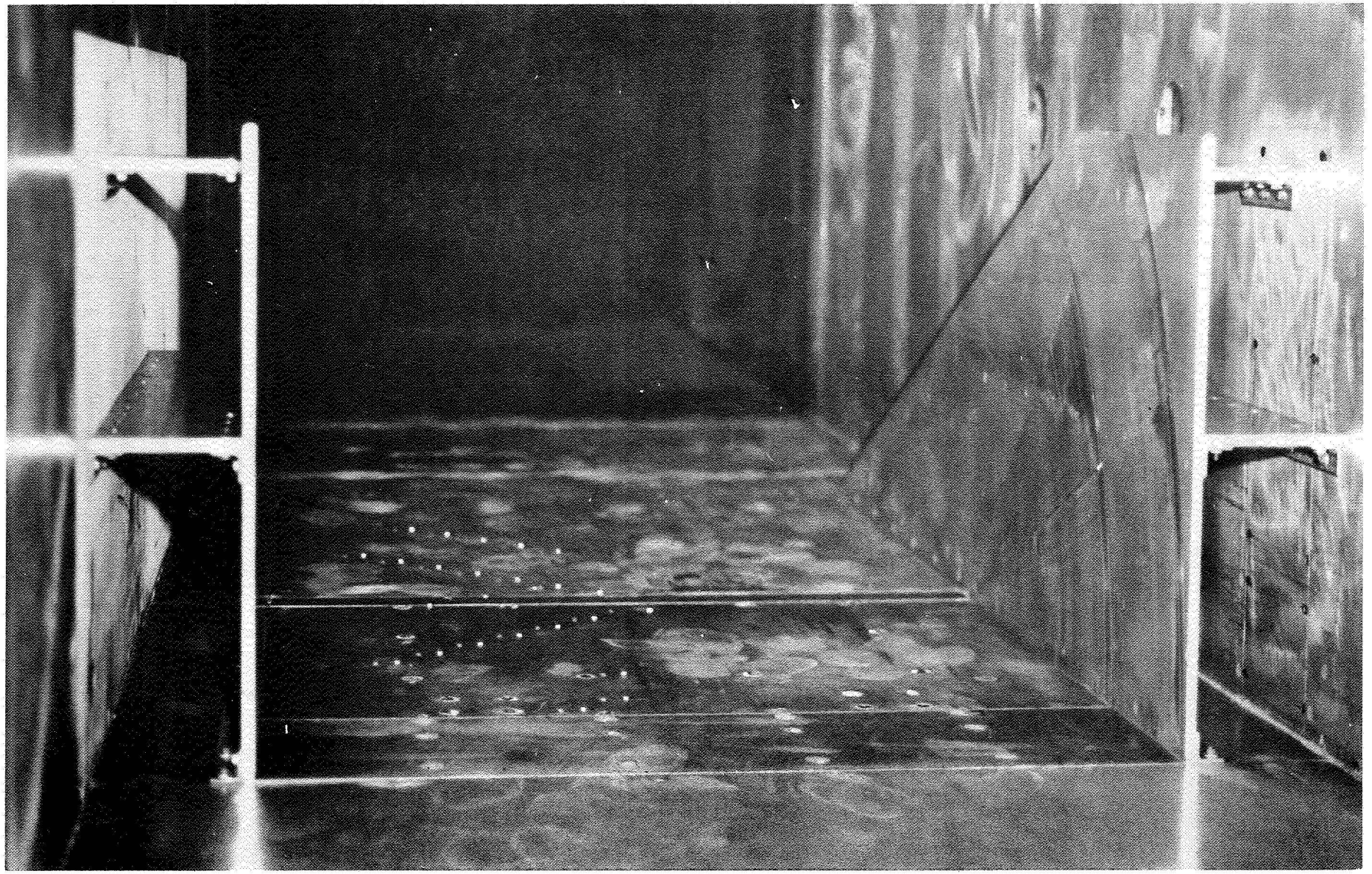

Figure 4. Installation Photograph

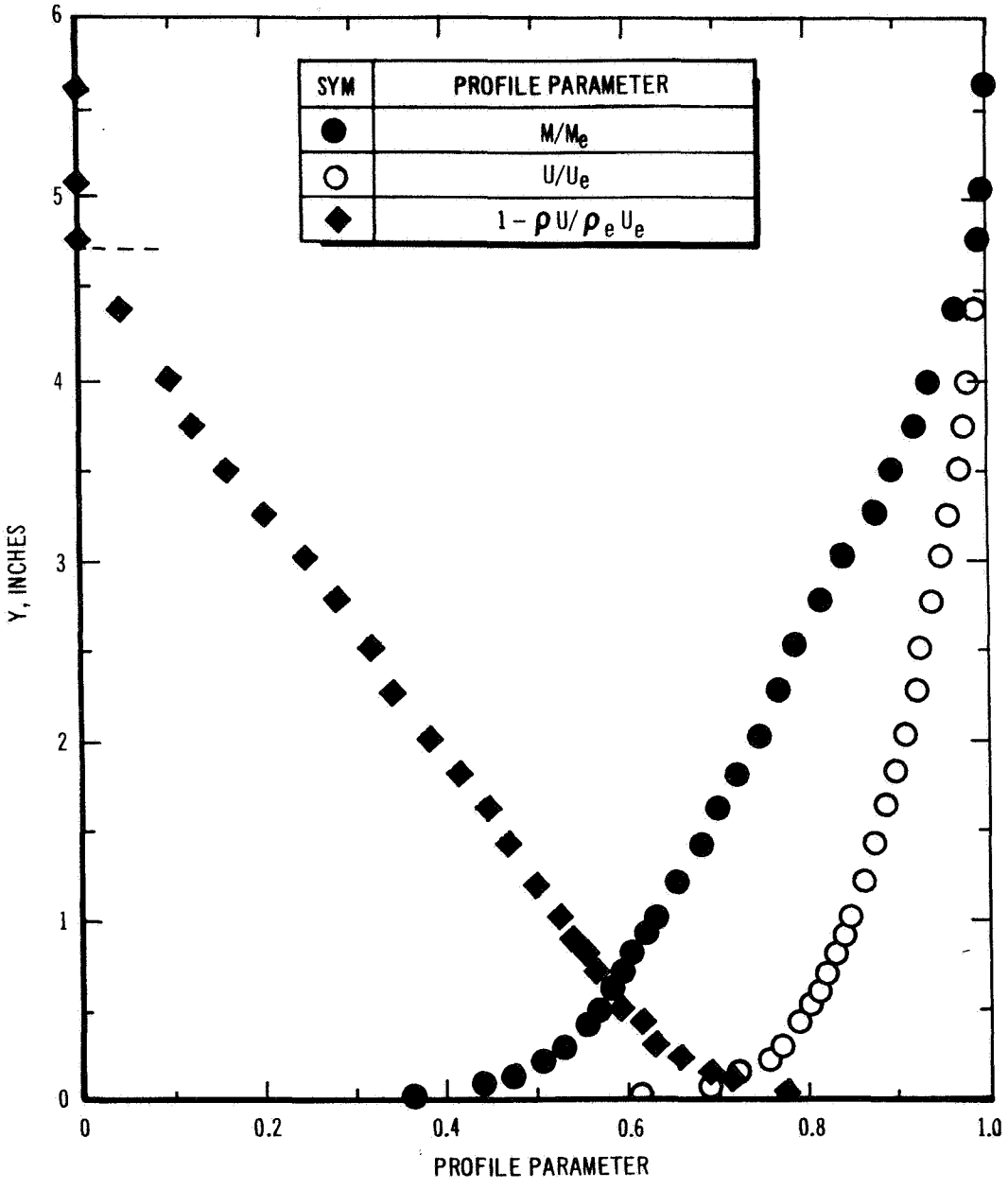

Figure 5. Boundary-Layer Profile at Tunnel Station 172.2 Inches. $M_e = 3.93$, $R_e = 1.71 \times 10^6$/Inch, $\delta = 4.7$ Inches.

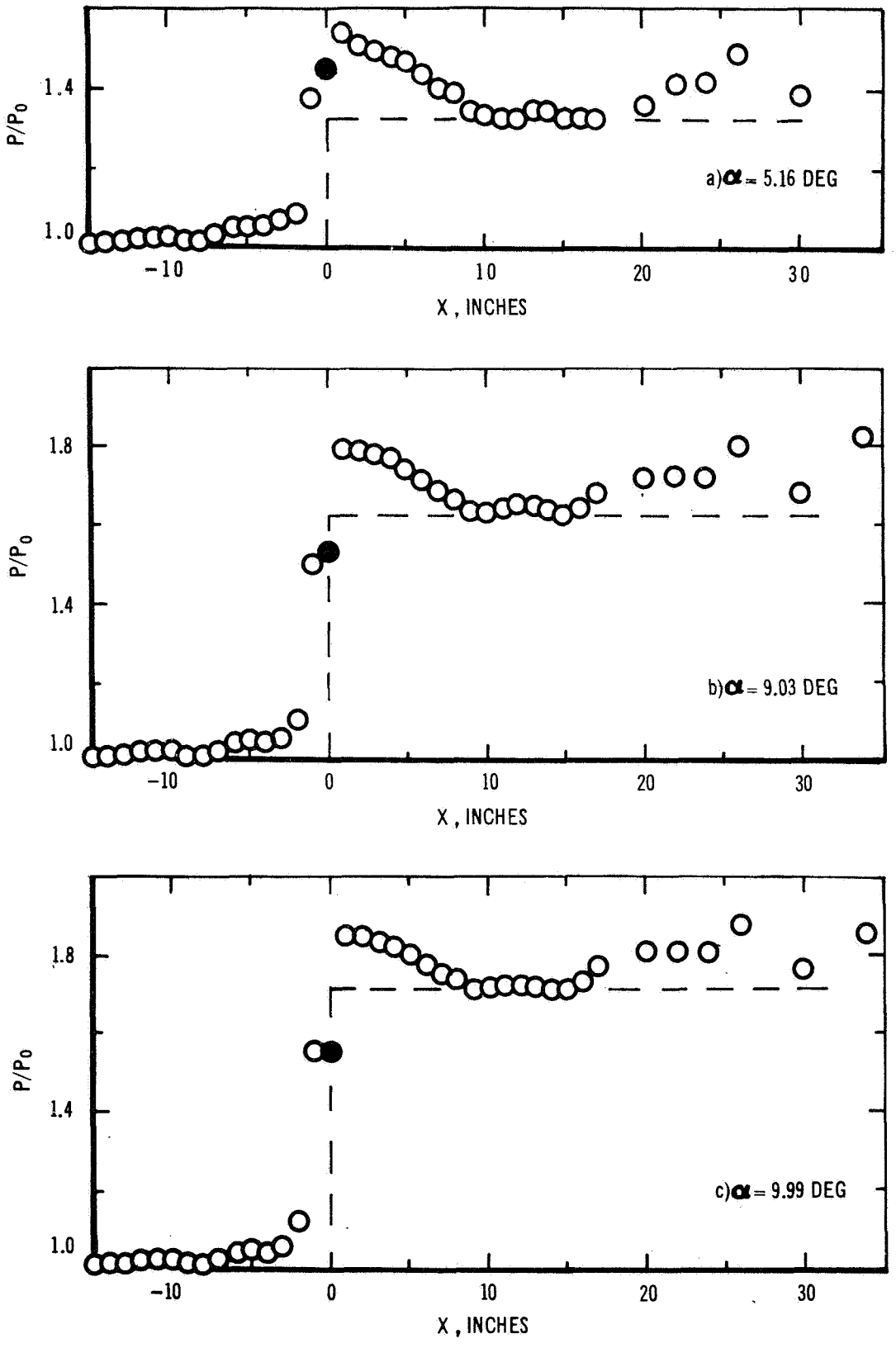

Figure 6. Pressure Distributions Along Model Centerline.
$M_0 = 1.95$, $R_0 = 0.580 \times 10^6$/in., $\delta_0 = 3.26$ in.

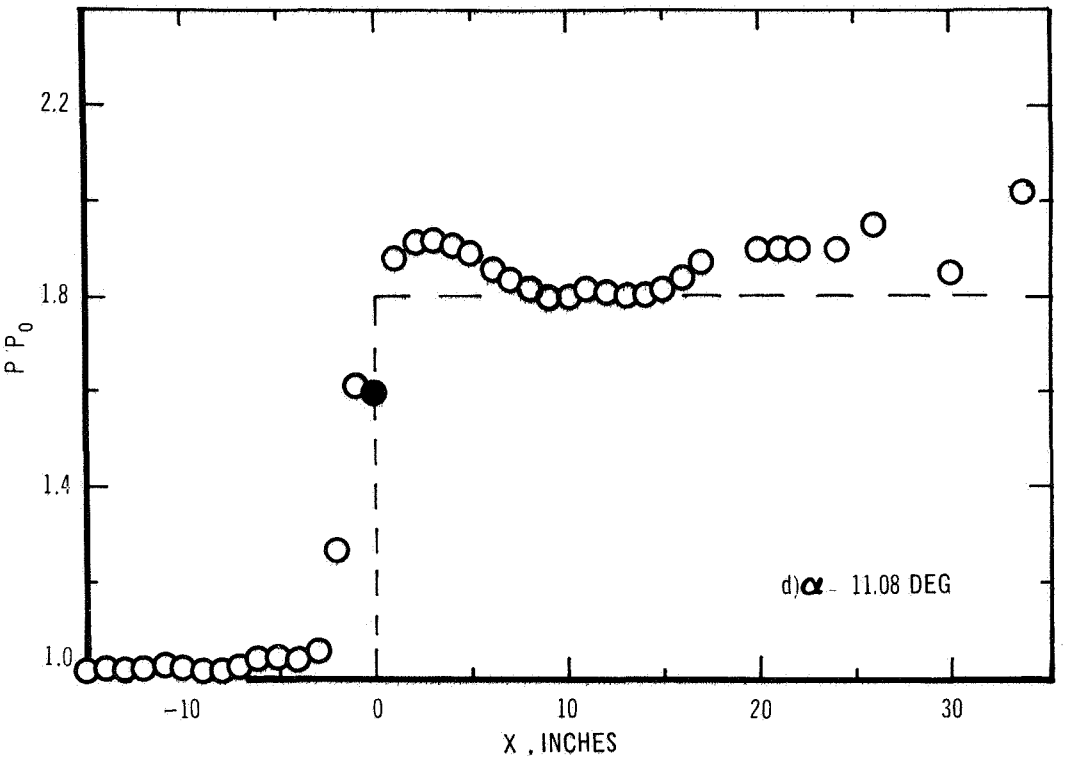

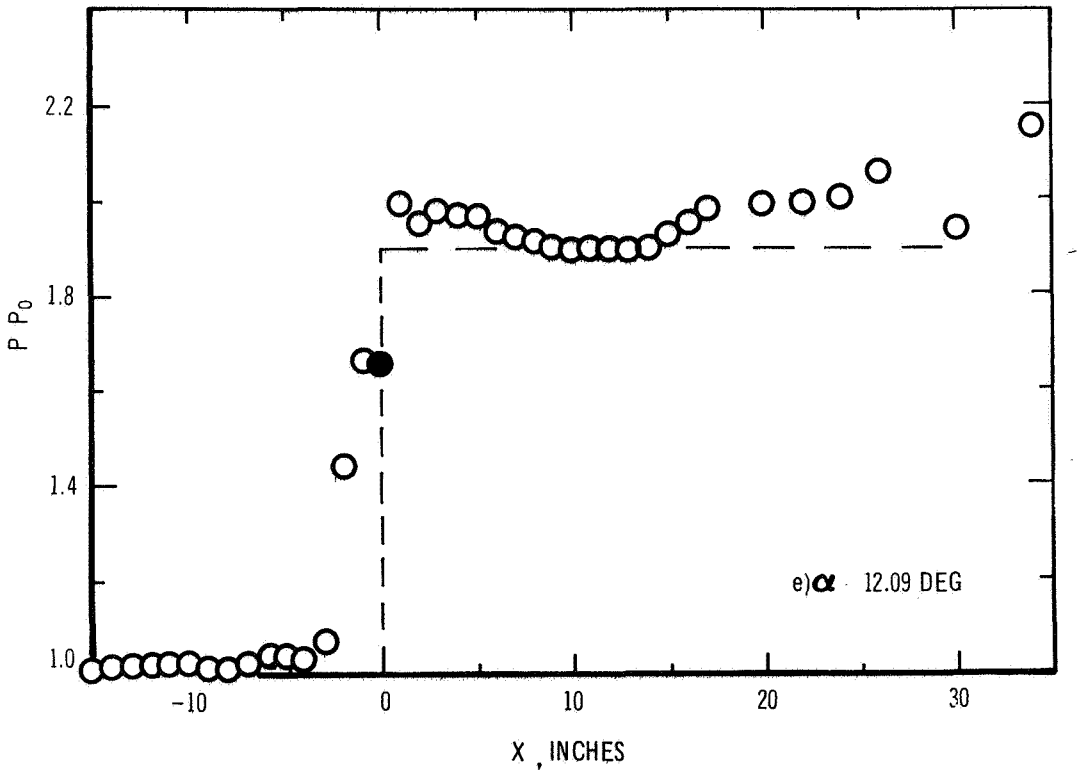

Figure 6. Continued

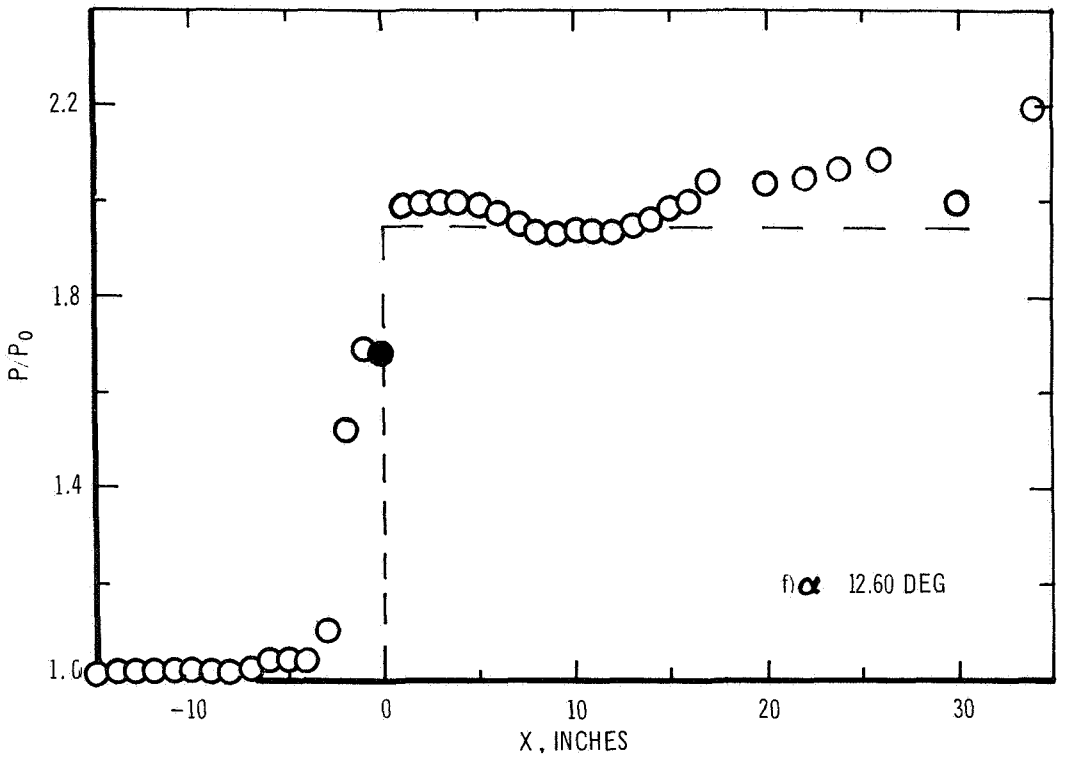

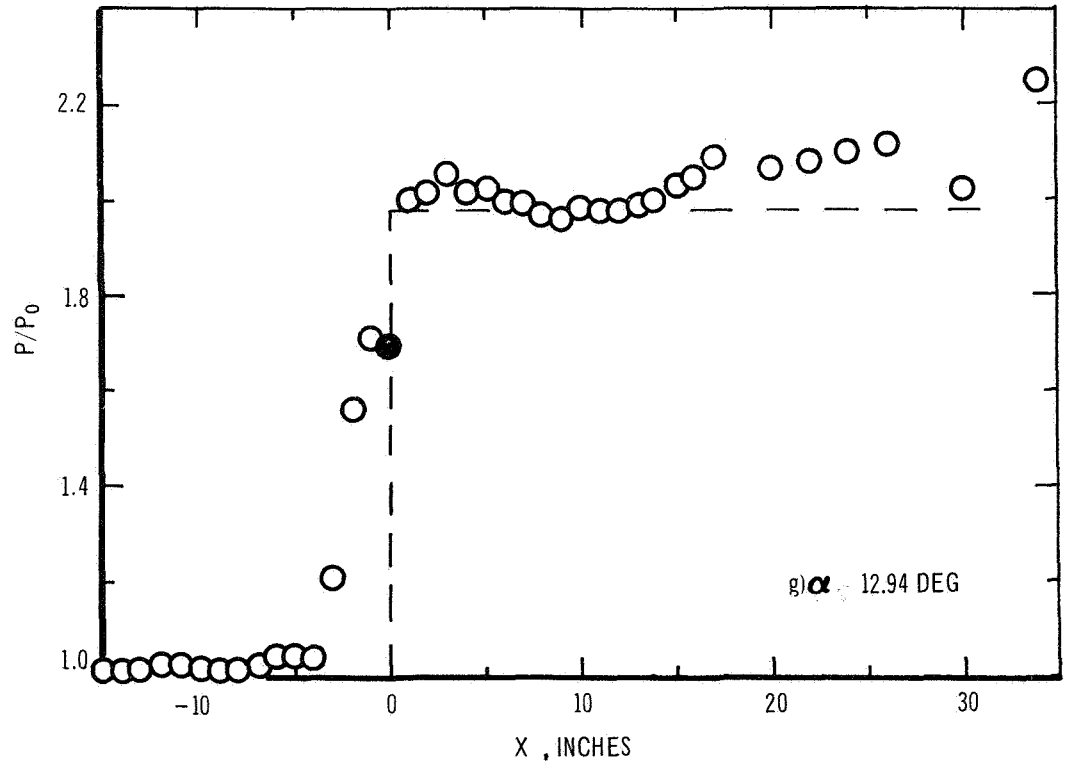

Figure 6. Concluded

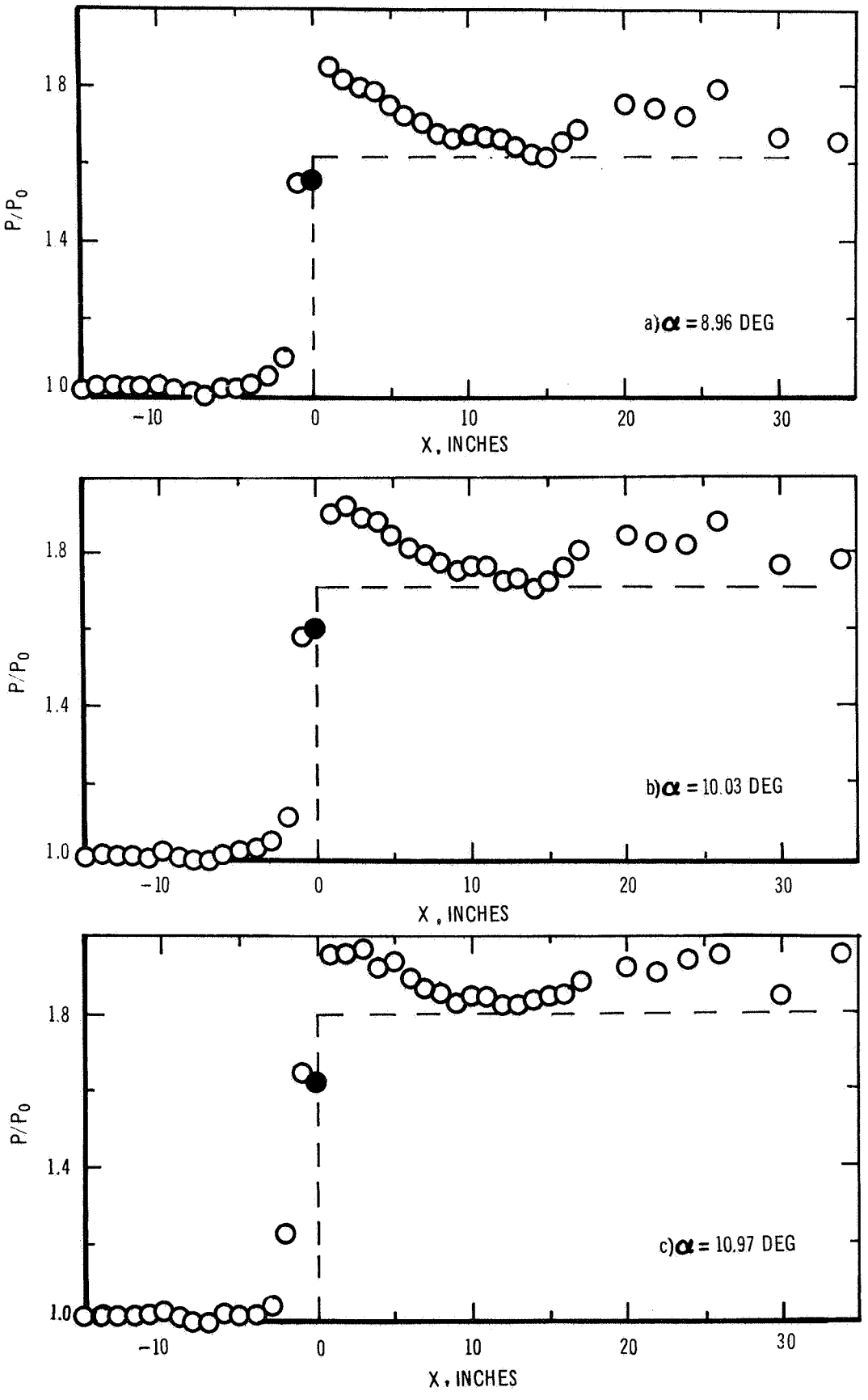

Figure 7. Pressure Distributions Along Model Centerline.
$M_0 = 1.95$, $R_0 = 1.022 \times 10^6$/In., $\delta_0 = 3.08$ In.

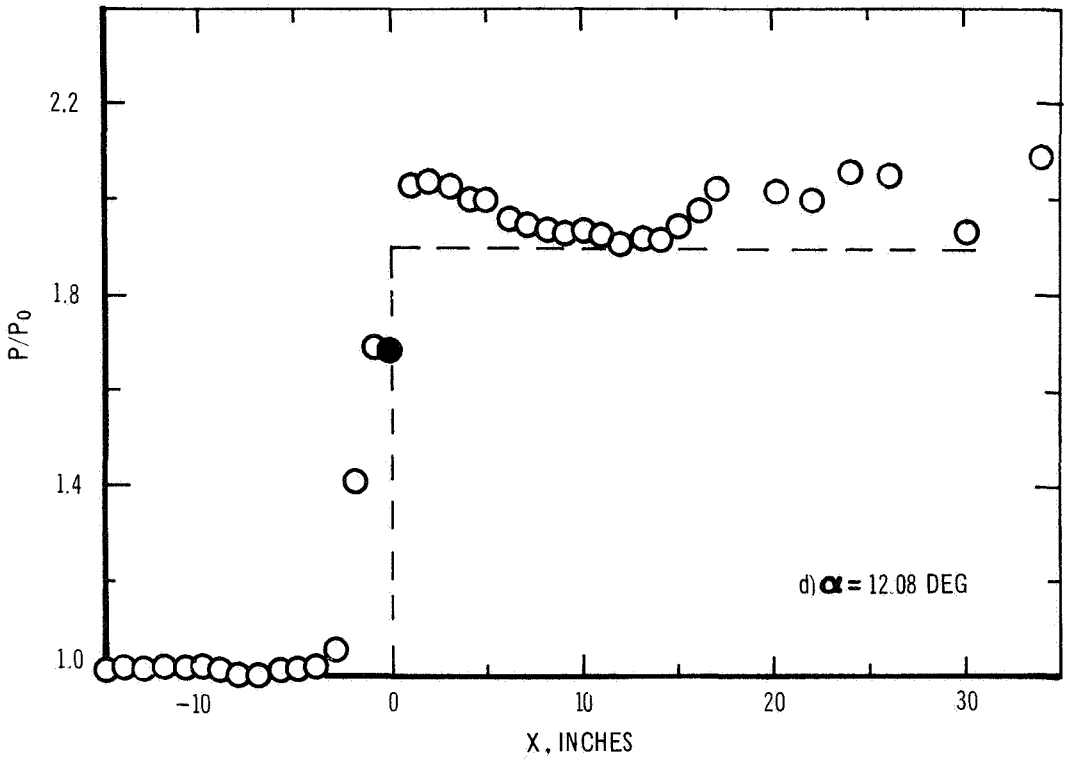

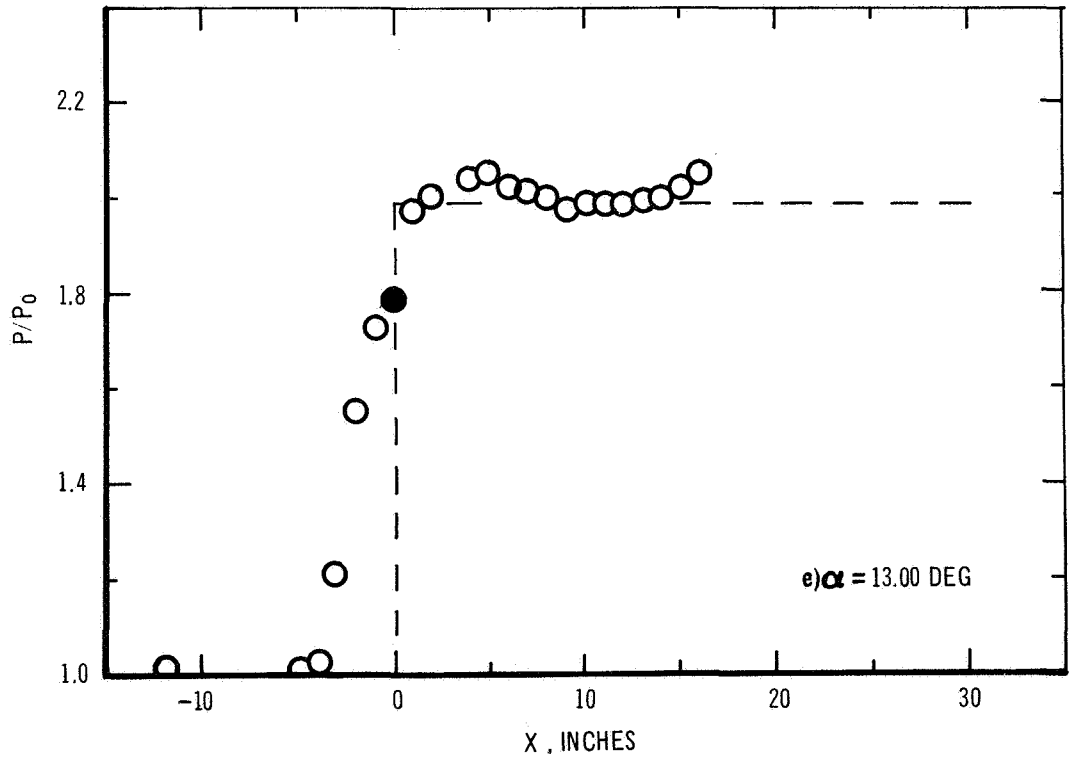

Figure 7. Concluded

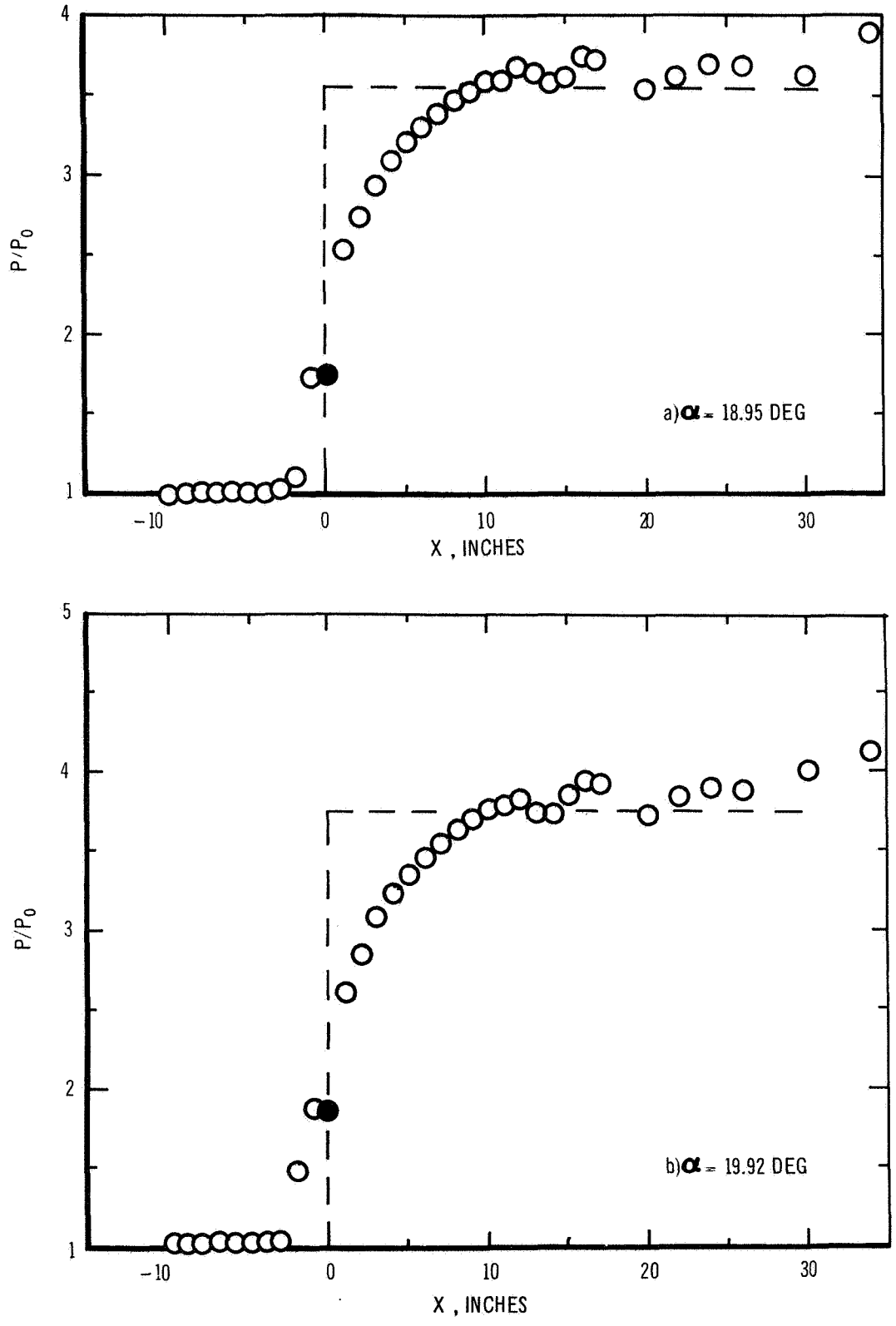

Figure 8. Pressure Distributions Along Model Centerline.
$M_0 = 2.95$, $R_0 = 0.411 \times 10^6$/in., $\delta_0 = 4.56$ in.

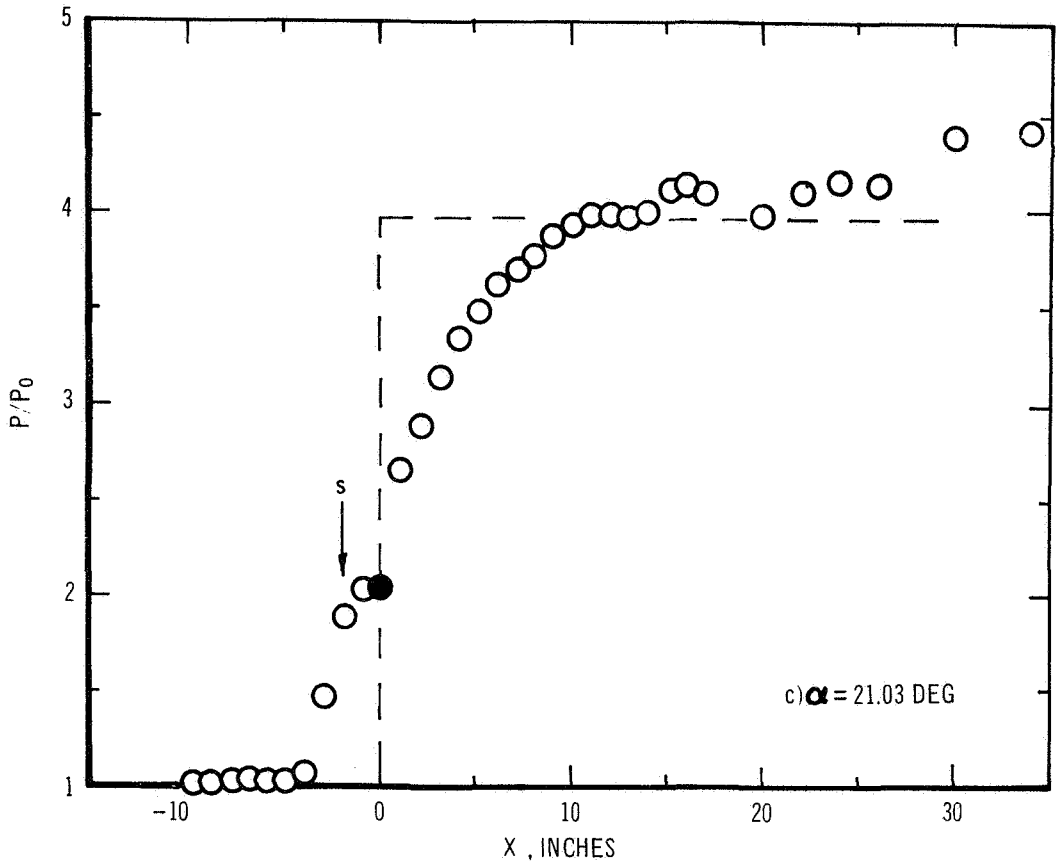

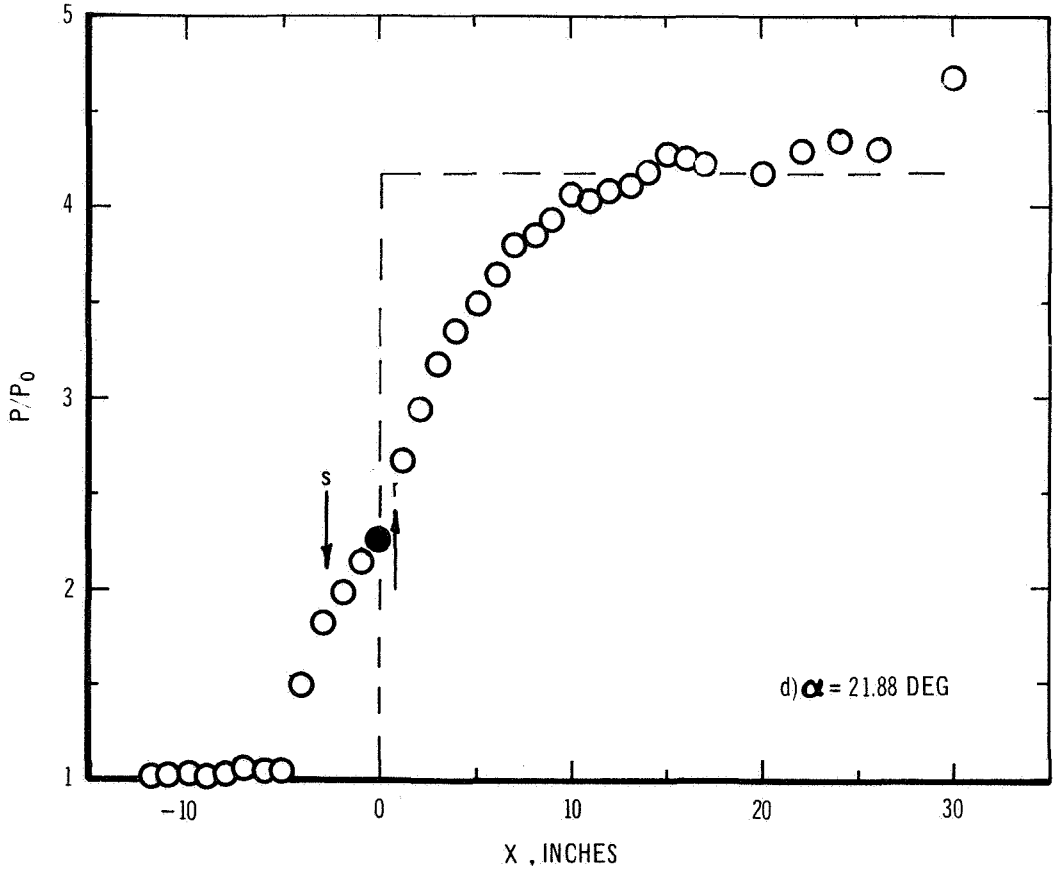

Figure 8.. Concluded

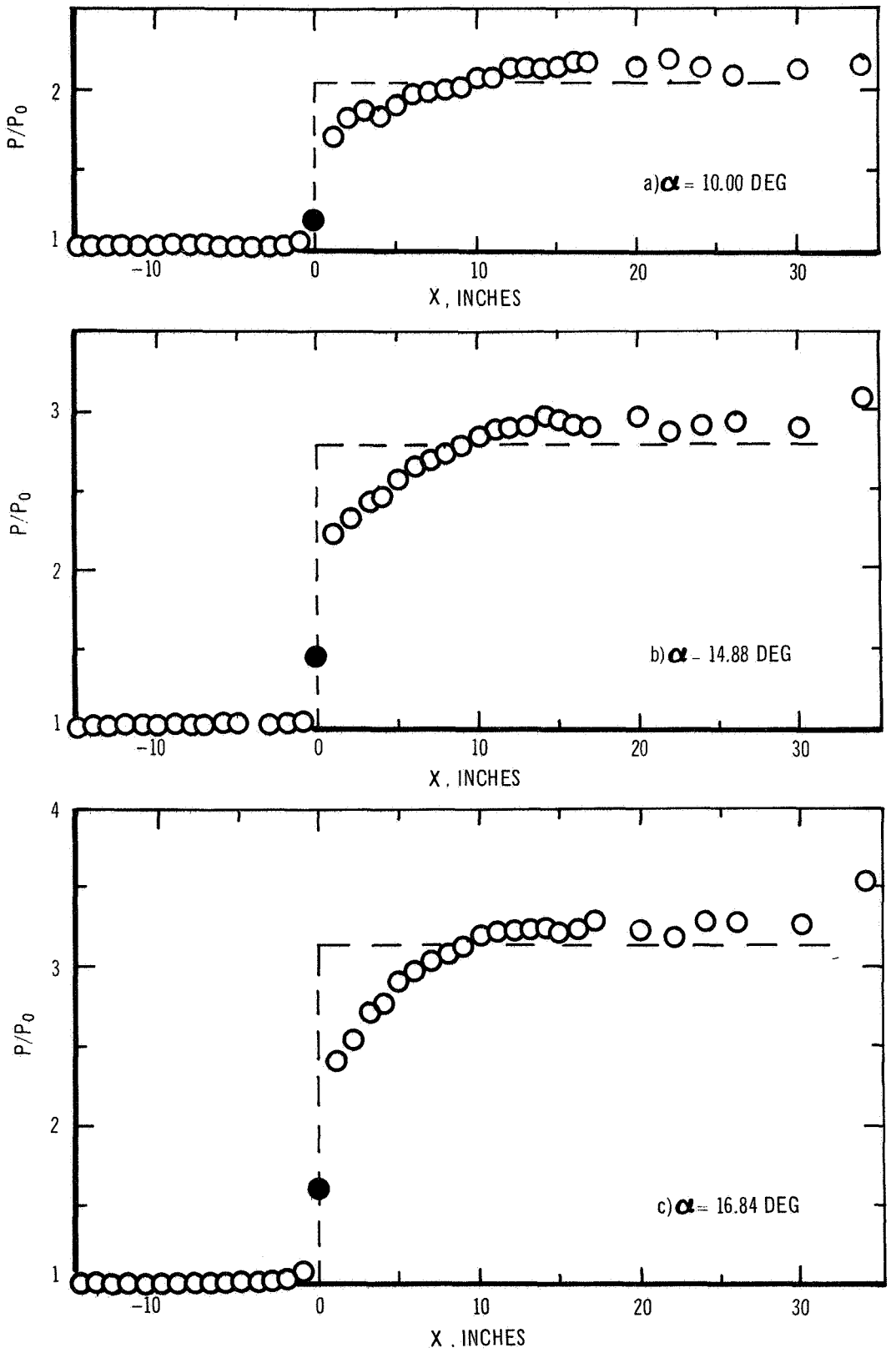

Figure 9. Pressure Distributions Along Model Centerline.
$M_0 = 2.95$, $R_0 = 0.752 \times 10^6$/in., $\delta_0 = 4.21$ in.

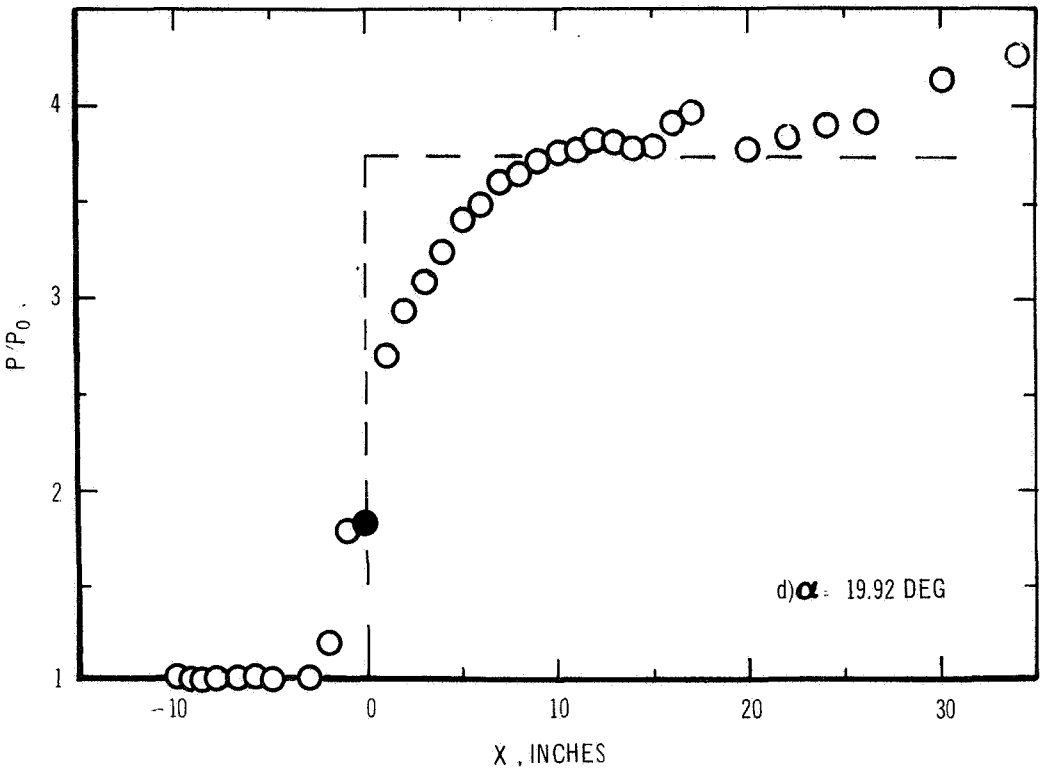

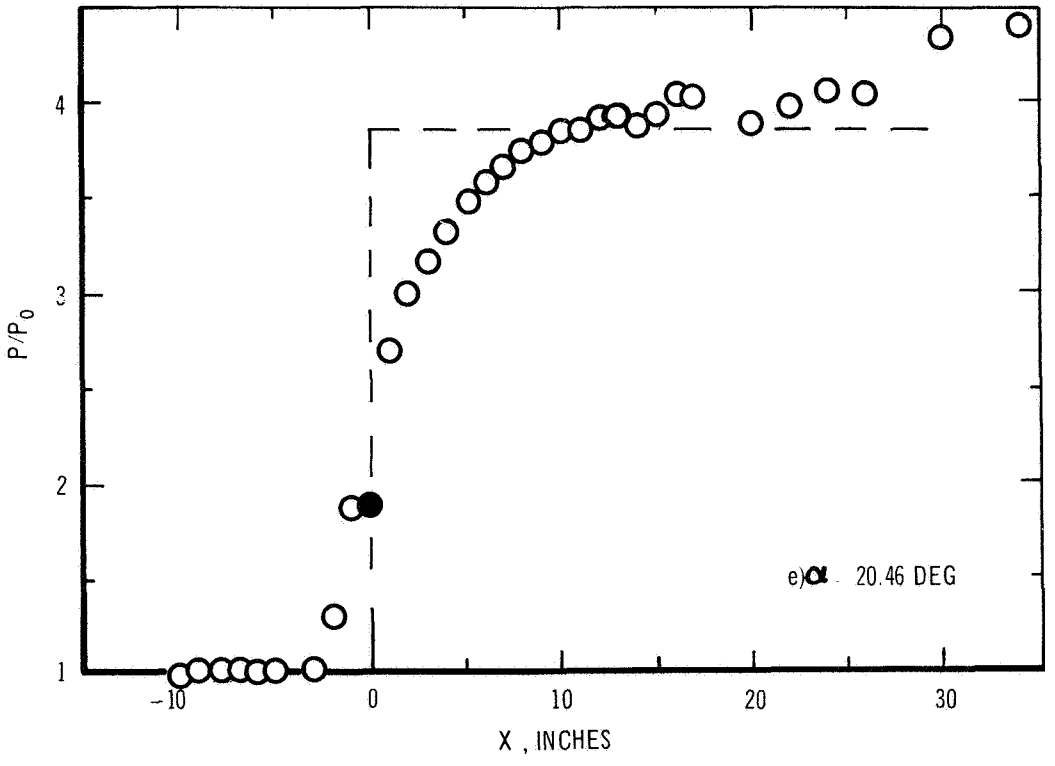

Figure 9. Continued

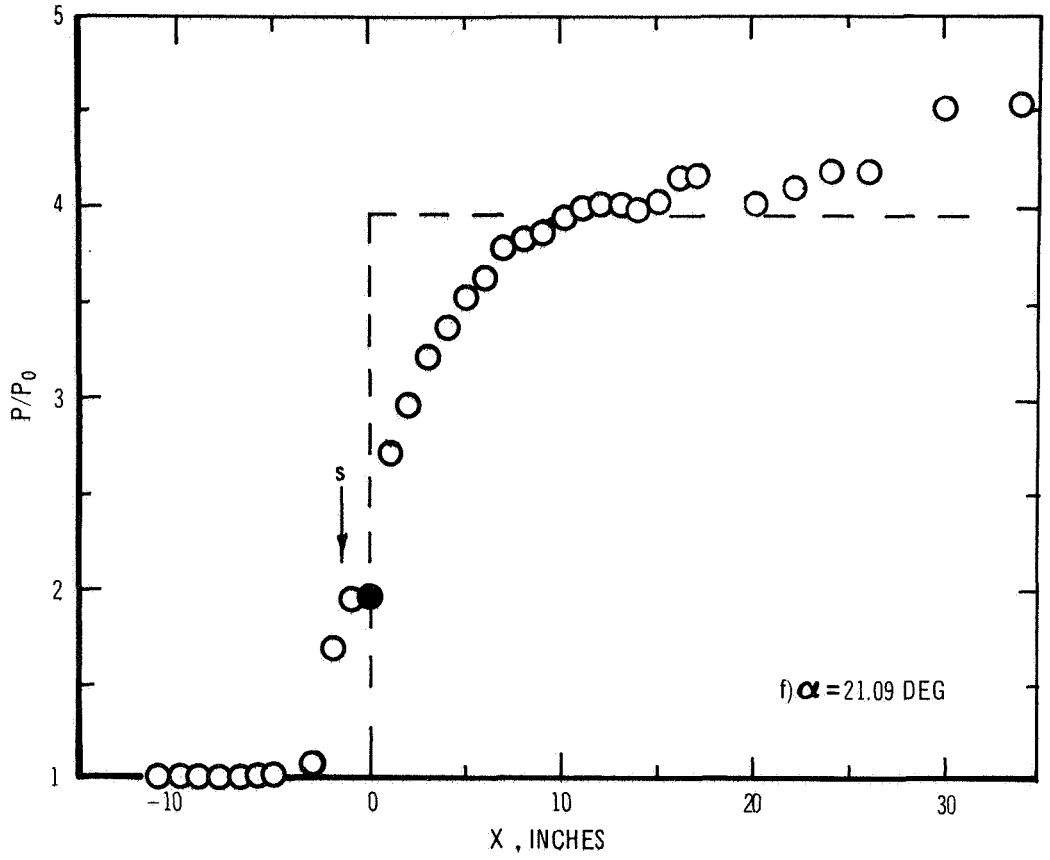

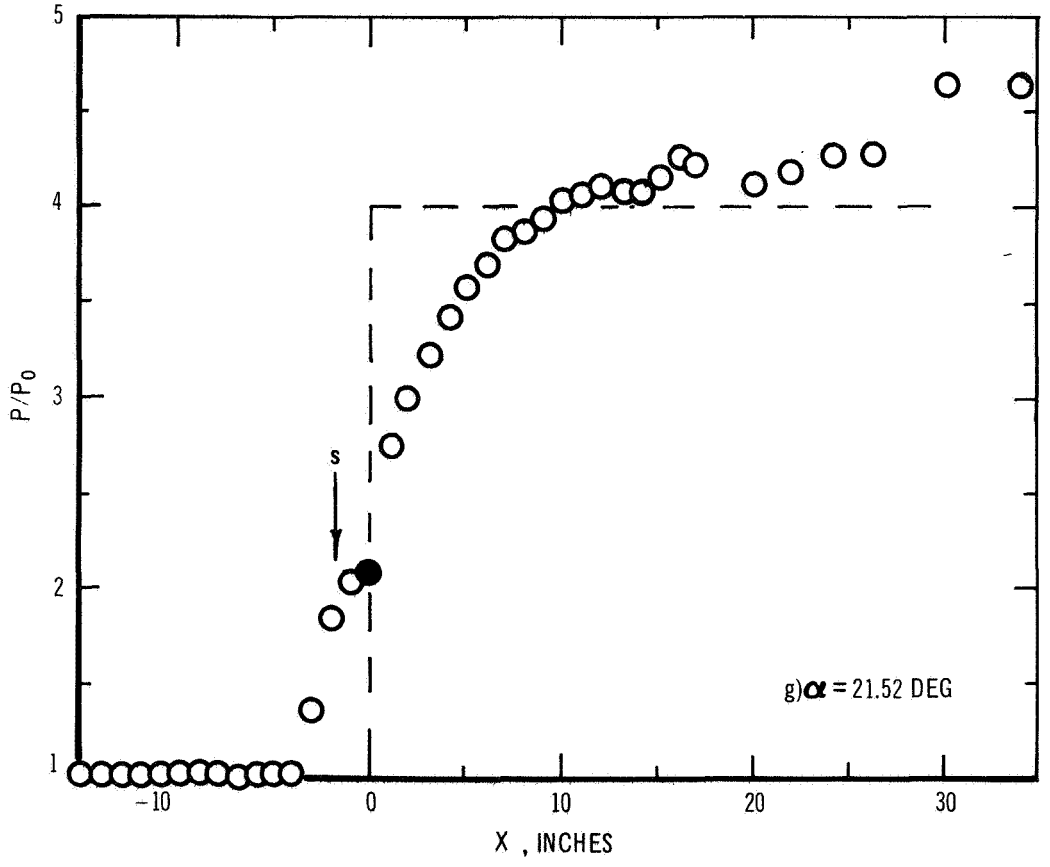

Figure 9. Continued

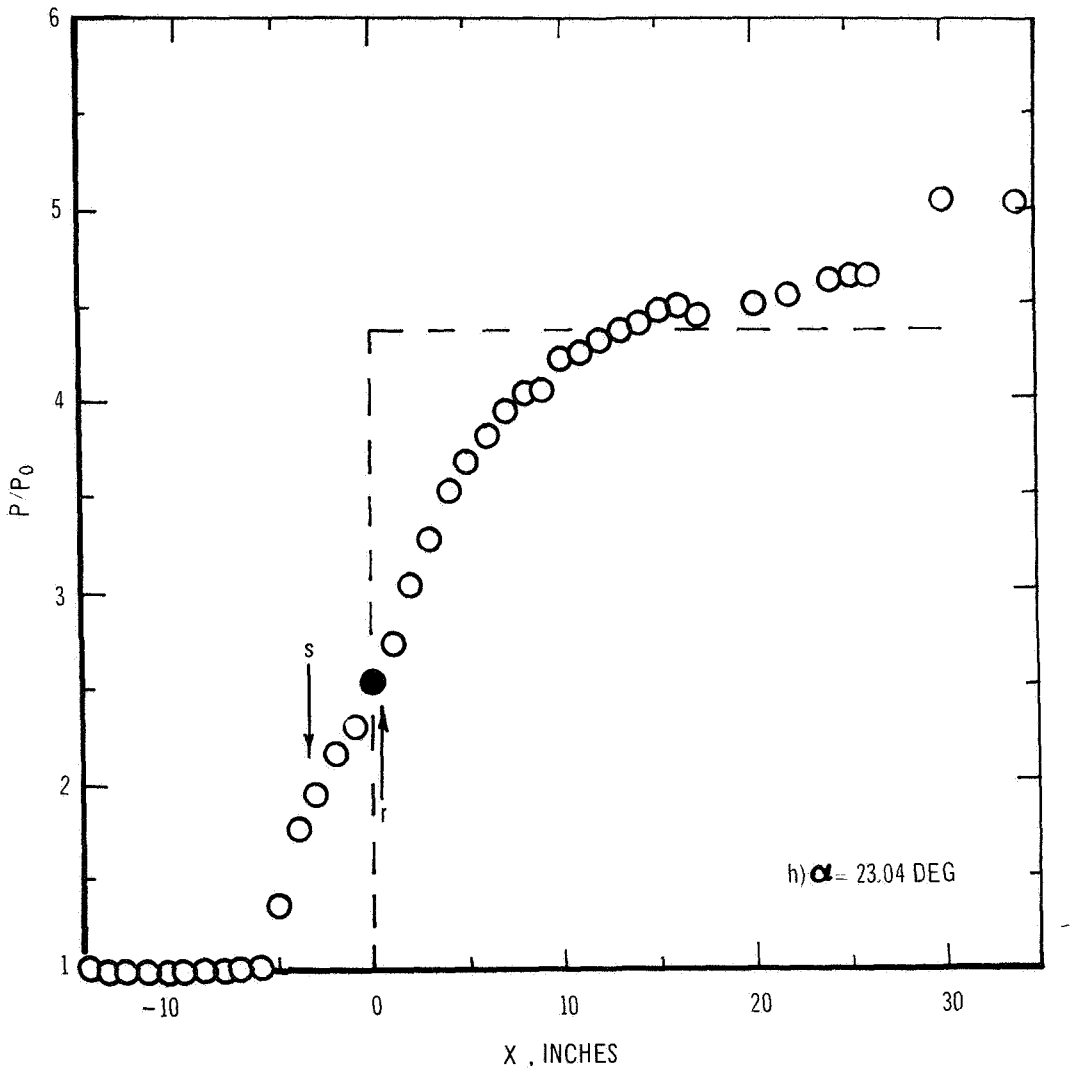

Figure 9. Continued

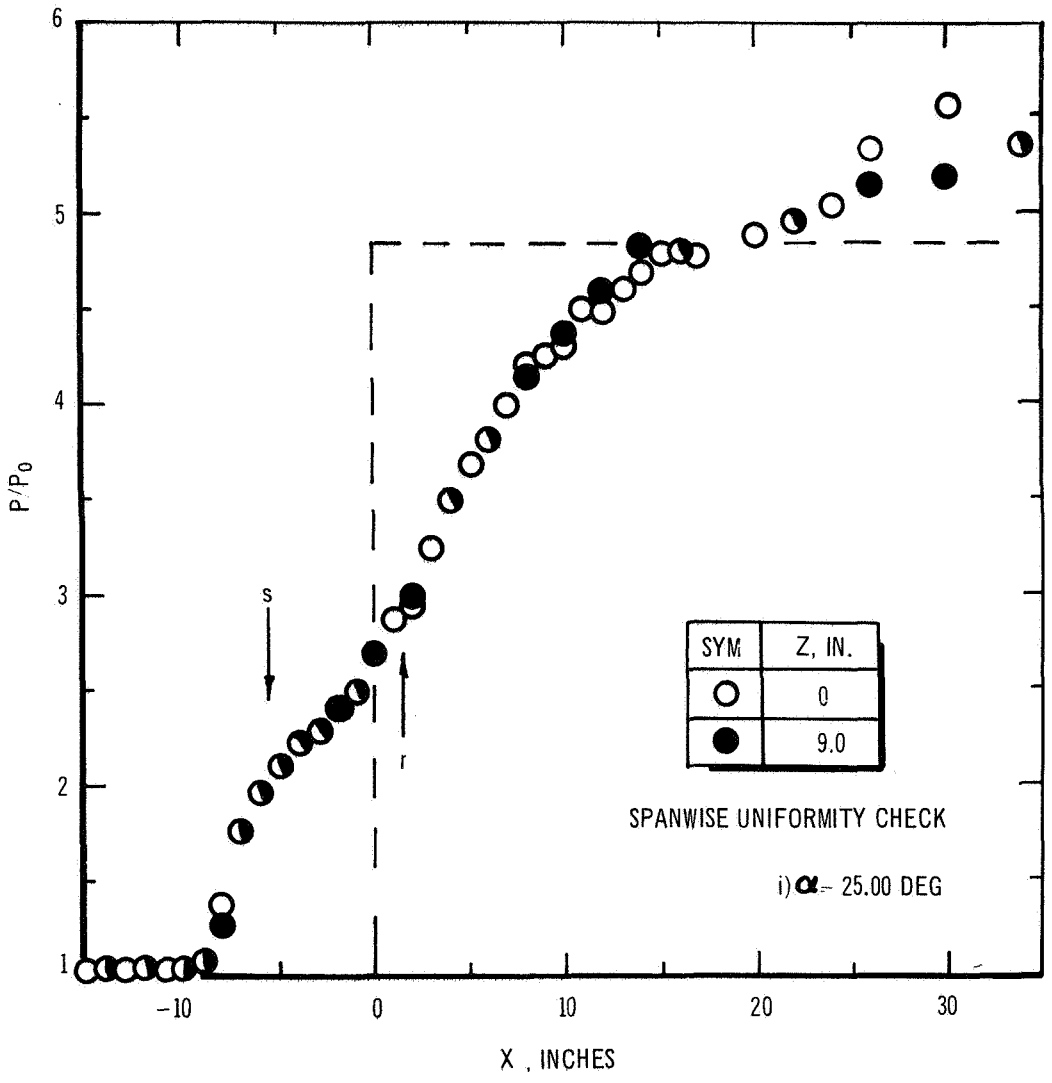

Figure 9. Concluded

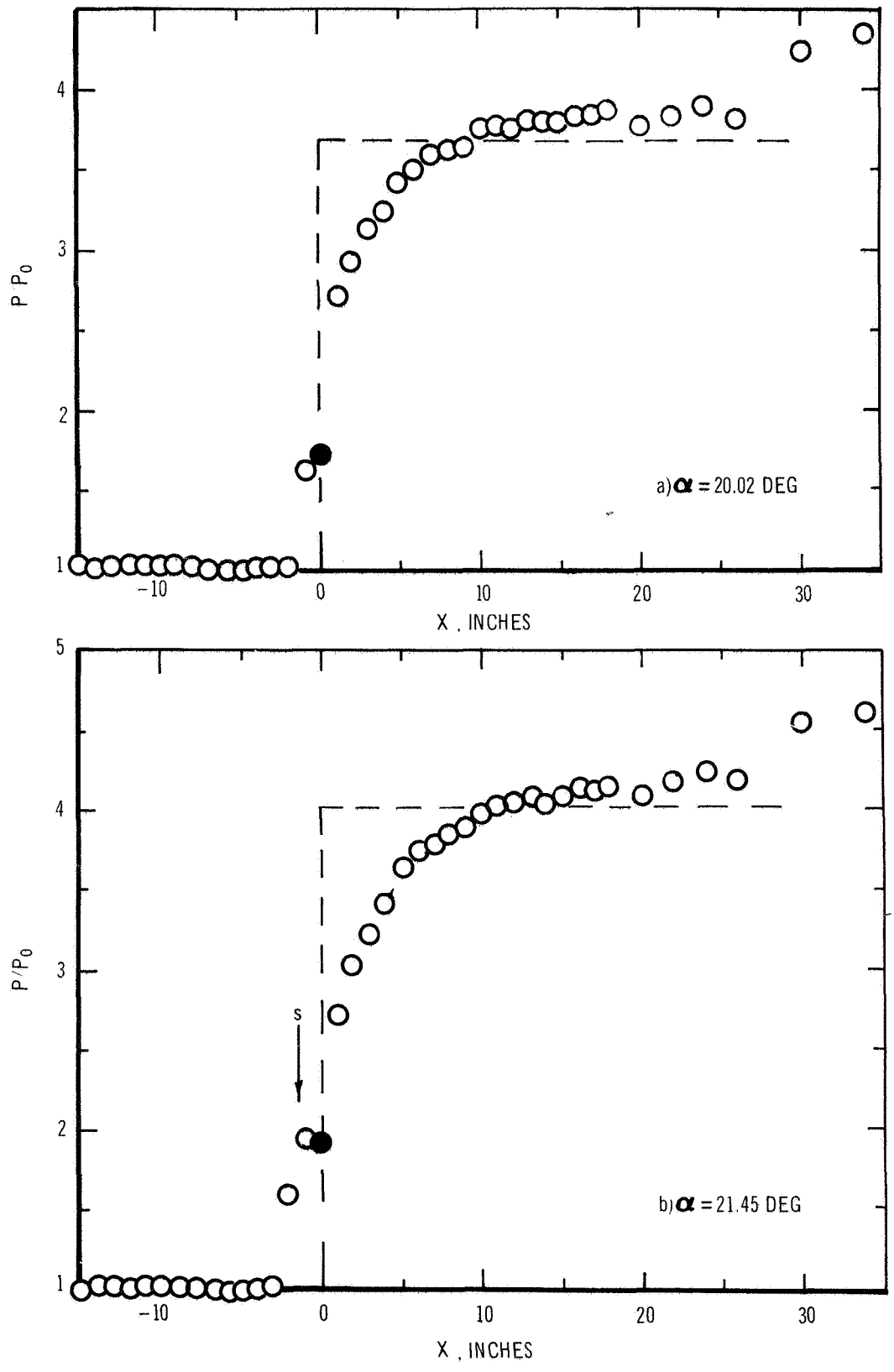

Figure 10. Pressure Distributions Along Model Centerline.
$M_0 = 2.95$, $R_0 = 1.509 \times 10^6$/In. $\delta_0 = 3.07$ In.

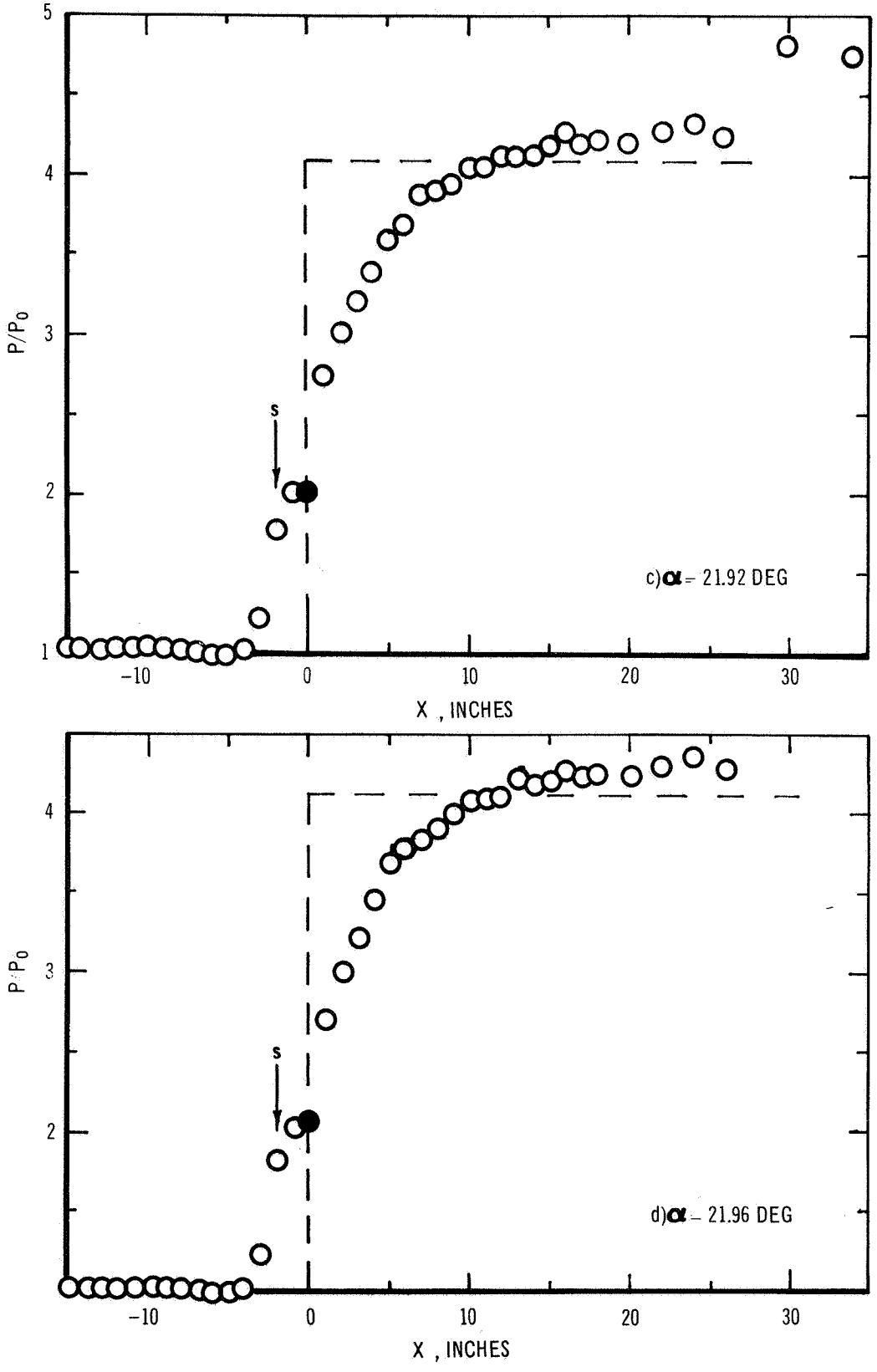

Figure 10. Continued

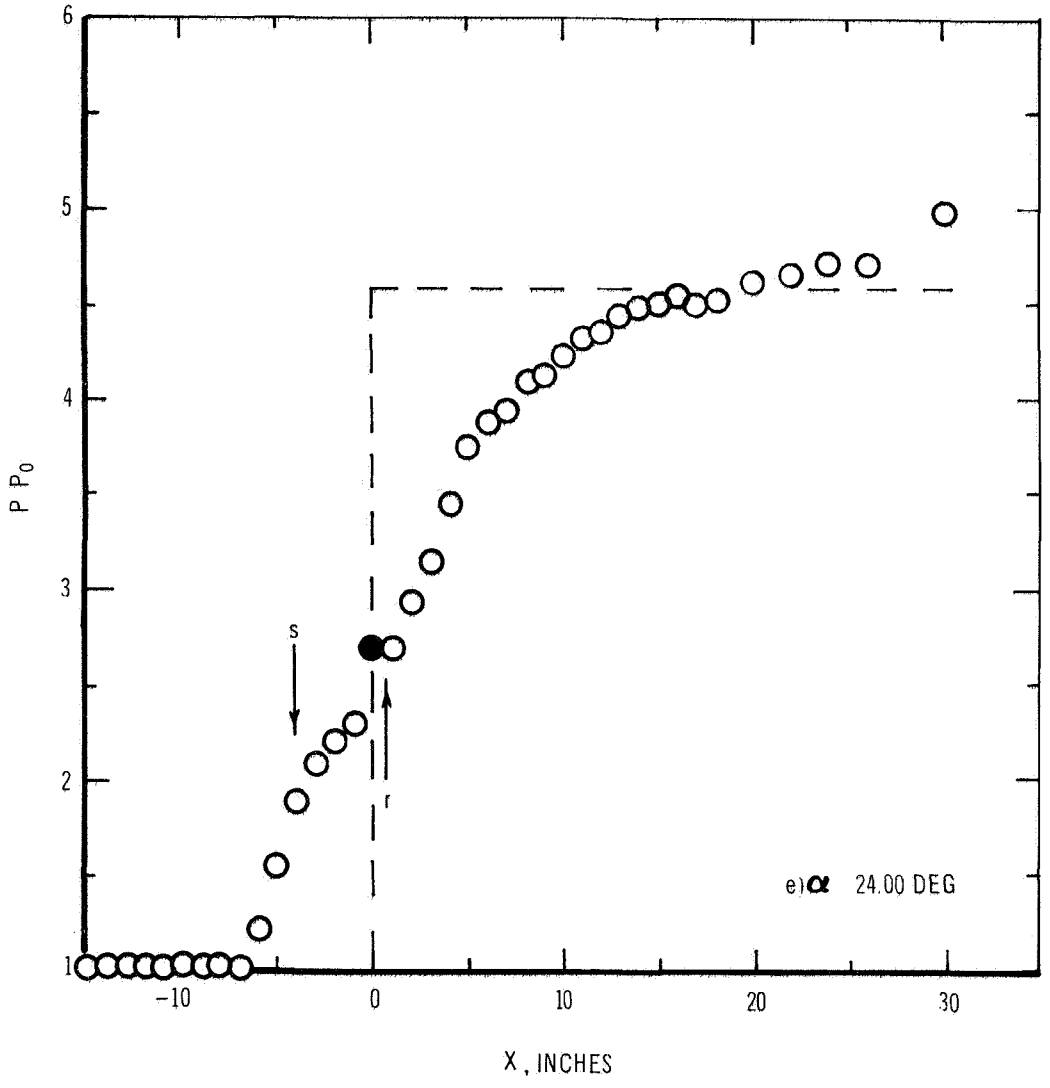

Figure 10. Concluded

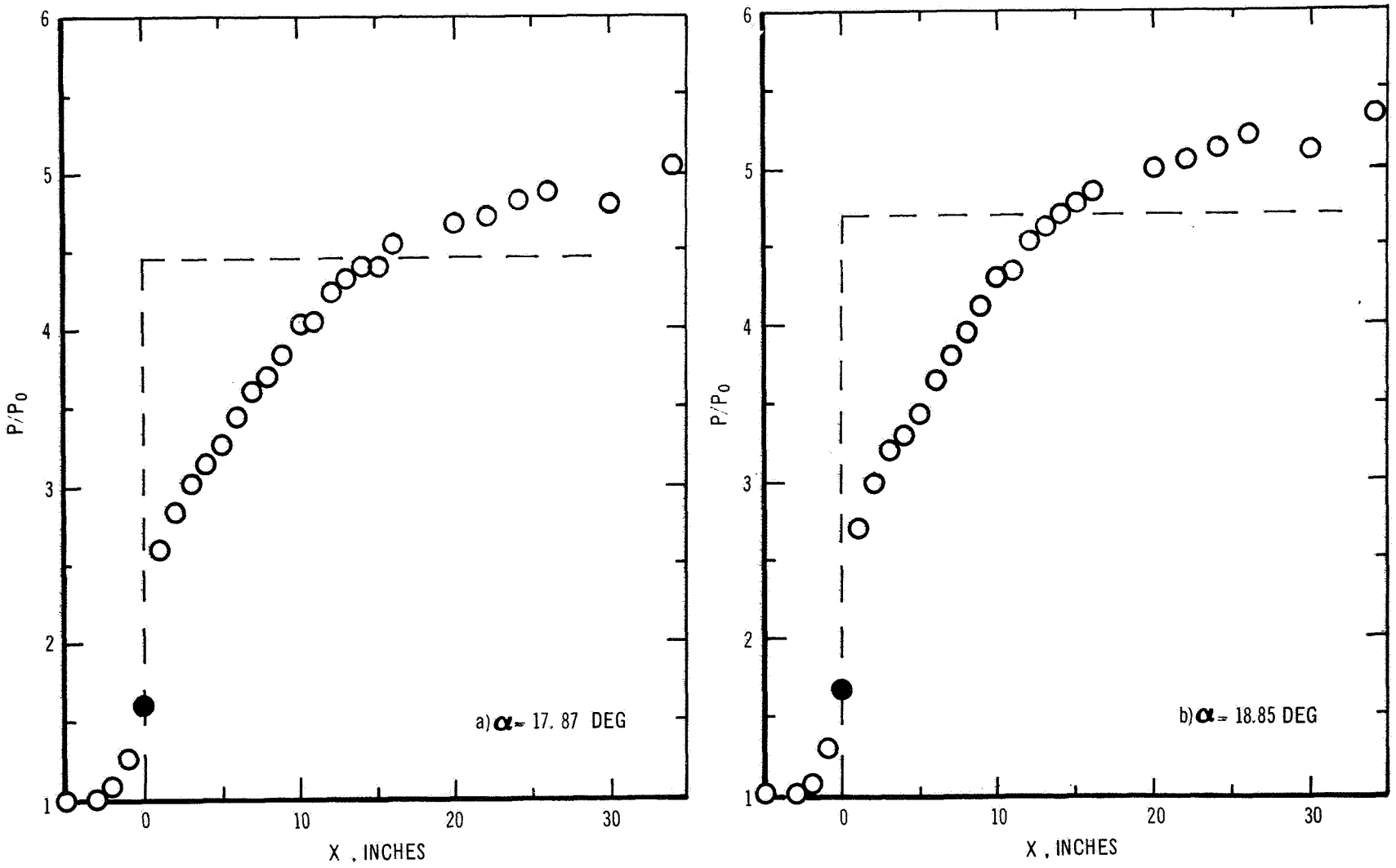

Figure 11. Pressure Distributions Along Model Centerline. $M_0 = 3.93$, $R_0 = 0.443 \times 10^6$/in., $\delta_0 = 5.36$ in.

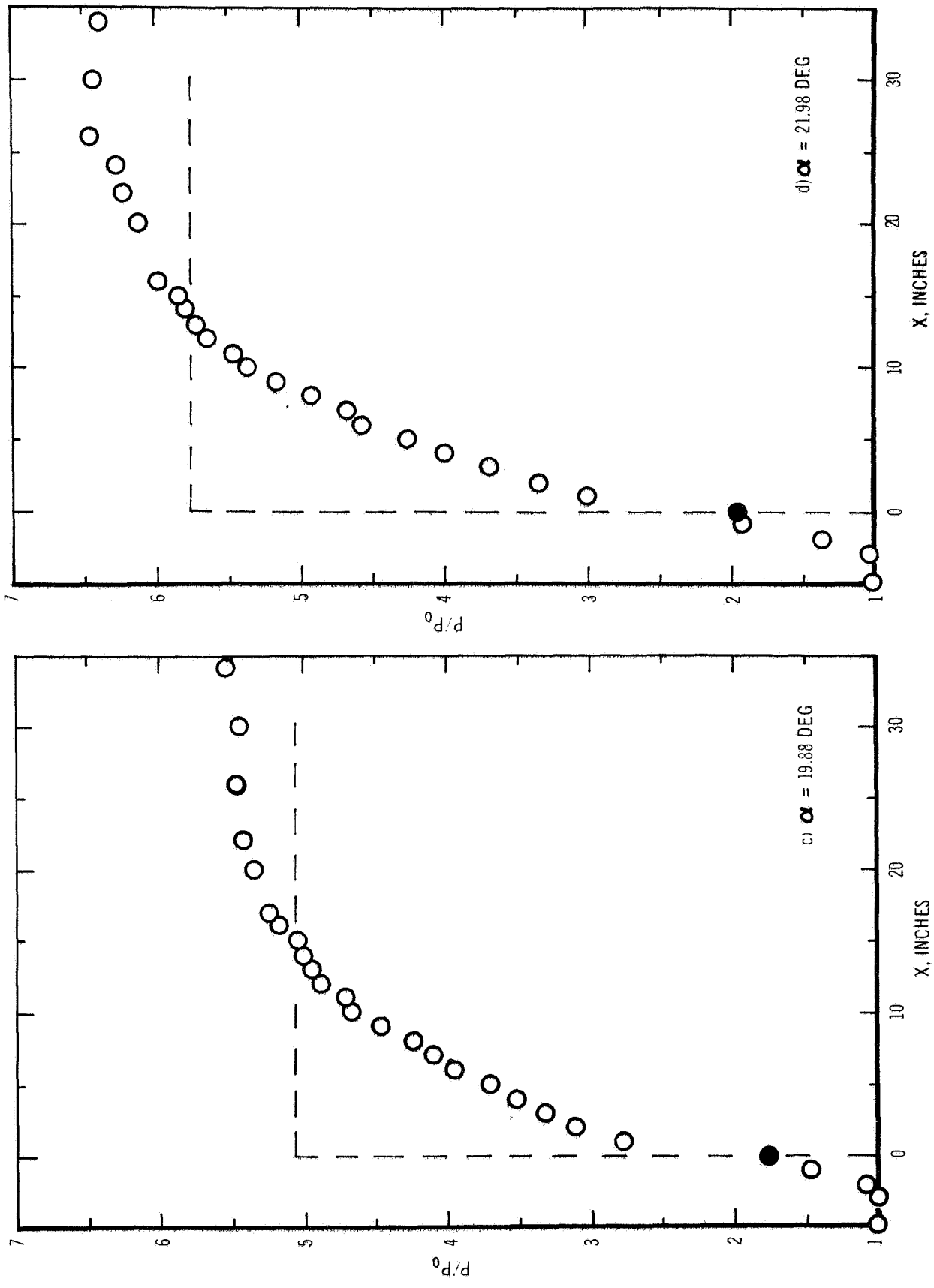

Figure 11. Continued

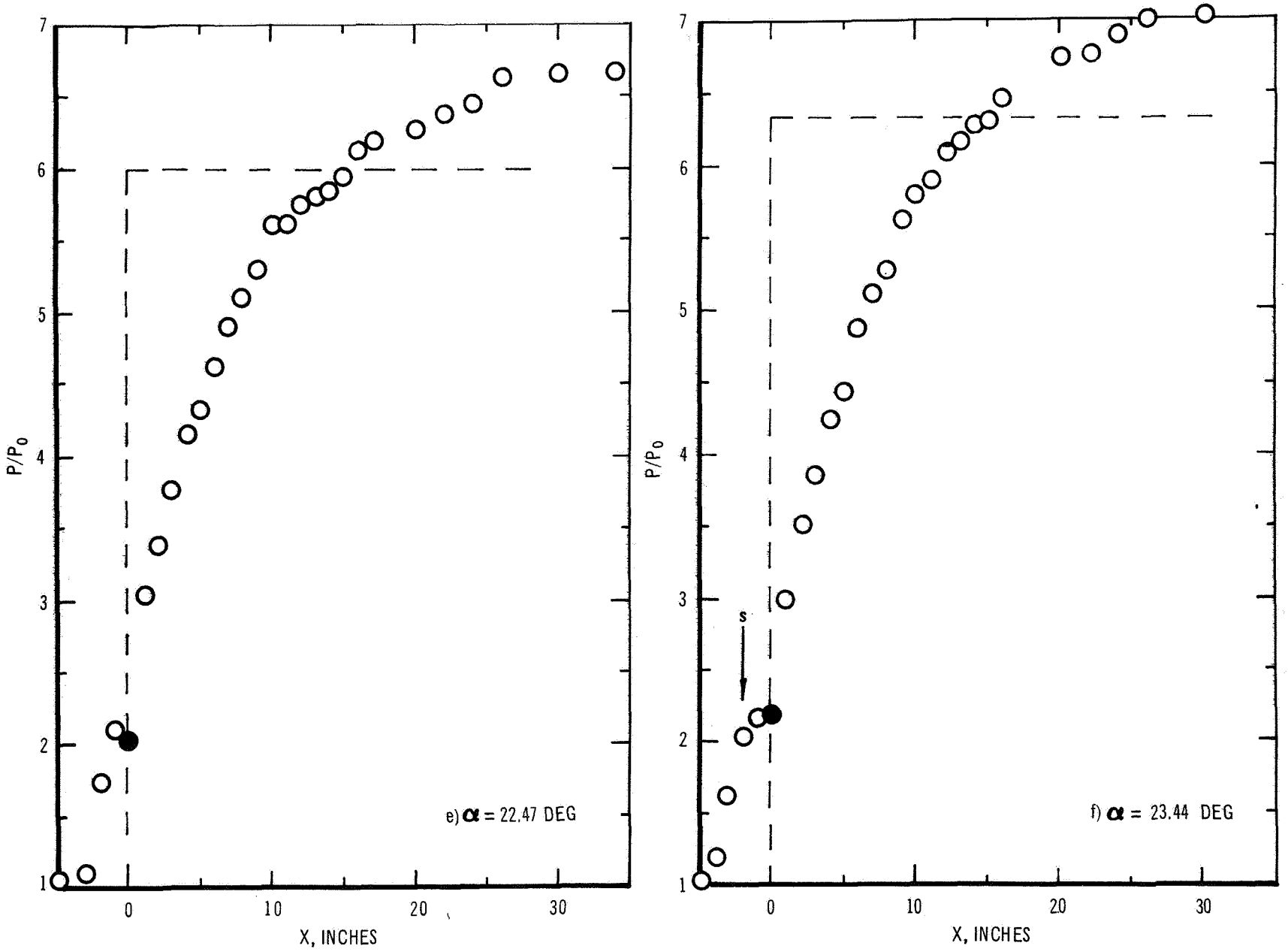

Figure 11. Continued

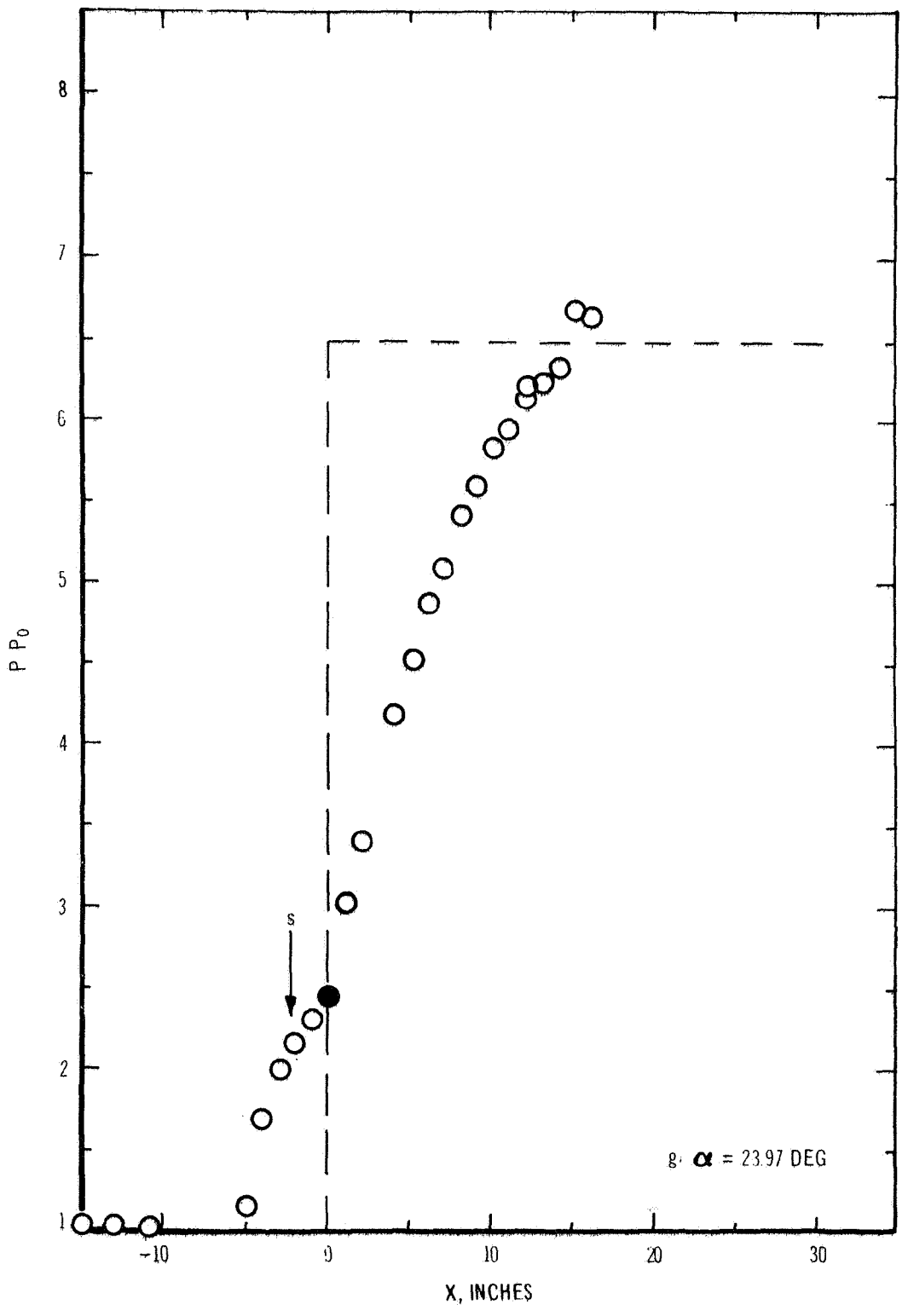

Figure 11. Continued

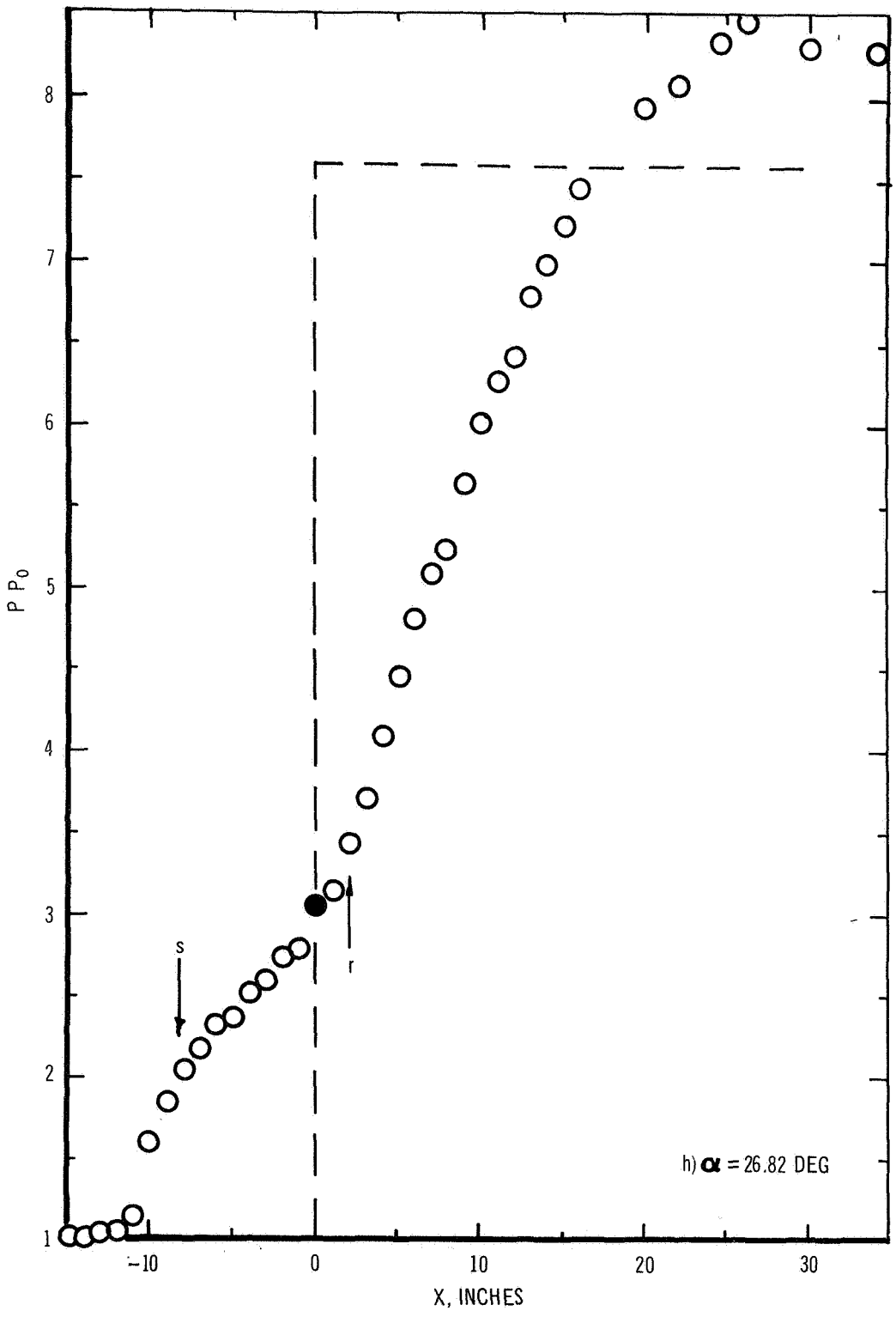

Figure 11. Concluded

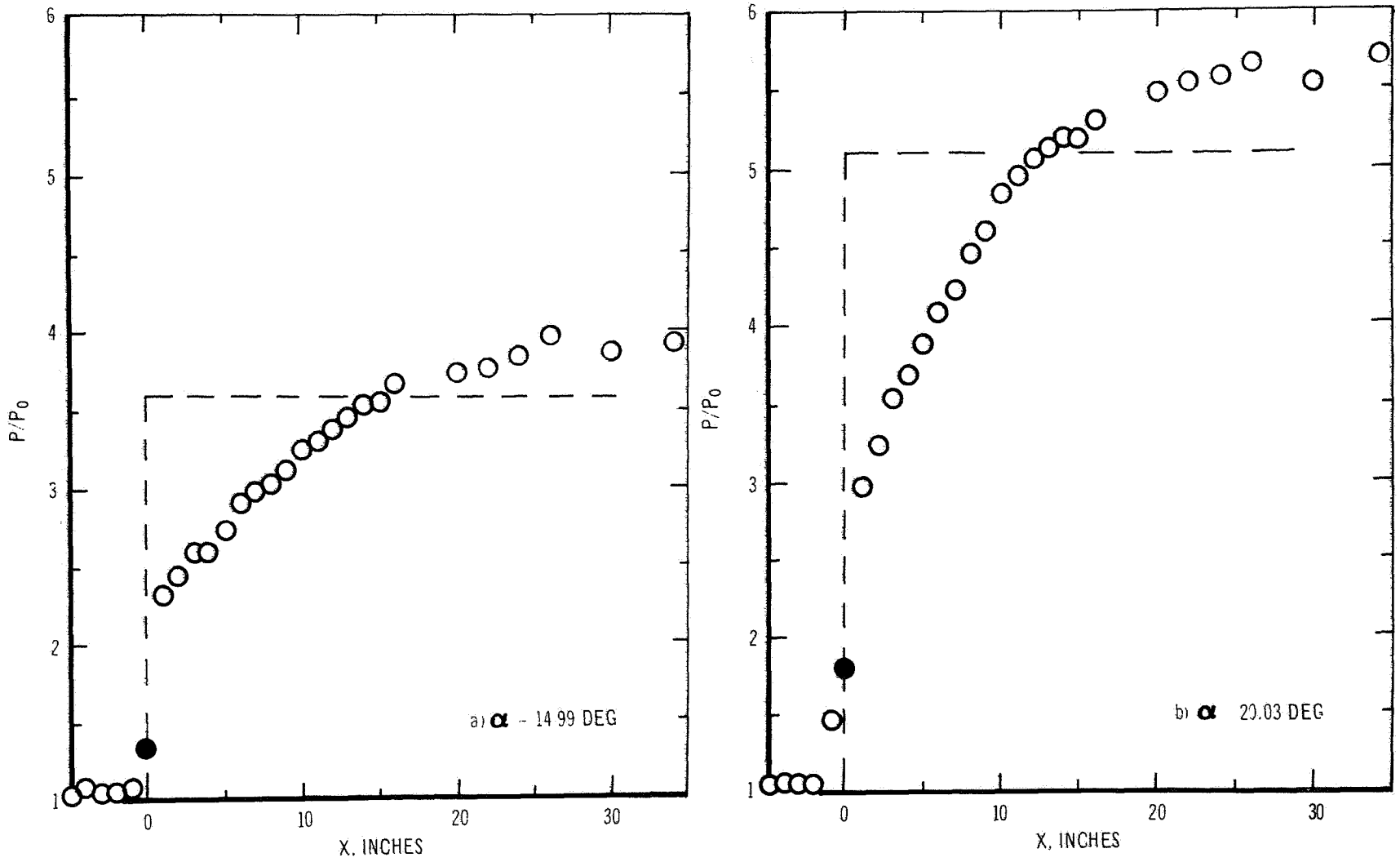

Figure 12. Pressure Distributions Along Model Centerline. M_0 = 3.93, R_0 = 0.734 x 10^6 in δ_0 = 5.04 in

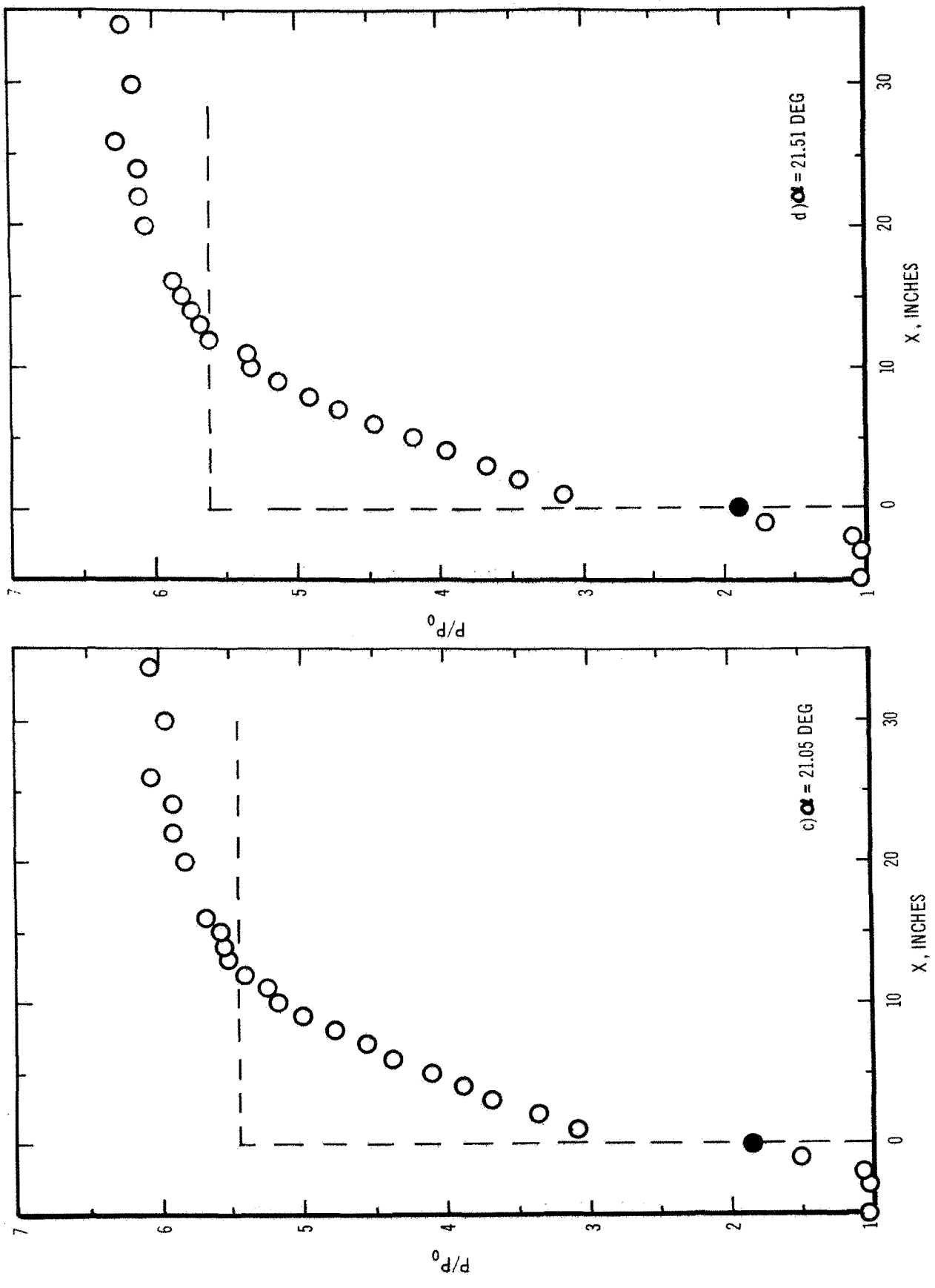

Figure 12. Continued

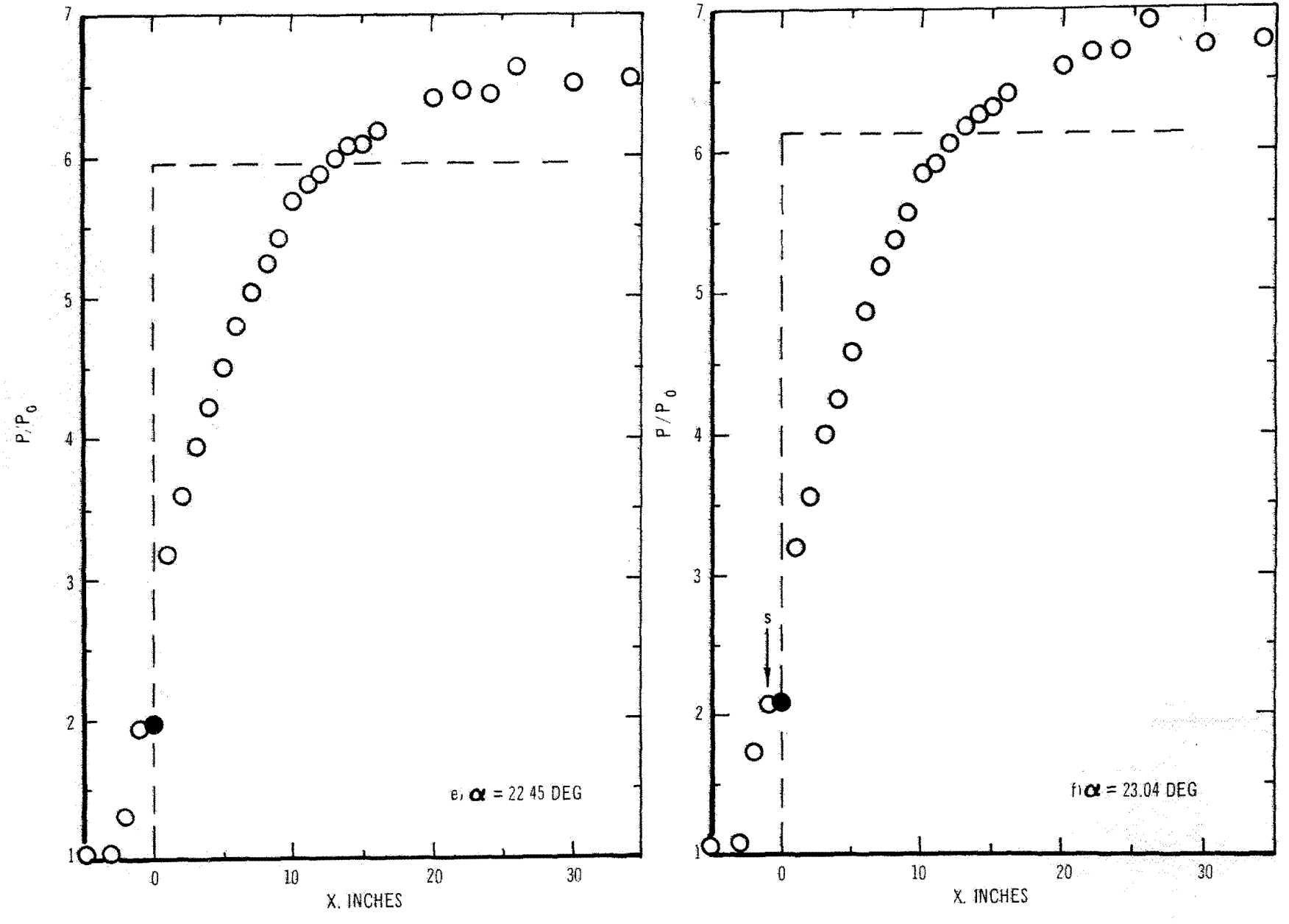

Figure 12. Continued

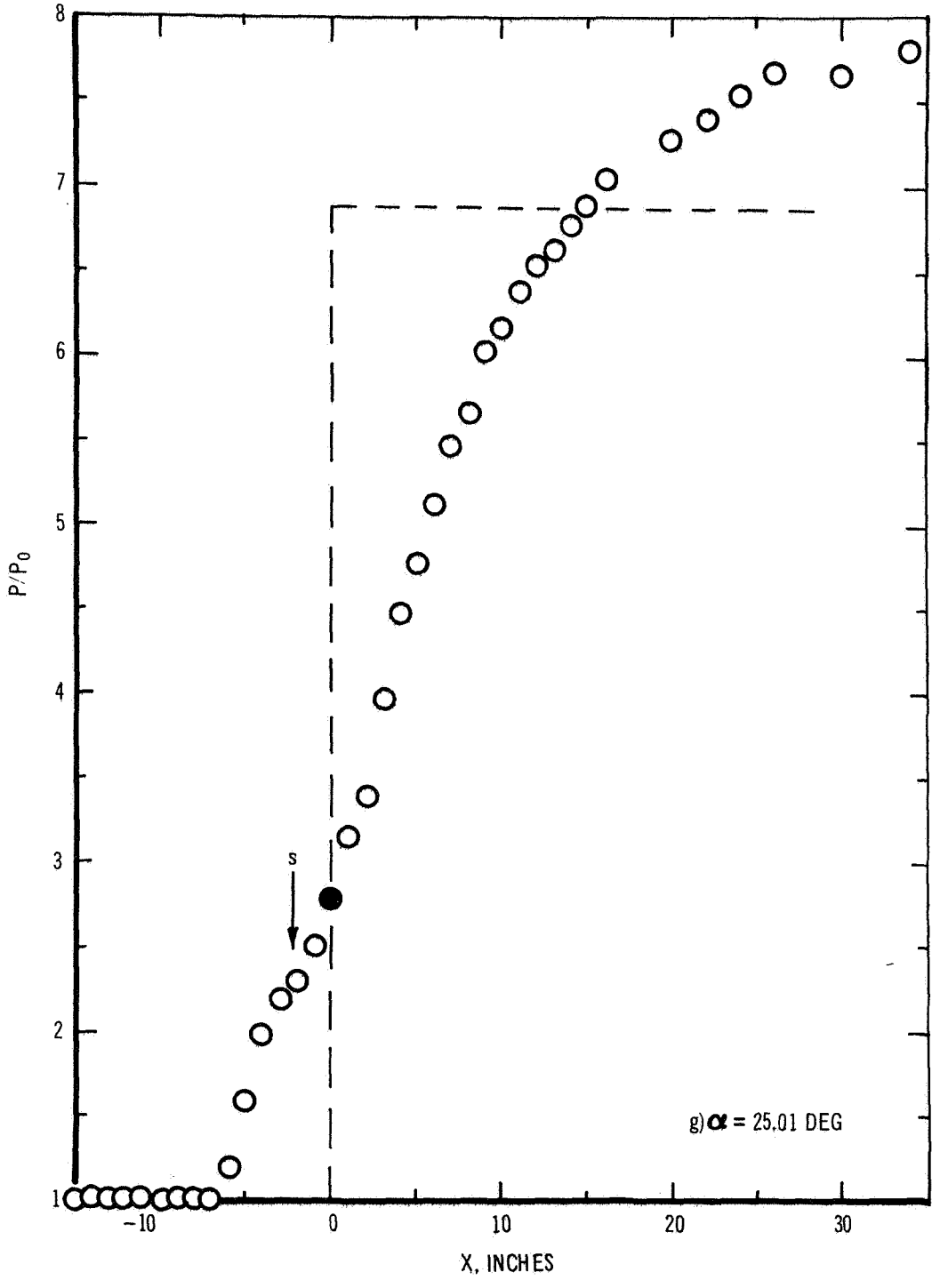

Figure 12. Concluded

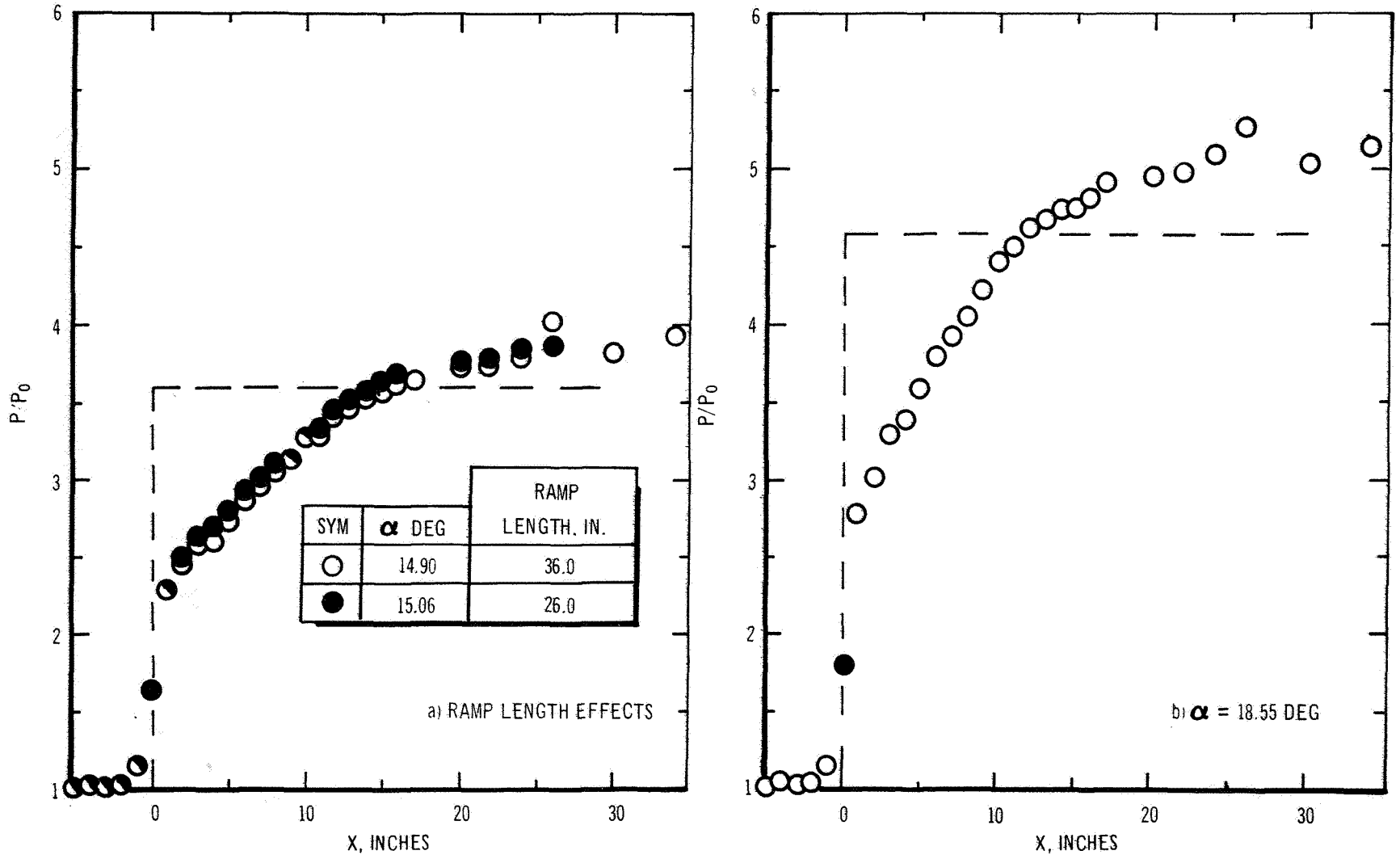

Figure 13. Pressure Distributions Along Model Centerline. $M_0 = 3.93$, $R_0 = 1.200 \times 10^6$/In., $\delta_0 = 4.75$ In.

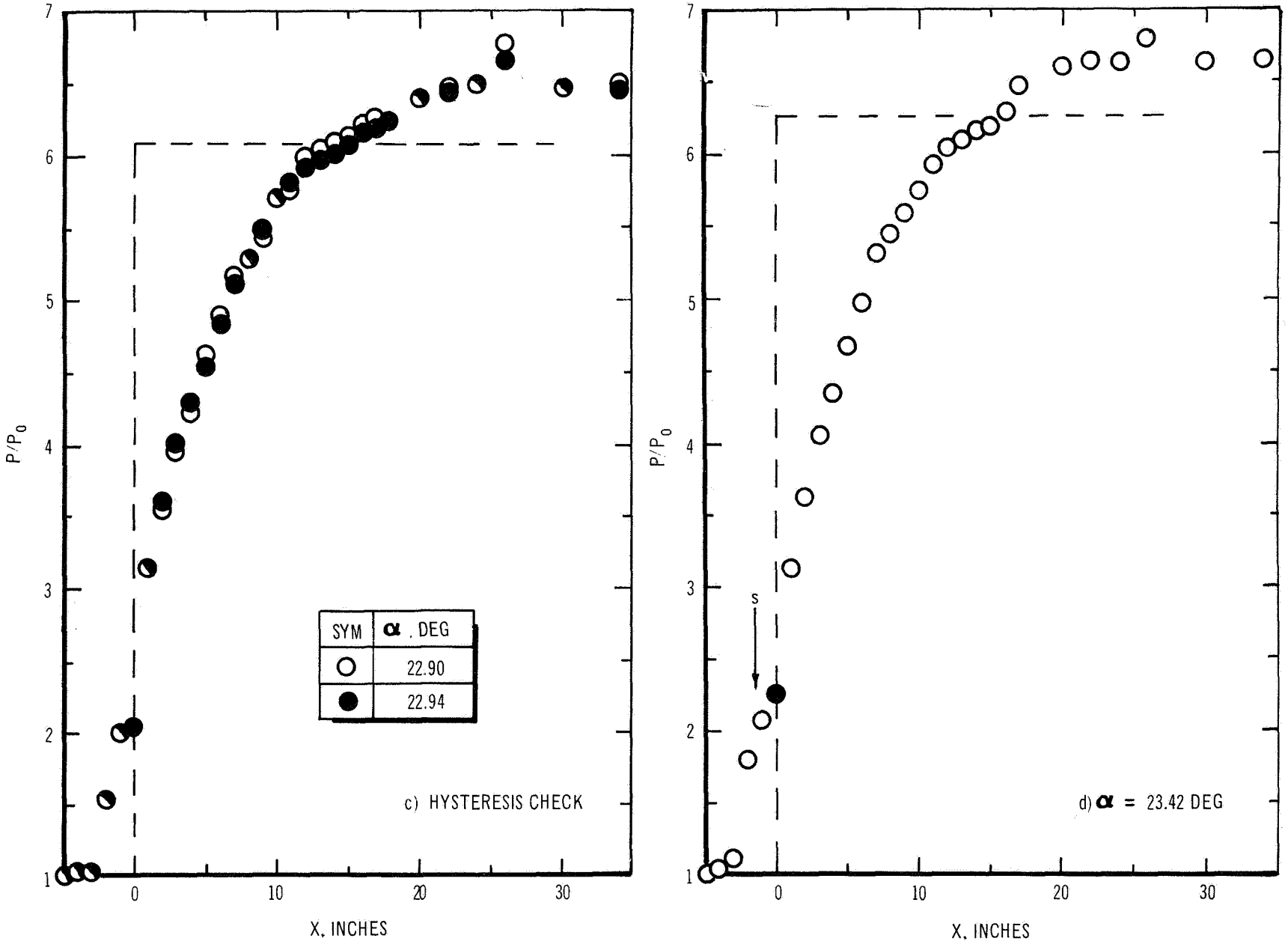

Figure 13. Continued

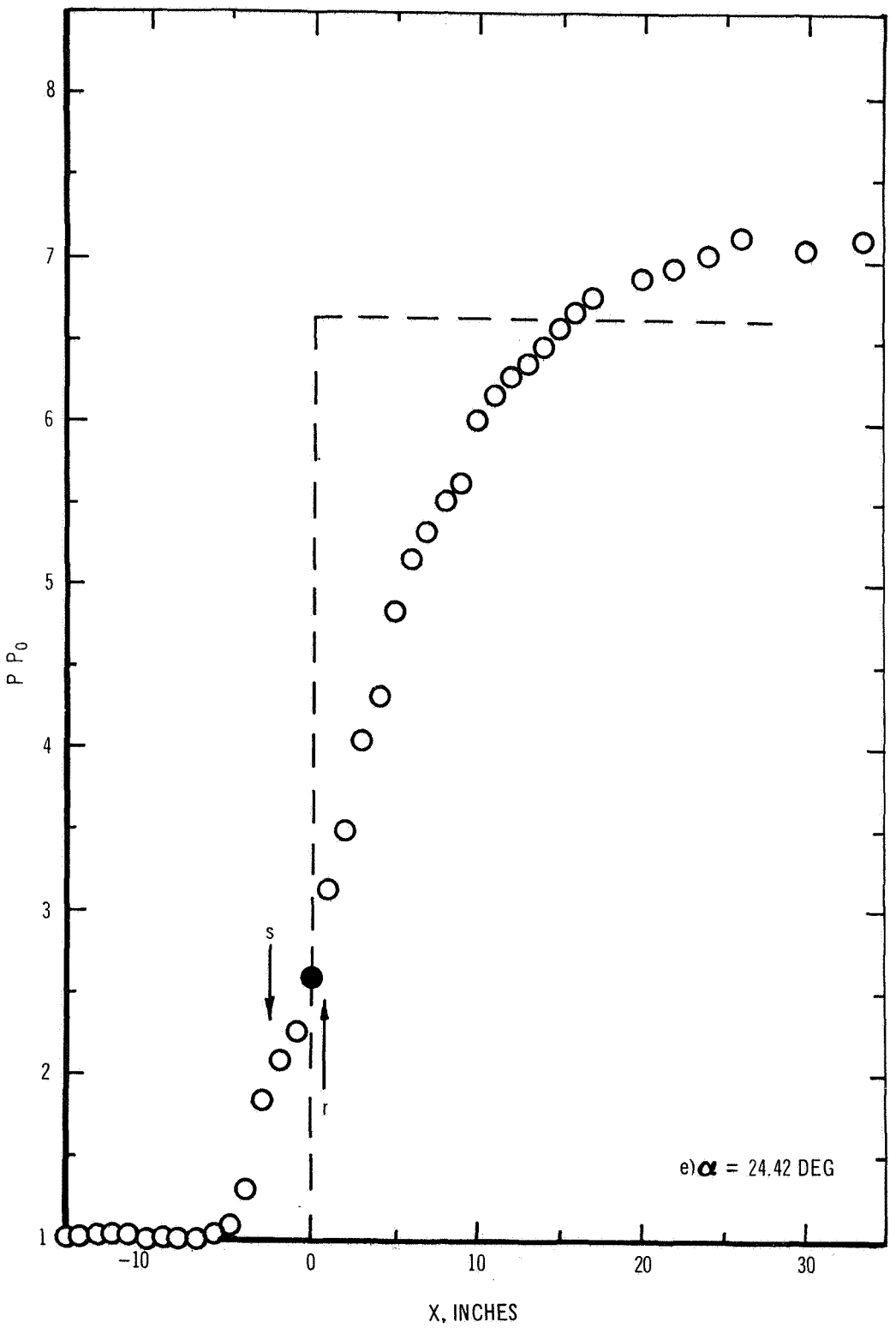

Figure 13. Continued

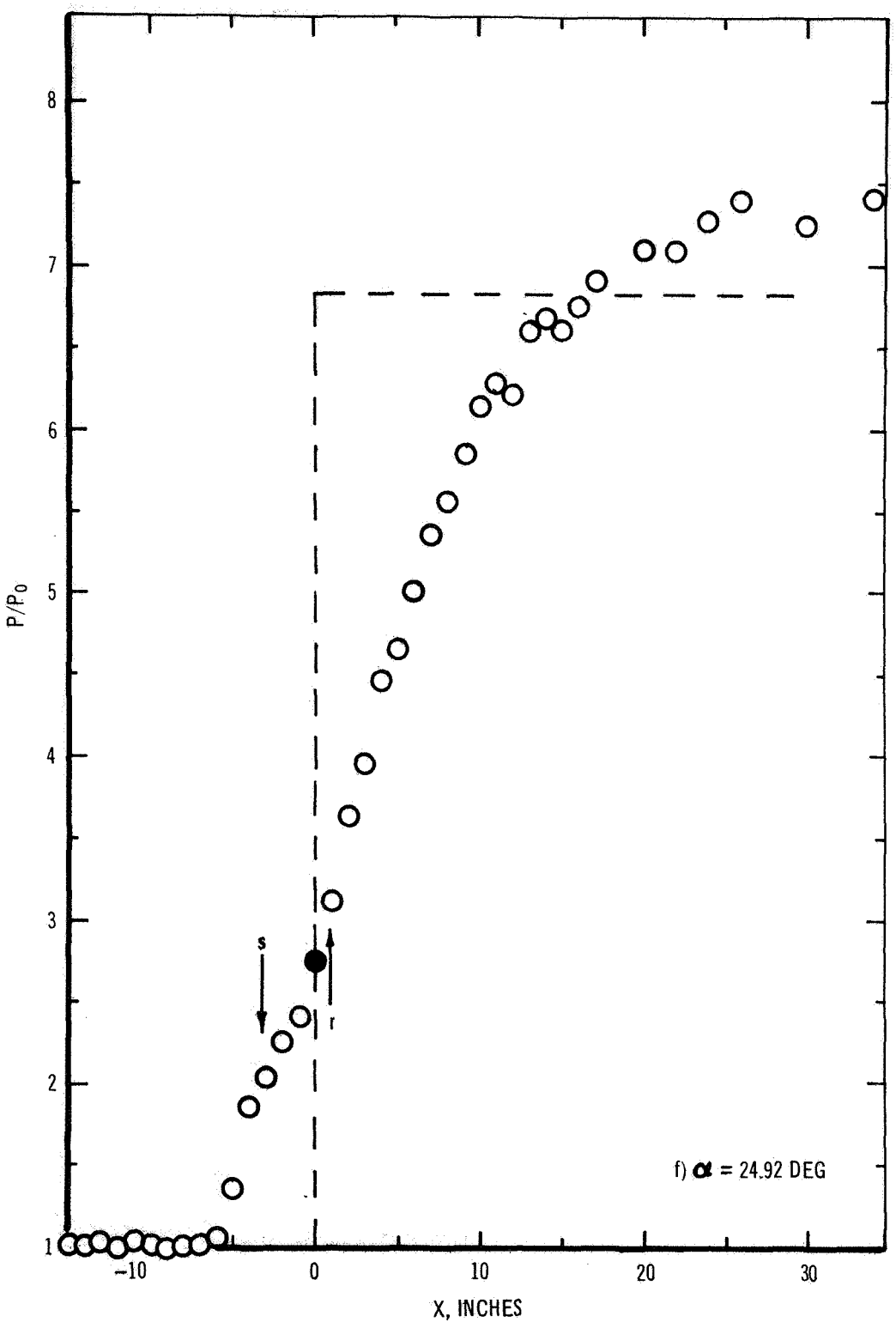

Figure 13. Continued

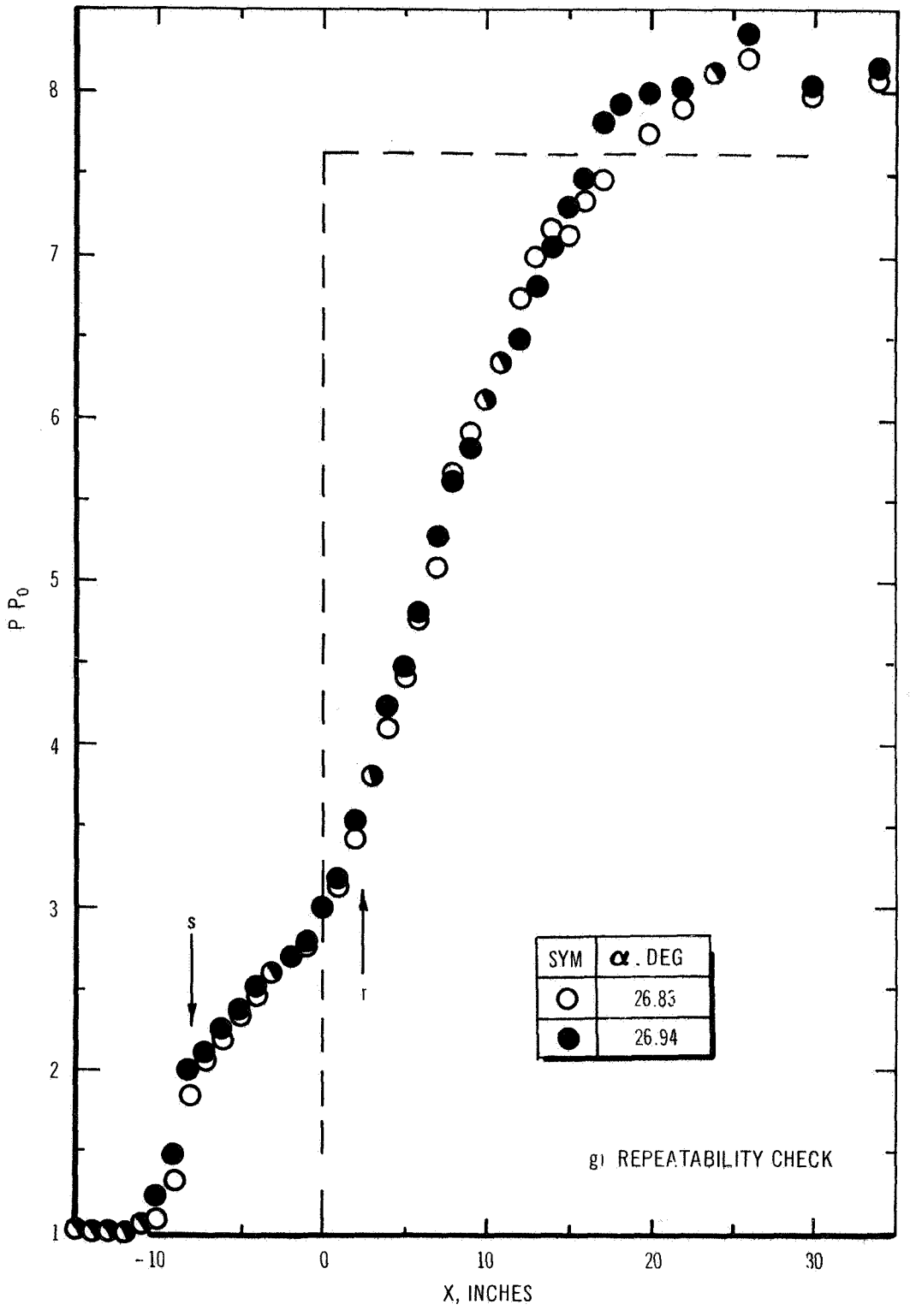

Figure 13. Concluded

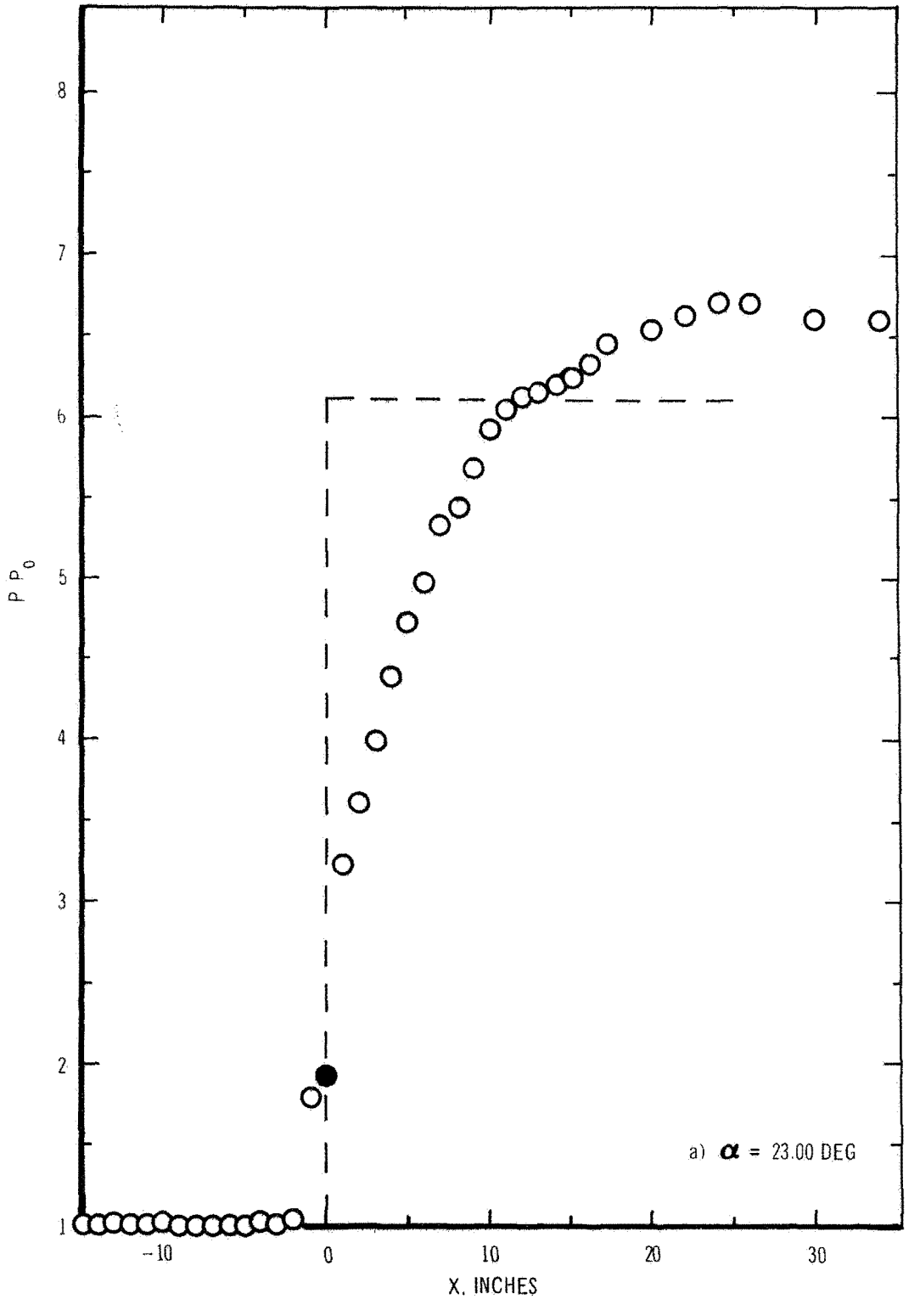

Figure 14. Pressure Distributions Along Model Centerline.
$M_0 = 3.93$, $R_0 = 1.743 \times 10^6$/in., δ_0 4.52 in.

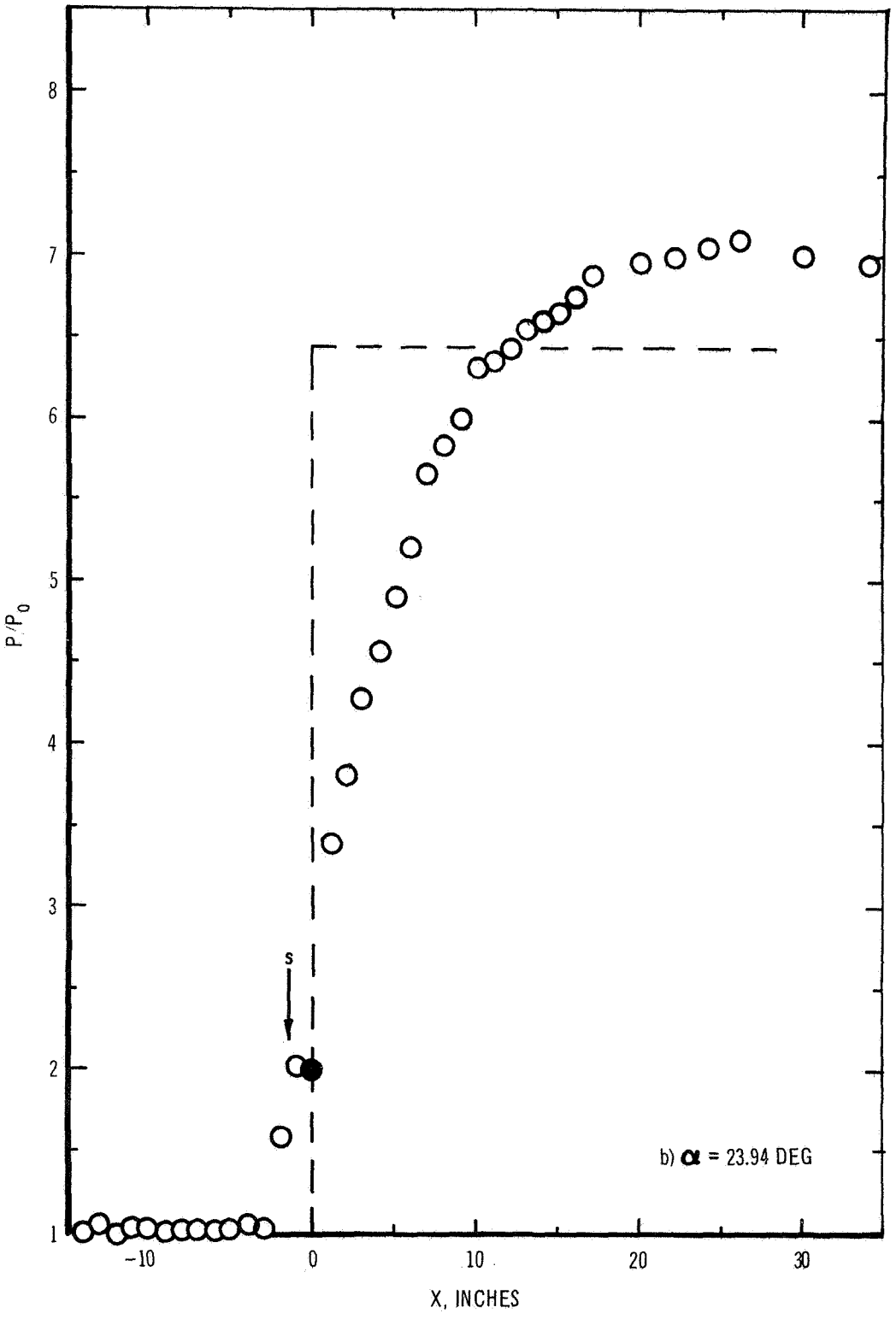

Figure 14. Continued

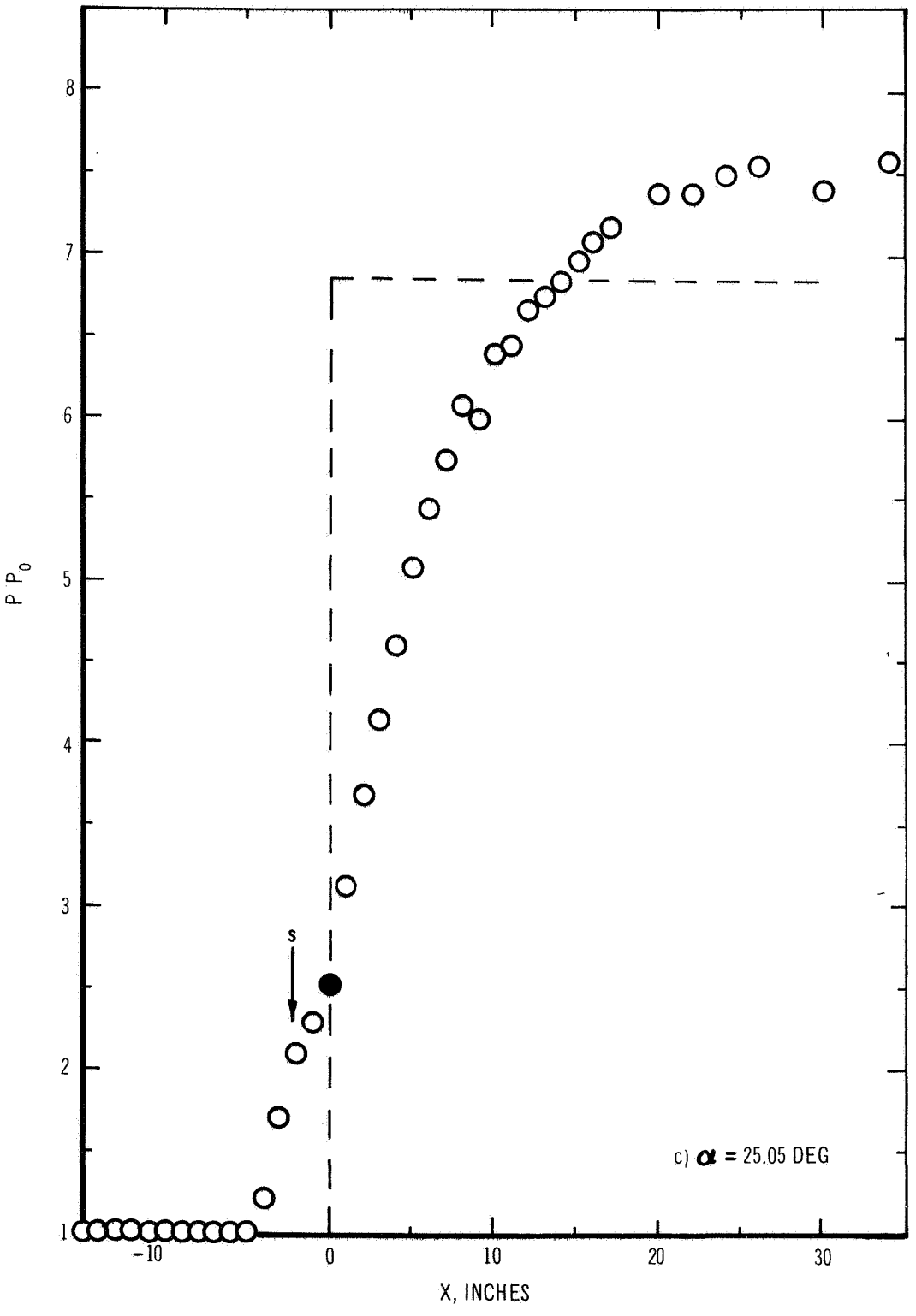

Figure 14. Continued

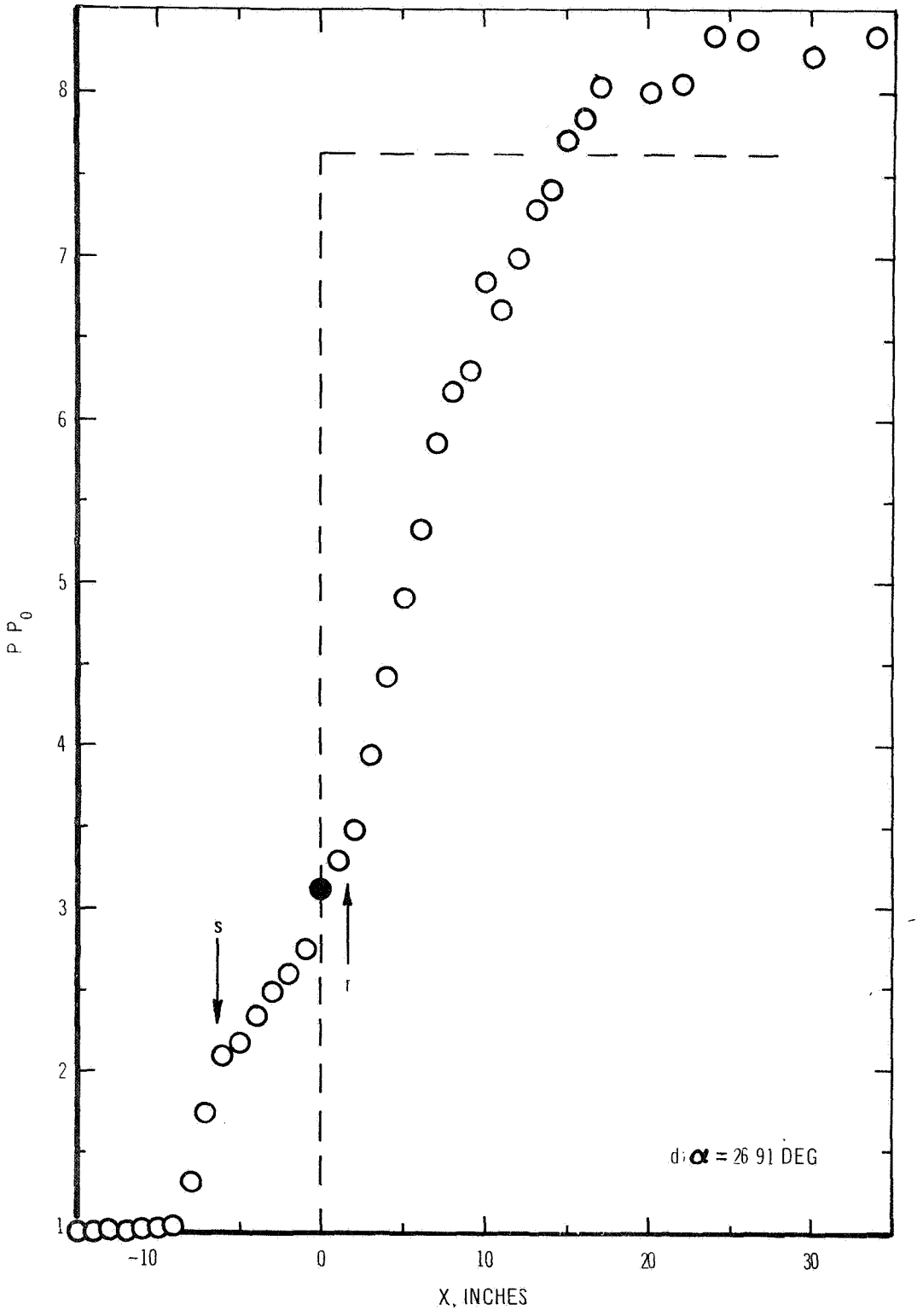

Figure 14. Concluded

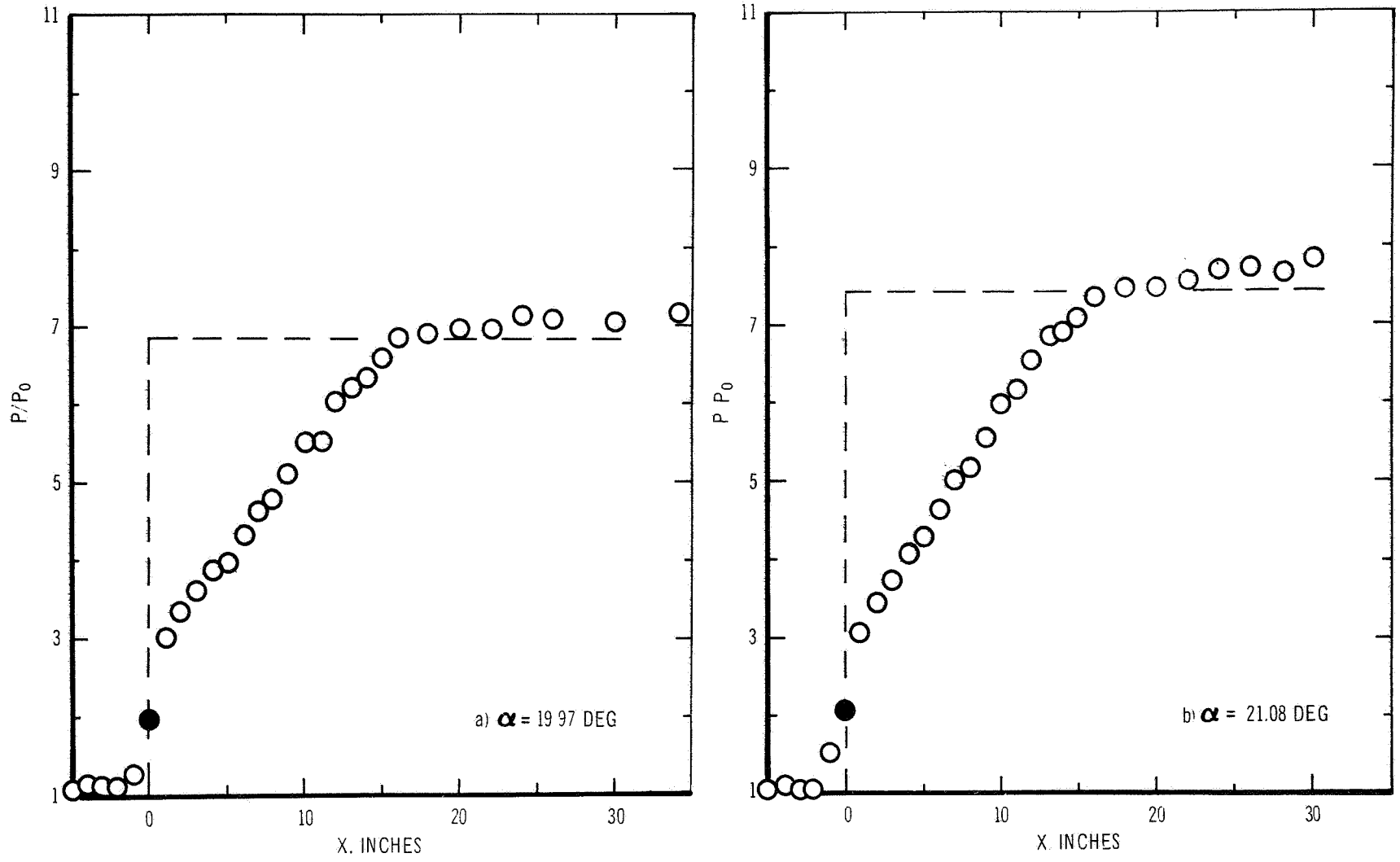

Figure 15. Pressure Distributions Along Model Centerline. M_0 - 4.92, R_0 0.560 x 10^6/in δ_0 - 5.81 in.

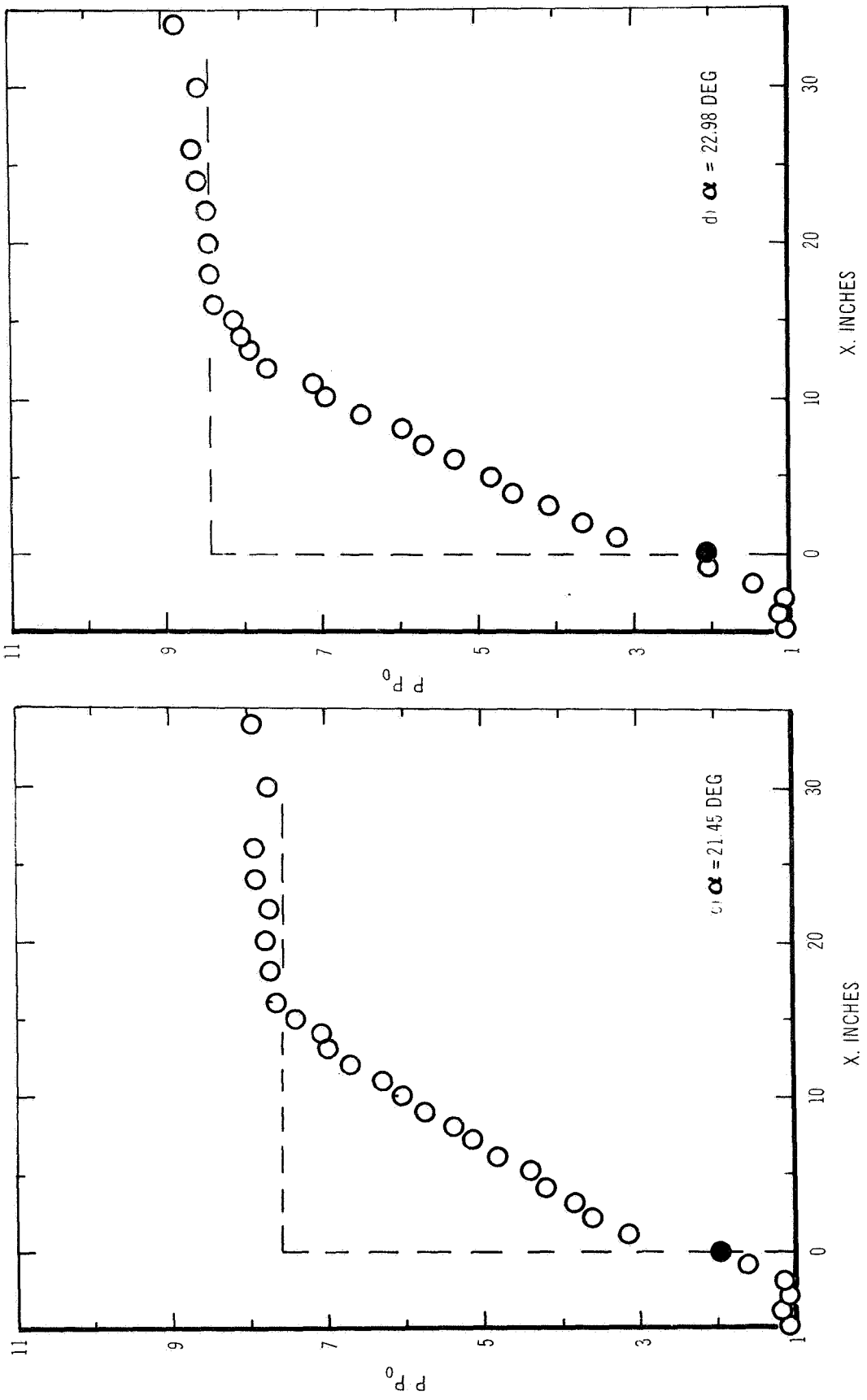

Figure 15. Continued

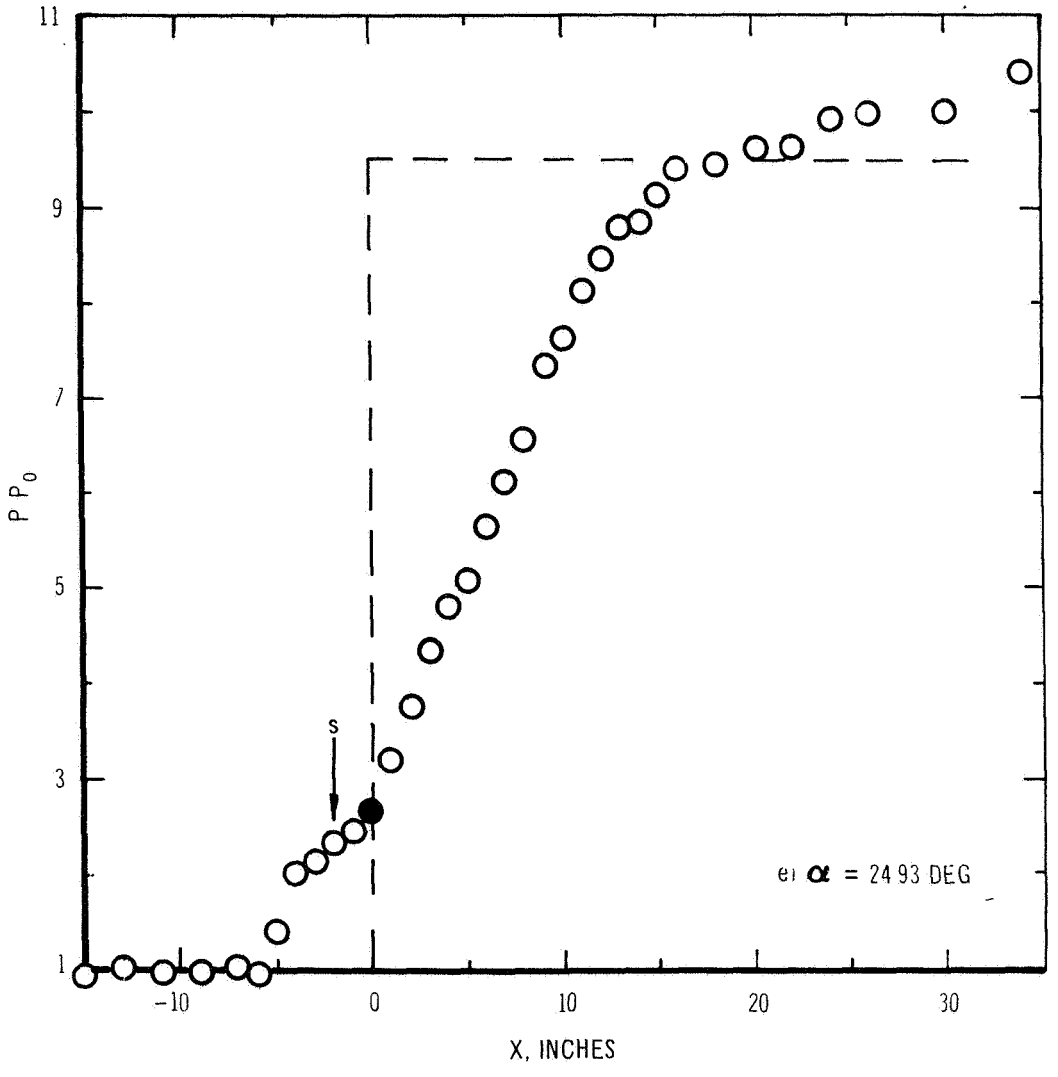

Figure 15. Concluded

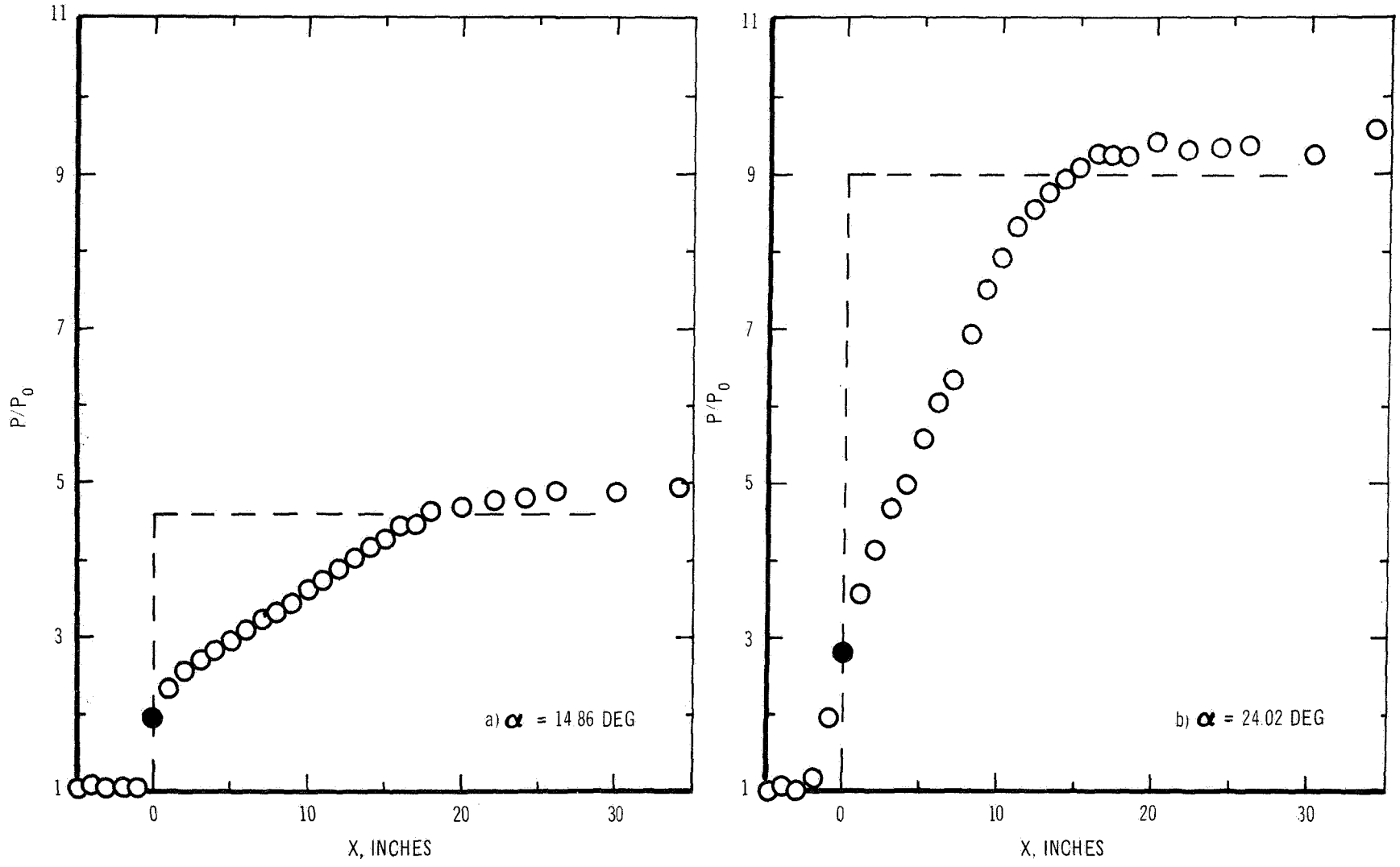

Figure 16. Pressure Distributions Along Model Centerline. M_0 = 4.92, R_0 = 0.959 x 10^6/in., δ_0 = 5.49 in.

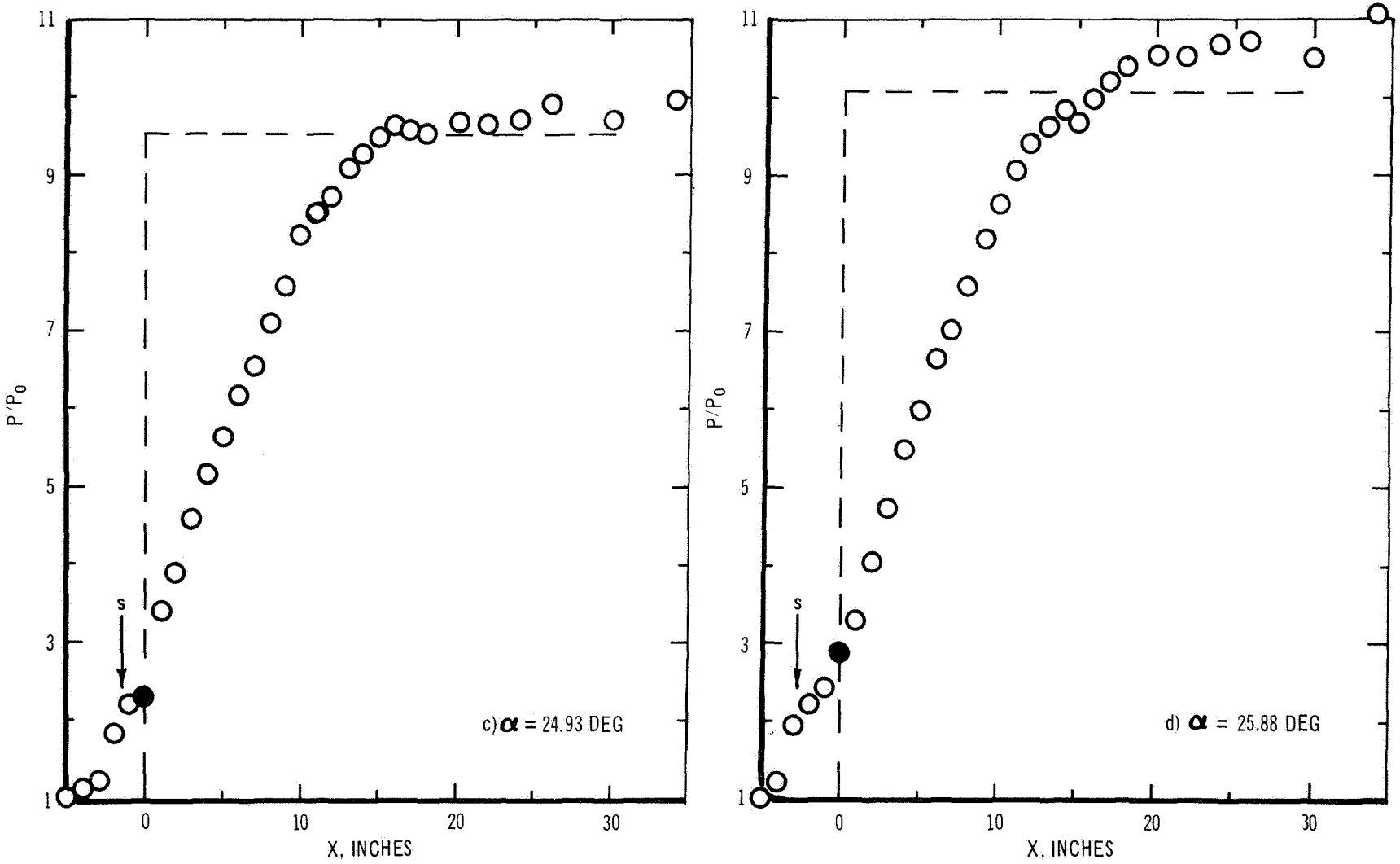

Figure 16. Continued

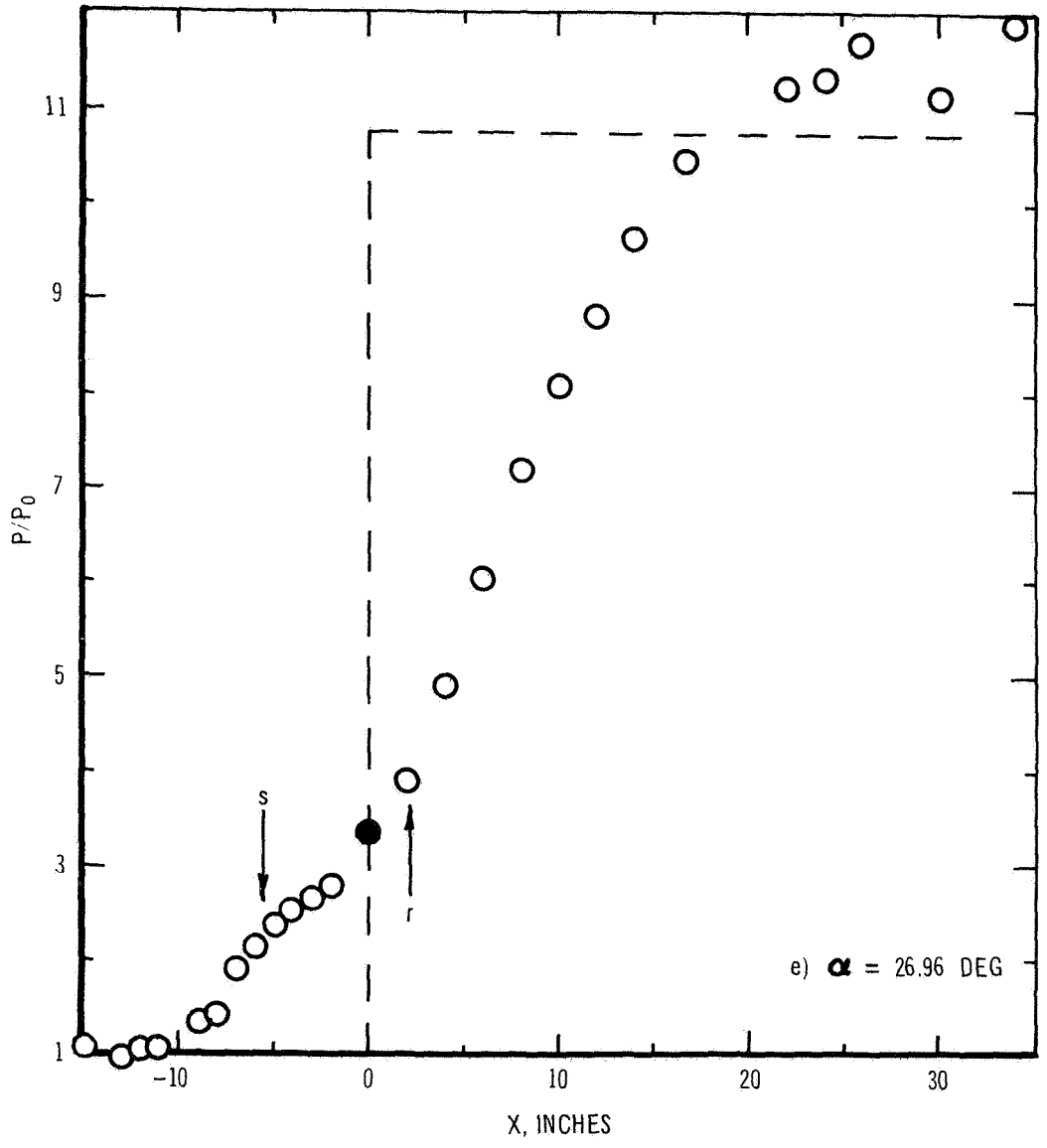

Figure 16. Concluded

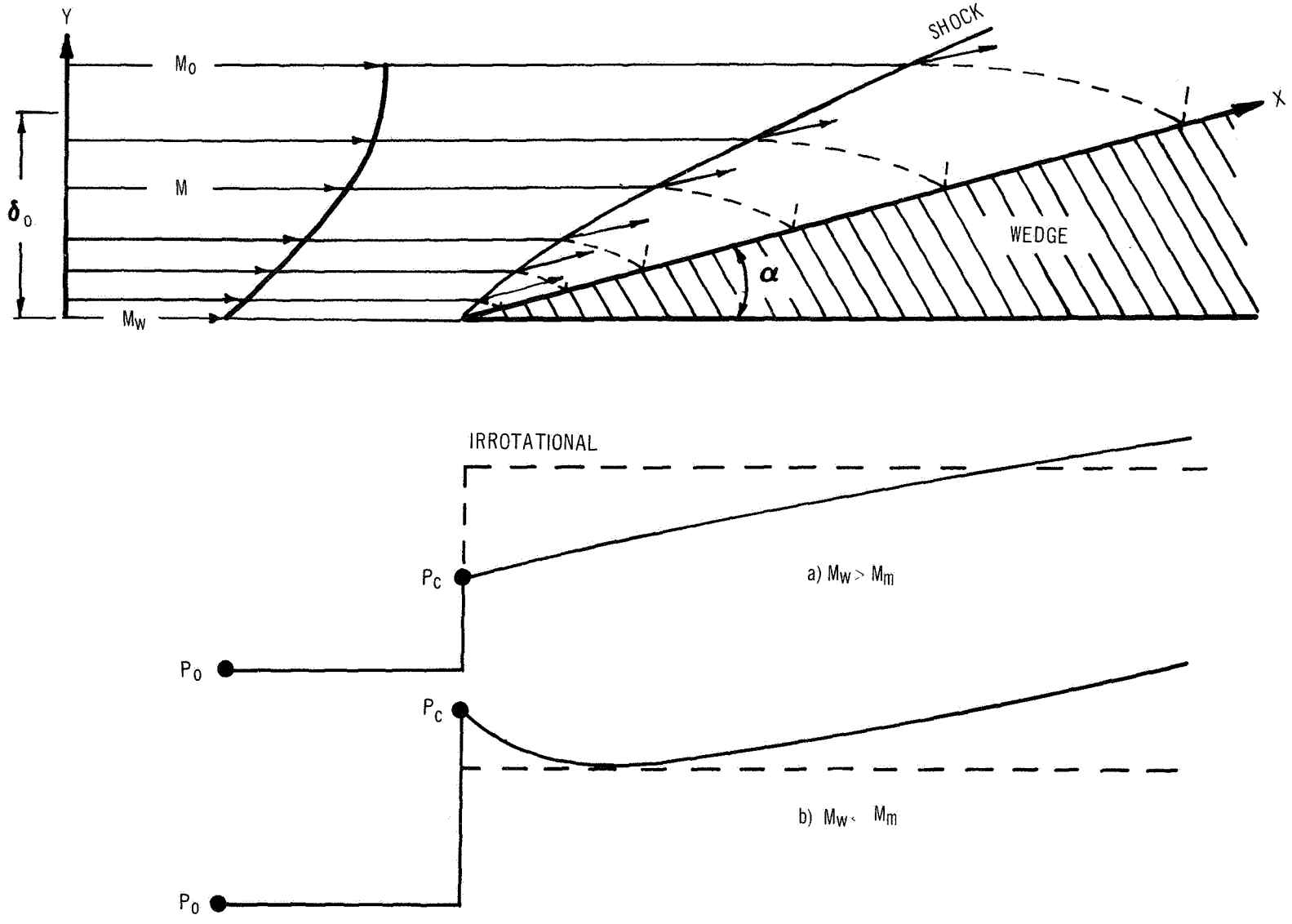

Figure 17. Inviscid Interaction of Boundary Layer With Compression Corner ($\alpha \cdots \alpha_i$)

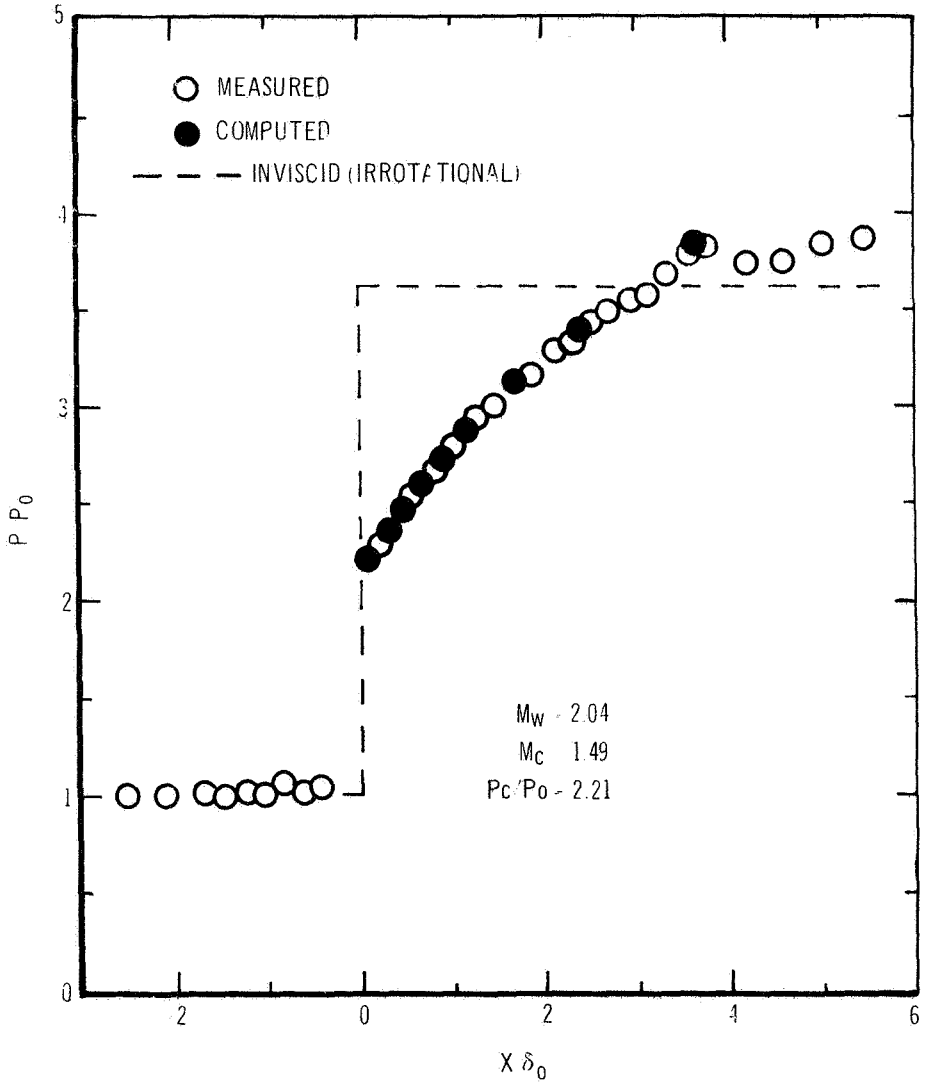

Figure 18. Surface Pressure Distribution. M_O 3.93, R_δ 5.55×10^6, δ_O 4.78 In., α 15 Deg.

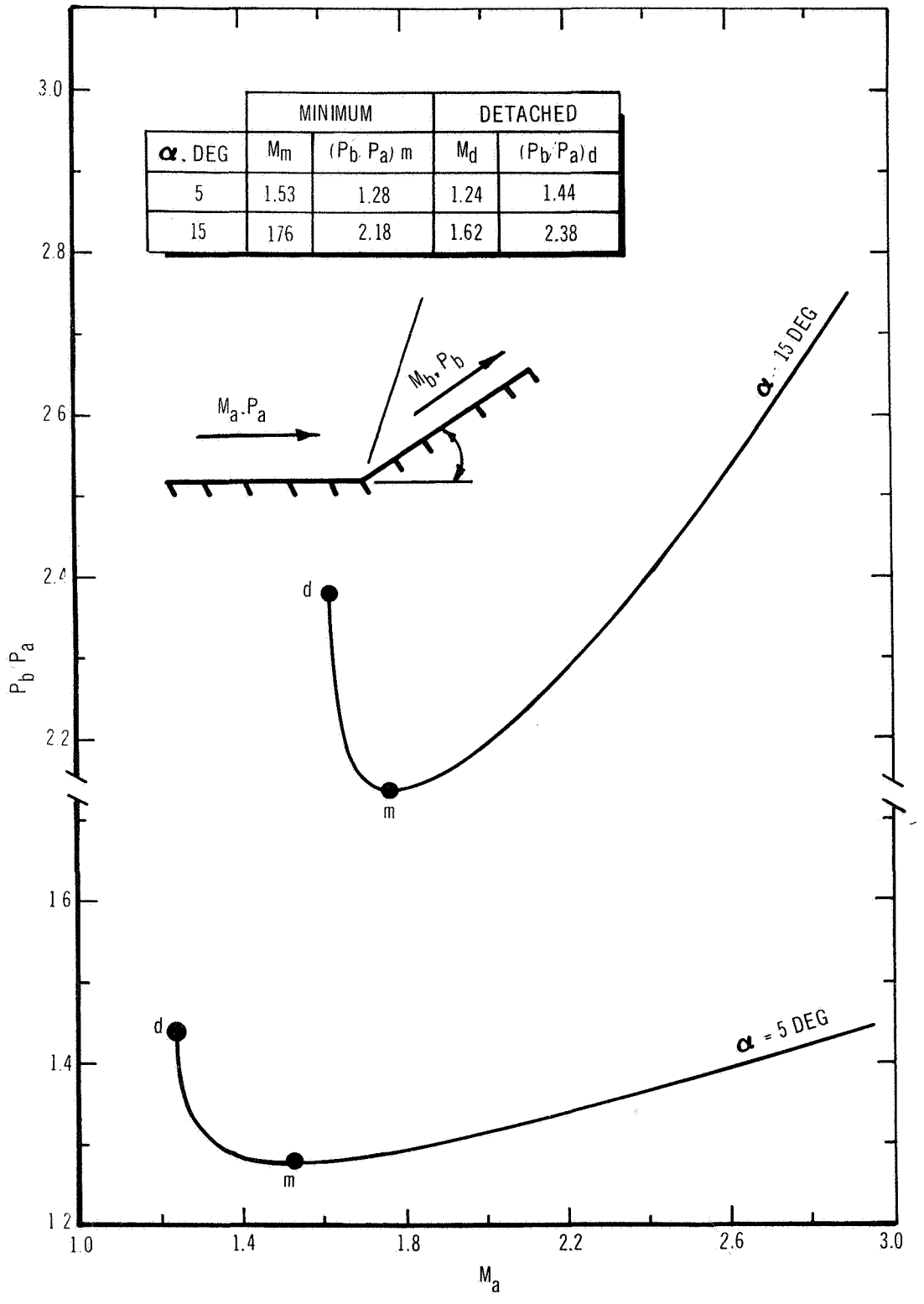

Figure 19. Pressure Rise Through a Shock

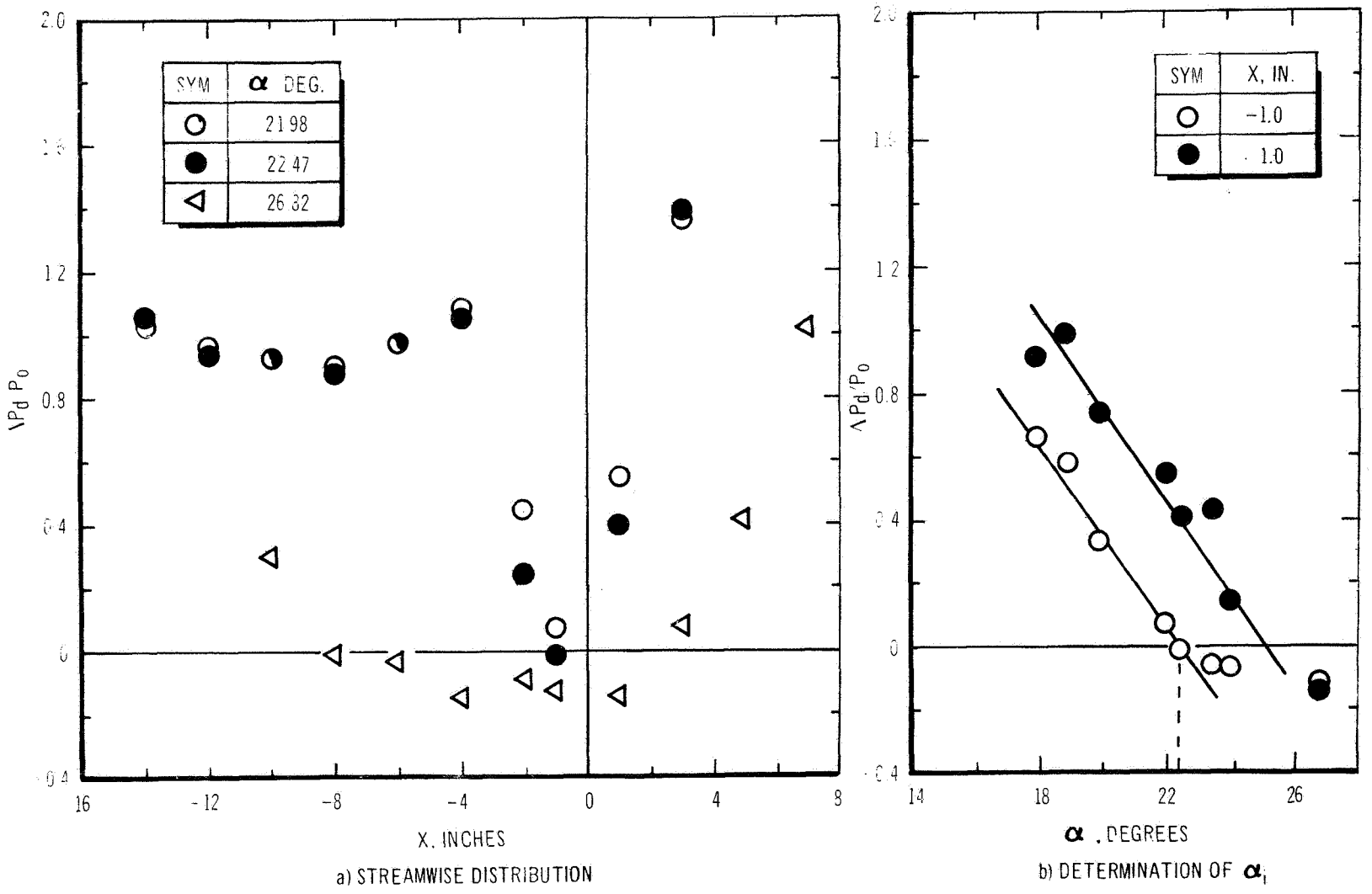

Figure 20 Typical Result Obtained From Orifice-Dam Technique. $M_0 = 3.93$, $R_0 = 0.443 \times 10^6$/In., $\delta_0 = 5.36$ In.

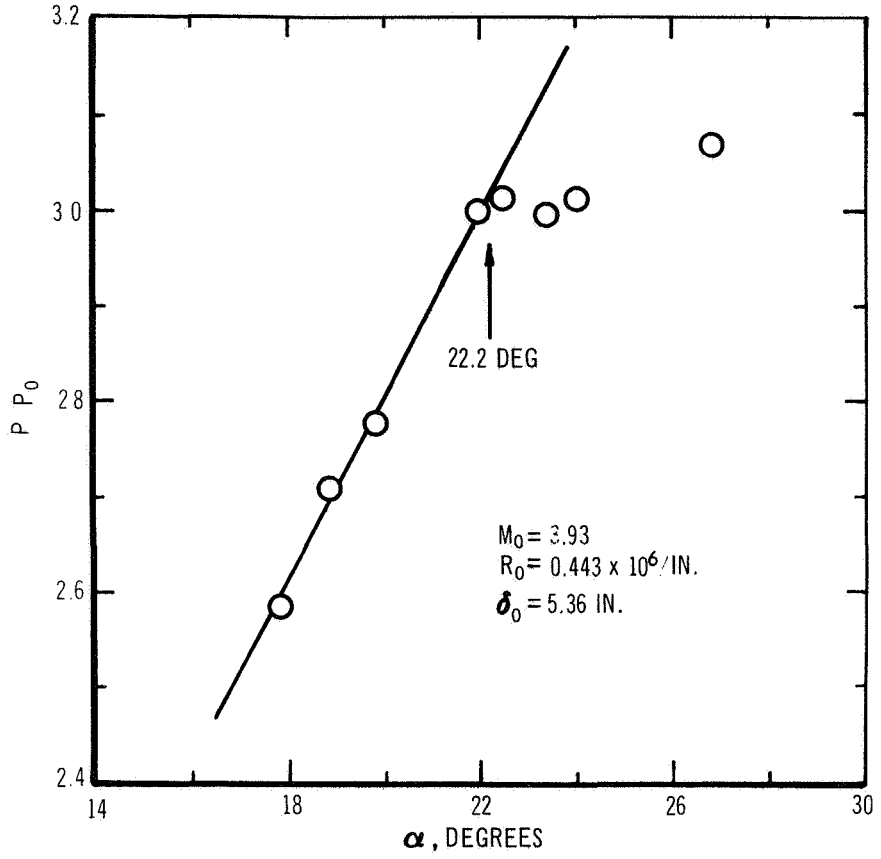

Figure 21. Surface Pressure Downstream (x = 1.0 Inch) of Corner

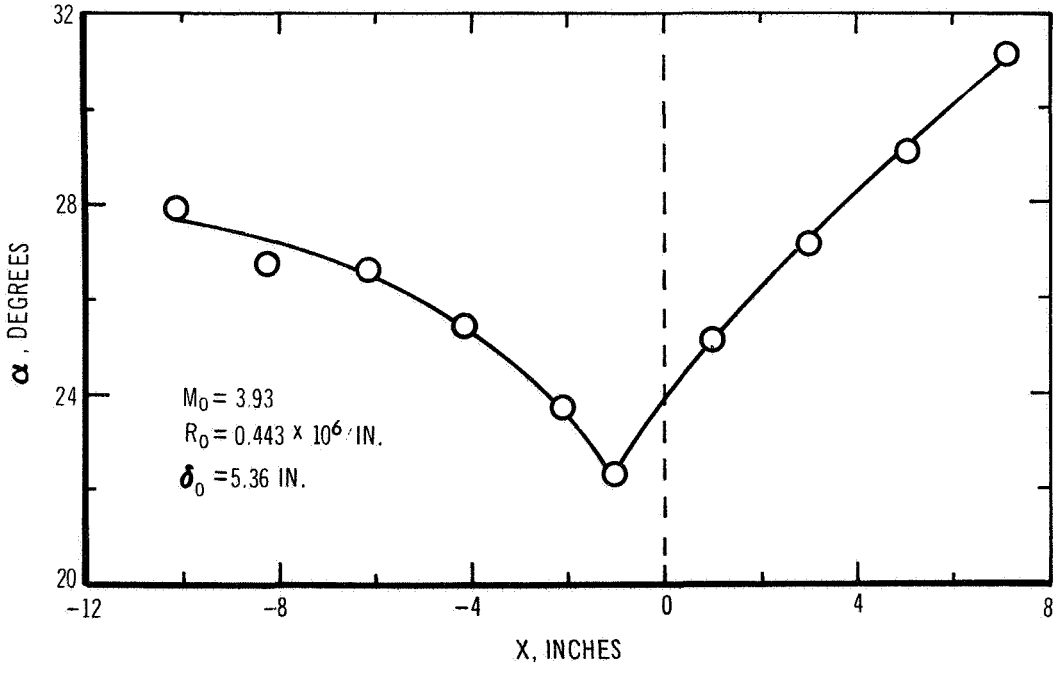

Figure 22. Location of Flow Reversal Points

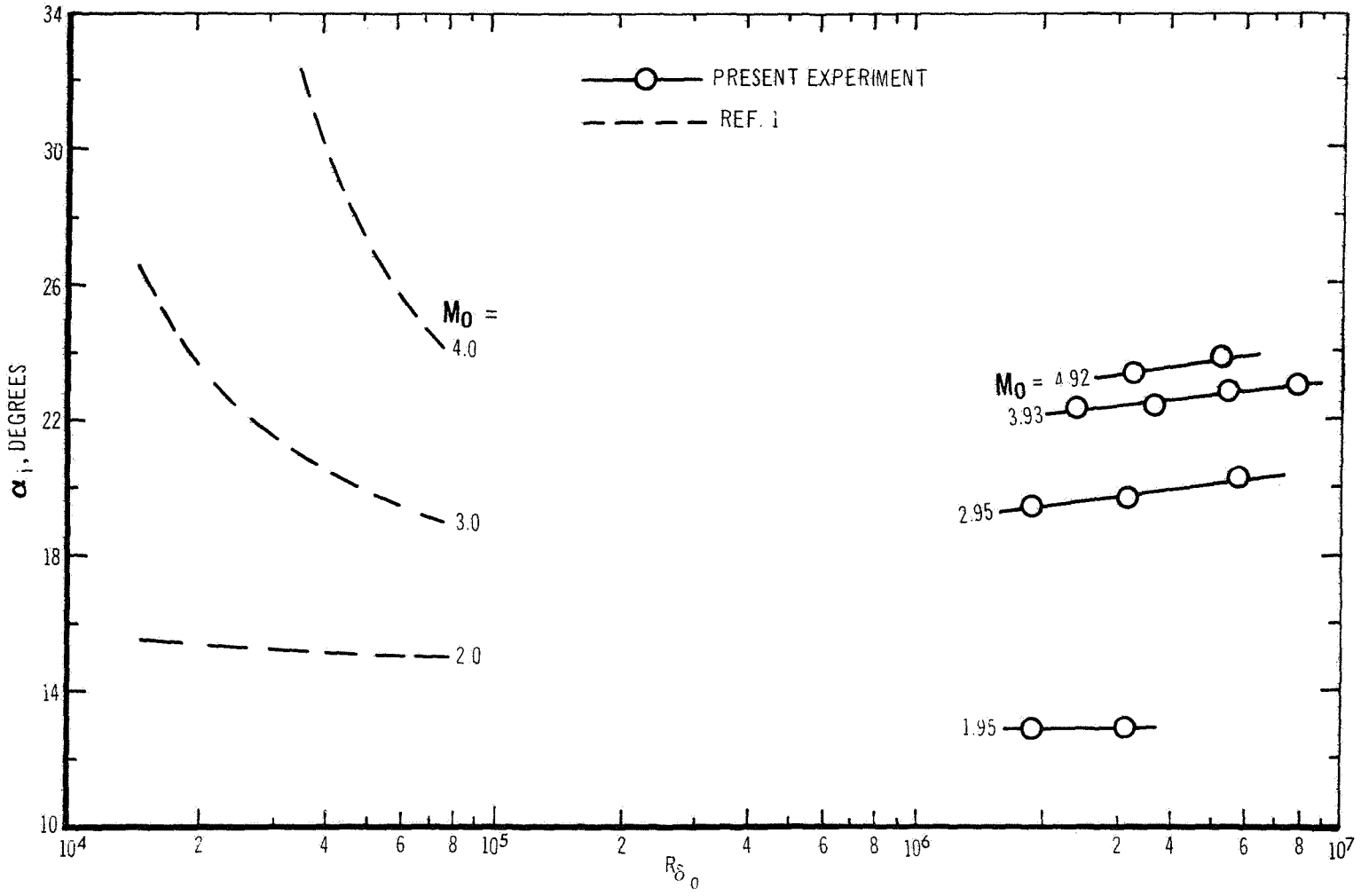

Figure 23. Compression Corner Angle for Incipient Separation of Turbulent Boundary Layer

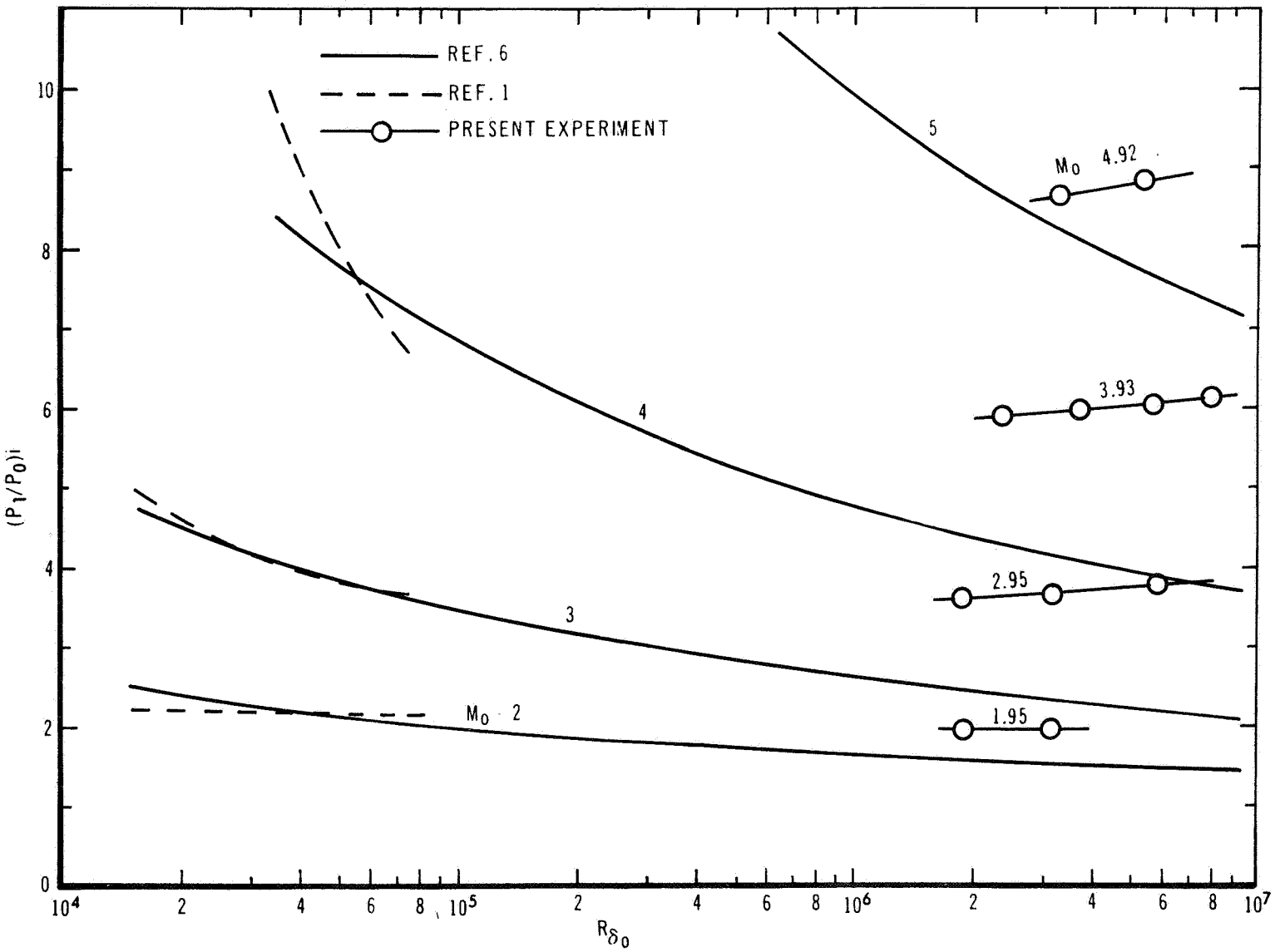

Figure 24. Pressure Rise for Incipient Separation of a Turbulent Boundary Layer.

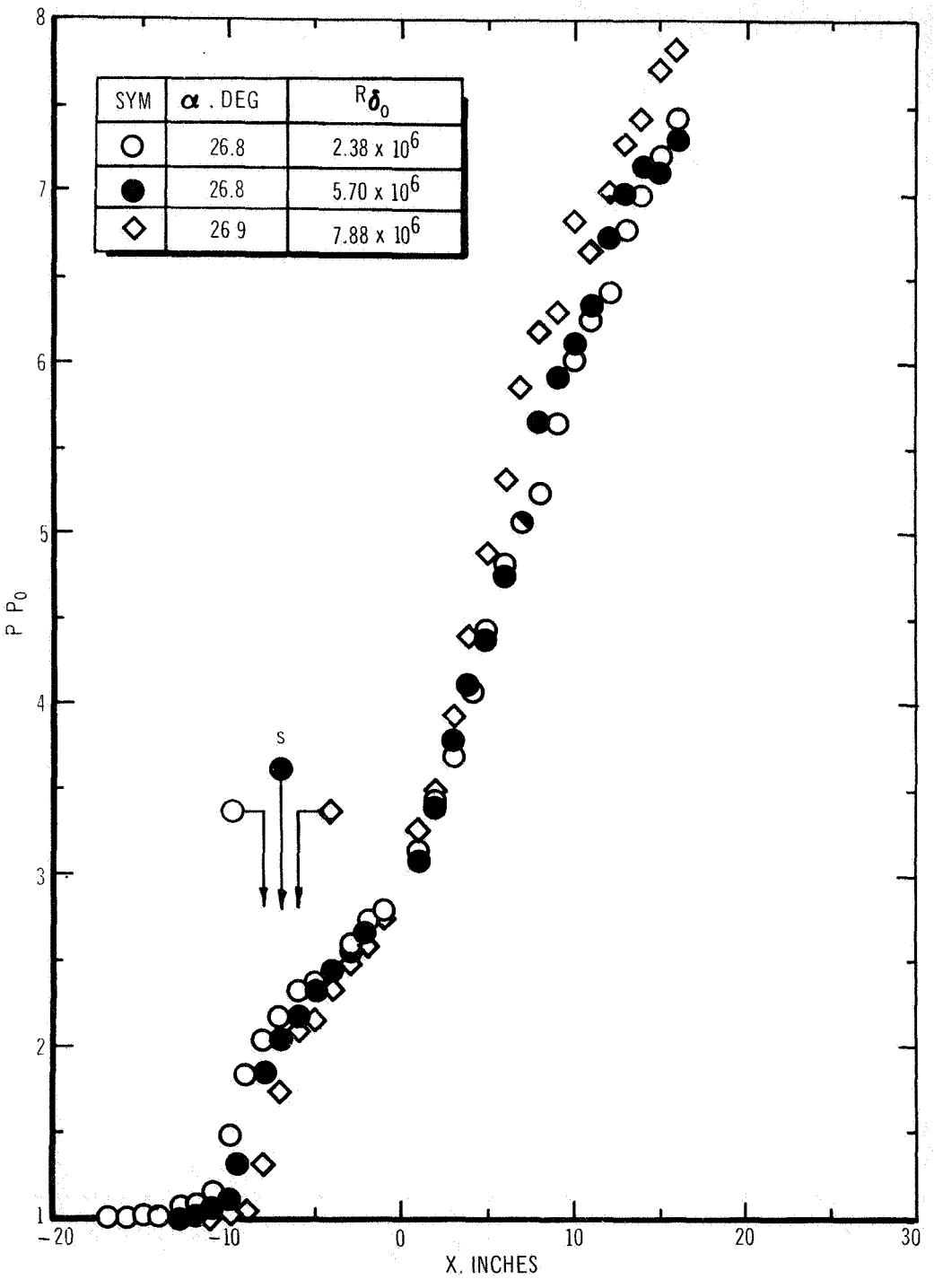

Figure 25 Reynolds Number Effect on Length of Separated Region M_0 3 93

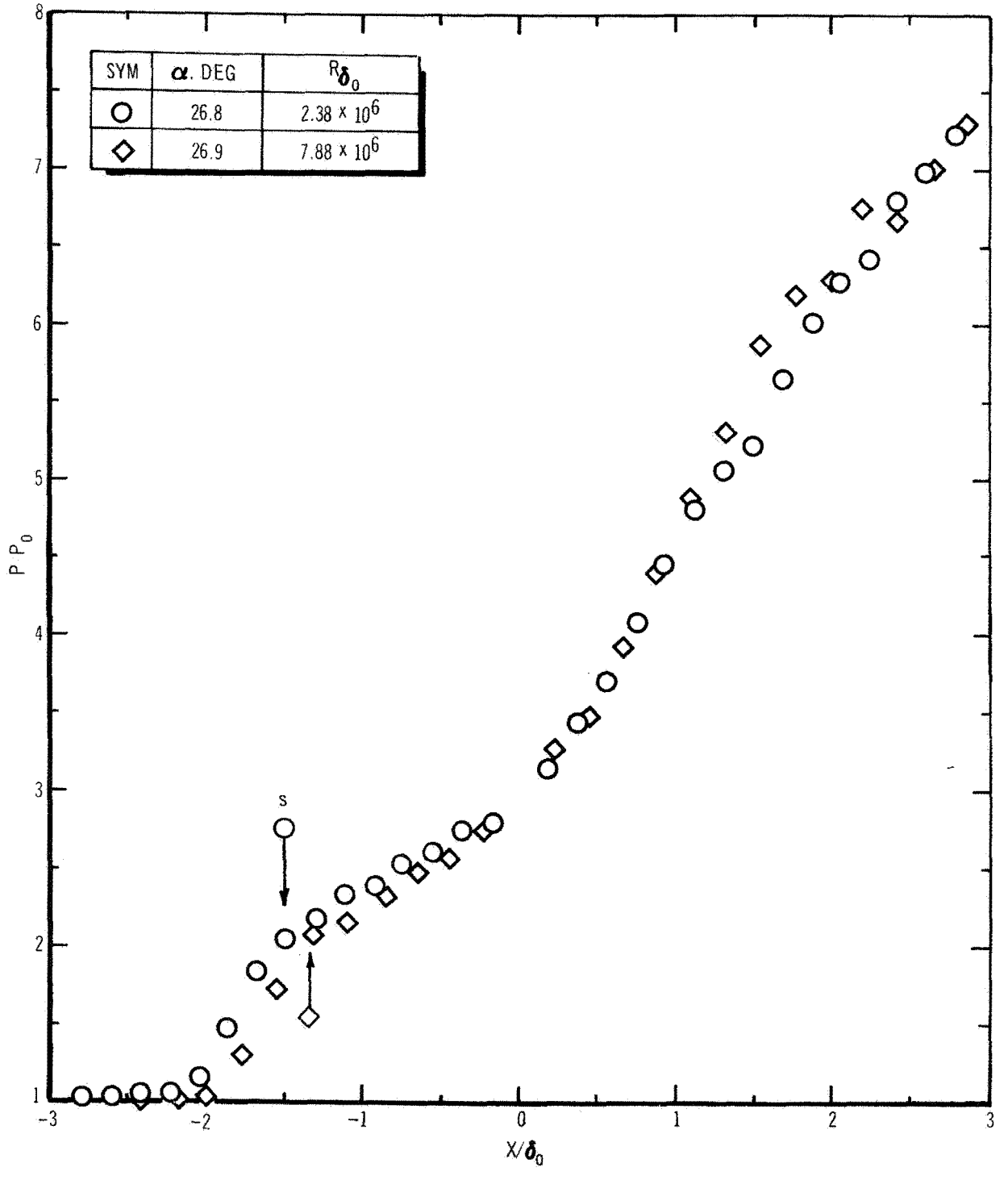

Figure 26. Reynolds Number Effect on Normalized Length of Separated Region. $M_0 = 3.93$